CHARACTERIZATION OF SHAPE MEMORY POLYMER FOAM:

BIOCOMPATIBILITY, VISUALIZATION AND HEMODYNAMIC INTERACTIONS

A Dissertation

by

JENNIFER N. RODRIGUEZ

Submitted to the Office of Graduate and Professional Studies of
Texas A&M University
in partial fulfillment of the requirements for the degree of

DOCTOR OF PHILOSOPHY

Chair of Committee,	Duncan J. Maitland
Committee Members,	Mark W. Lenox
	Fred J. Clubb
	Matthew W. Miller
Head of Department,	Gerard L. Cote

May 2014

Major Subject: Biomedical Engineering

ABSTRACT

Cerebral aneurysms are unstable localized dilations of an artery wall located in the vasculature of the brain that are susceptible to rupture. Current treatments of aneurysms, both surgical and endovascular, involve isolation of the weakened area of artery from the rest of the vasculature. However, current filling methods do not result in optimal healing. Therefore, we are developing an alternative filling method using shape memory polymer (SMP) foams. This dissertation addresses multiple post processing methods and characterization of these SMP foams. The goals for characterizations addressed include 1) microstructure, 2) radio-opacity, 3) biocompatibility, 4) mechanical reticulation, 5) flow visualization via magnetic resonance imaging and 6) permeability measurements.

The microstructure of the SMP foams was imaged via micro-computed tomography imaging methods at high resolution, 4 μm/voxel. At this resolution we were able to resolve membranes, struts and obtain 3D models of the foam for computational fluid dynamic simulations. Histogram data of average pore cells sizes in multiple axes were also measured. It was shown that these materials are anisotropic and heterogeneous.

Increased radio-opacity via loading methods resulted in x-ray based visualization of devices made of these materials during endovascular implantation. The addition of high-z element particulates for radio-opacity resulted in a stronger or composite version of the material.

It was shown that these shape memory polymer foams were biocompatible when implanted in a porcine aneurysm model. The implants elicited healing, were completely isolated from the parent vessel and covered with a complete endothelial cell layer at

ninety days.

A non-destructive mechanical reticulation device was made to puncture the membranes of the foams and thereby increase flow permeation. The permeability, or pressure drop induced by the samples was measured. Permeability results showed that with the increased amount of mechanical reticulation resulted in increased permeability of these materials. Flow visualization within the samples was achieved via MRI at sub pore cell resolution.

All of this research aids in not only the understanding but also the development of these materials as a viable medical device for the treatment of intracranial aneurysms and other vascular applications.

DEDICATION

I would like to dedicate this dissertation to my family and friends, especially my parents, Nanci J. and Samuel B. Rodriguez for their continued emotional and financial support throughout this educational experience. I would like to also thank colleagues, collaborators and mentors whom have helped me along the way, including collaborators at Lawrence Livermore National Laboratory and Kaiser Permanente: Thomas S. Wilson, Jason M. Ortega, Ward Small, I.V., and Dr. Jonathan Hartman, collaborators here at Texas A&M University who have been of great support in research: Matthew W. Miller, Fred J. Clubb, Mark W. Lenox, and my adviser, Duncan J. Maitland. I would like to additionally thank my adviser for his support and belief in my abilities to accomplish this work.

Through the accomplishment of this goal I have improved not only as a researcher, but overall as a person. This educational adventure would not have been possible without all of your support; for which I am eternally grateful.

Thank you.

ACKNOWLEDGEMENTS

I would like to thank my colleagues in the Biomedical Device and the Cardiovascular Pathology Laboratories at Texas A&M University for their collaboration, encouragement, expertise and support. I would like to thank the Biomedical Engineering Department's faculty and staff for making my time at Texas A&M University a smooth educational experience. I would like to extend an extra thanks to Carl Johnson, of the biomedical engineering department's machine shop, for his expertise in design and fabrication of parts. I also want to extend my gratitude to the Alfred P. Sloan Foundation Minority Ph.D. Program, which generously provided funding for instruments, computers and computer programs necessary for this research. This work was supported by the National Institutes of Health and National Institute of Biomedical Imaging and Bioengineering Grant R01EB000462.

Thanks to my family and friends in both the state of Texas and California for their encouragement and motivation of completion.

I would like to again express my gratitude to my mother and father, Nanci and Samuel Rodriguez, for their continued support, encouragement, patience and love. One last expression of thanks to Amber and Zorro (12/14/01 - 01/10/14), for being part of this journey with me and making Texas feel more like home.

I would like to acknowledge my co-authors for the first paper included in this dissertation, section two, Fred J. Clubb, Thomas S. Wilson, Matthew W. Miller, Teresa W. Fossum, Jonathan Hartman, Egemen Tuzun, Pooja Singhal and Duncan J. Maitland, entitled "In vivo response to an implanted shape memory polyurethane foam in a porcine

aneurysm model". The authors also expressed their thanks to Jordan Conway for his assistance in the preparation of the final manuscript.

Secondly, I would like to acknowledge my co-authors for the second paper in this dissertation, section three, which included Ya-Jen Yu, Matthew W. Miller, Thomas S. Wilson, Jonathan Hartman, Fred J. Clubb, Brandon Gentry and Duncan J. Maitland entitled, "Opacification of Shape Memory Polymer Foam Designed for Treatment of Intracranial Aneurysms". The authors acknowledged Amanda Connor, Josh Bergerson, Casey McCurrin, Stephen Darrouzet, Brent Volk and Keith Hearon for their technical support on the research published in this article.

Thirdly, I would like to acknowledge my co-authors for the third paper in this dissertation, section four, which included Matthew W. Miller, Anthony Boyle, Cheng-Kang Yang, Thomas S. Wilson, Ward Small, Landon Nash, Hunter Skoog and Duncan J. Maitland entitled, "Reticulation of low density shape memory polymer foam for vascular occlusion". The authors would like to thank Carl Johnson and Todd Landsman for their assistance in fabrication of the reticulation devices.

Lastly, I would like to acknowledge my co-authors for the fourth paper in this dissertation, section five, which included John Horn, Mark W. Lenox, Jason M. Ortega, Robin Terry and Duncan J. Maitland.

All of the work reported in this dissertation was supported by the National Institutes of Health/National Institute of Biomedical Imaging and Bioengineering Grant R01EB000462 and some of this work was partially performed under the auspices of the

U.S. Department of Energy by Lawrence Livermore National Laboratory under Contract DE-AC52-07NA27344.

NOMENCLATURE

MRV	Magnetic Resonance Velocimetry
MRI	Magnetic Resonance Imaging
P	Pressure
T	Time
μ-CT	Micro Computed Tomography
CT	Computed Tomography

TABLE OF CONTENTS

Page

LIST OF FIGURES

LIST OF TABLES

1. INTRODUCTION

A cerebrovascular accident (CVAs) is a sudden lack of oxygen to a portion of the brain, resulting in death of the adjacent brain cells, due to a blockage in the vasculature or hemorrhage, commonly known as ischemic or hemorrhagic stroke respectively.[12] CVAs occur in more than 700,000 Americans per year,[12, 93, 13] and approximately 100,000 of the 700,000 occur after an aneurysm rupture.[12, 5, 6] Cerebral aneurysms are localized dilations of the artery wall located in the vasculature of the brain, and are unstable in structure due to a lack of an intimal elastic lamina and a thickened hyalinized intima and thus, have the tendency to rupture.[55] Upon aneurysm rupture, a subarachnoid hemorrhage, occurring in approximately 10 per 100,000 people,[23, 56] results in a cerebrovascular accident, a potentially fatal or a severely debilitating event.[23]

These cerebral arterial malformations are often spherical in shape and are commonly referred to as berry aneurysms, which affect approximately 3-5% of the general population.[92, 23] Berry aneurysms are congenital, or linked to genetic inheritance, with an increased susceptibility to develop lesions at different sites within the cerebral vasculature, especially within the circle of Willis.[90, 23] Due to the high impact on patient mortality and morbidity, early and effective treatment of a berry aneurysm prior to rupture is imperative for increasing the patient's survival rate and quality of life.[23]

The current FDA approved treatments for such aneurysms involve isolation of the weakened vessel via surgical clipping,[62] endovascular embolization through the use of flexible platinum coils, called Guglielmi Detachable Coils (GDC), inserted into the dome of the aneurysm, or filling with an in-situ polymerizing radiopaque material, such

as Onyx Liquid Embolic Eystem (Onyx HD-500) (Onyx; MicroTherapeutics, Irvine, CA, USA). Both the GDC coils and the polymerizing material are introduced to the aneurysm dome via a micro catheter. These filling treatments involve isolation of the weakened area of artery from the rest of the vasculature, resulting in the remodeling of the endothelium, the innermost layer of the artery. Further, these treatments are not perfect in avoiding aneurysm rupture and subsequent hemorrhage, but they have greatly improved the outcome compared to untreated aneurysms.[12]

The current treatments for intracranial aneurysms give options for interventionists; however there are limitations and risks associated with each of the designs. Surgical clipping involves a craniotomy, an invasive surgery of the brain, which can have serious inherent risks to the patient. Furthermore, surgical clipping is not always possible due to an inaccessible location of the aneurysm within the brain or the patient being a nonviable candidate for surgery due to age or weakness. As a result of these limitations on surgical clipping, endovascular treatment by filling devices has become the preferred treatment among physicians.[23]

Of the two available filling treatments, GDC platinum coils are the favored treatment for cerebral aneurysms.[62] The mechanism of aneurysm treatment by GDC is to fill the sac with multiple clot-promoting platinum coils one-at-a-time until the volume appears to be filled, as observed via fluoroscope imaging.[37] Specifically, the coils are navigated through the arterial system from the femoral artery to the site of the aneurysm, guided by contrast enhanced fluoroscope images of the patient, utilizing the Seldinger method, which involves placement of the micro catheter over a micro guidewire to

navigate the tortuous vasculature of the brain.[83, 23] Filling of the aneurysm is then achieved when there is a lack of contrast medium injected into the dome; at that point no more coils would be inserted. Although inherently extremely flexible, the platinum coils are available in engineered variations that tailor the flexibility, thickness and length. In addition, GDCs have the ability to wind themselves into a circular shape until they create a scaffold for which blood can coagulate and form a stable clot. Each platinum coil is detached at a solder point via electrical current, causing the coil to become positively charged.[23] This positive charge makes the coil attractive to the negatively charged blood components[23, 37] and thus initiates a clot via electrothrombosis.[37]

While being the favored treatment for intracranial aneurysms, GDCs do possess drawbacks, such as coil compaction and subsequent formation of new side aneurysms adjacent to the original aneurysm,[40] low packing volume (less than 50% of the volume[68, 44, 49]) leading to recanalization or refilling,[38] migration of loose coils into the parent artery [96], and although rare, potential puncture of the aneurysm dome.[26] Additionally, GDCs are not very successful at treating aneurysms with neck diameters greater than 4 mm.[68] In these large neck aneurysms, approximately one-third of GDC treated aneurysms either rebleed or recanalize.[30, 63, 75, 89] Therefore, although GDC treatment is the preferred filling method by interventionlists, there is room for improvements in the safety and efficacy of these devices.

A more recent method of filling and isolation of the aneurysm involve a soft spongy material. Onyx is a material that is mechanically more compliant with the arterial wall than the GDC metal coils, potentially having a better in-vivo healing response and

overall stability in comparison to the GDC filling method. Because Onyx is a spongy polymer only after in-situ polymerization, it has the potential to migrate,[94] or leak out, of the dome of the aneurysm while still in its liquid state. The consequences associated with the migration are substantial due to the potential to block one of the parent or downstream arteries and thereby causing infarction. In addition, Onyx has been proven to be a viable treatment for small-necked aneurysms over time,[18] but is not as stable for permanent treatment of giant aneurysms.[18]

The drawbacks of the commonly accepted treatments have spurred developments of alternative aneurysm filling methods. Some of these technologies include treatment with multiple commercial devices[42], hydrogel polymer[38], hybrid metal and hydrogel coils[1], and polymer foams for filling of the dome.[98, 99, 68, 86]

This dissertation focuses on technology which involves shape memory polymer (SMP) foams that have been developed as an aneurysm filling method[87, 25, 68] and vascular occlusion device. SMP foams are materials that have the ability to be fabricated into an initial shape, such as a sphere. This initial geometry can then be deformed subsequent to raising the material's temperature above its transition temperature, for these materials its glass transition temperature, through application of a force. A continued application of the force while cooling the material below its glass transition temperature, programs the material into a secondary shape. An example of a secondary shape is a crimped, small diameter cylinder. When the polymer is in a cylinder of small diameter it is in a secondary, or temporary shape. The aneurysm or artery filling device

would remain in its temporary shape until it is delivered to the dome of the aneurysm, or patent artery respectively.

These SMP foams are based off of polyurethane chemistry[97] and have potentially superior biocompatibility *in-vivo.*[15] Although superior healing may result from the use of SMP polymer foams as a filling material, these polymer foams are not visible under conventional patient imaging modalities, which hinders their use by clinicians. Part of this research sought to resolve the lack of radio-opacity of low-density SMP foams and thus advance this technology toward a marketable medical device. Another aspect to this research involved characterization of the materials via imaging and mechanical methods, such as mechanical testing and characterization of foams while under the influence of flow. Another aspect of characterization includes the in vivo tissue response of these foams to implants within porcine aneurysm and vascular occlusion models. Radio-opacity, tissue interaction and hemodynamic interactions were determined in this research.

2. *IN VIVO* RESPONSE TO AN IMPLANTED SHAPE MEMORY POLYURETHANE FOAM IN A PORCINE ANEURYSM MODEL*

2.1 Overview

Cerebral aneurysms treated by traditional endovascular methods using platinum coils have a tendency to be unstable, either due to chronic inflammation, compaction of coils, or growth of the aneurysm. We propose to use alternate filling methods for the treatment of intracranial aneurysms using polyurethane based shape memory polymer (SMP) foams. SMP polyurethane foams were surgically implanted in a porcine aneurysm model to determine biocompatibility, localized thrombogenicity, and their ability to serve as a stable filler material within an aneurysm. The degree of healing was evaluated via gross observation, histopathology and low vacuum scanning electron microscopy (LV-SEM) imaging after zero, thirty and ninety days. Clotting was initiated within the SMP foam at time zero (less than one hour exposure to blood prior to euthanization), partial healing was observed at thirty days, and almost complete healing had occurred at ninety days in vivo, with minimal inflammatory response.

---

* Reprinted with permission from "In vivo response to an implanted shape memory polyurethane foam in a porcine aneurysm model" by Jennifer N. Rodriguez, Fred J. Clubb, Thomas S. Wilson, Matthew W. Miller, Theresa W. Fossum, Jonathan Hartman, Egemen Tuzun, Pooja Singhal and Duncan J. Maitland, 2014. Journal of Biomedical Materials Research Part A, Volume 102, pages 1231-1242, Copyright 2014 Wiley Periodicals, Inc., License Number: 3345431422339.

2.2 Introduction

2.2.1 Cerebral aneurysms and subarachnoid hemorrhage

Aneurysms are geometric structural abnormalities of the vasculature manifested as a bulging or out pouching of the vessel wall. These can occur almost anywhere in the body but are particularly worrisome when they are present in the intracranial circulation. Due to the thinned, weakened wall, aneurysms are at risk of rupture, and in the United States, approximately one in 50 adults has an unruptured aneurysm.[62] Upon rupture, a subarachnoid hemorrhage (SAH) is said to have occurred, and this can be a severely debilitating or fatal event.[7] Approximately 30,000 people per year in the United States suffer SAH from a ruptured cerebral aneurysm.[62]

2.2.2 Current treatments and limitations

Current treatment of these arterial abnormalities involves isolation from the normal vasculature, and subsequent stabilization of the vulnerable portion of the artery. Isolation methods involve either surgical clipping or filling of the aneurysm with platinum coils, thereby preventing subsequent rupture. Surgical clipping, although highly effective for treating aneurysms,[44] involves invasive surgery in the form of a craniotomy. Additionally, for patients who are not viable candidates for surgery or whose aneurysm is in an area of the brain in which surgical access involves increased risk, surgery is either not an option or not the preferred option.[20,62,47] For these patients and many treatment centers, filling methods are the preferred treatment of aneurysms.[10, 11]

Filling methods involve endovascular navigation to the site of the aneurysm with the aid of fluoroscopy and intra arterial injection of iodinated contrast for vessel and aneurysm opacification. The aneurysm is then entered with a microcatheter and filled, reducing the pressure on the aneurysm wall and promoting clotting and healing within the aneurysm. For optimal treatment, the filling material would become incorporated into the aneurysm sac and isolated from the parent vessel by the formation of an endothelial cell layer and neointima proliferation across the neck of the aneurysm. This encasing of the filler and restoration of the parent vessel essentially isolates the aneurysm sac from blood flow, permanently stabilizing the weakened portion of the artery and preventing subsequent rupture.

Various materials are currently used for endovascular treatment of aneurysms. The most common is a soft, wound platinum coil. There are variations of this, including hydrogel- coated coils and polyglycolic polylactic acid coated or impregnated coils. These devices have proven to be clinically successful at filling small aneurysms (<4 mm in diameter).[68] However, these devices could be improved with respect to their biological activity [50] and safety of delivery.[26] Previously it has been demonstrated by Murayama et al.[63] and Szikora et al.[88], despite the relatively inert nature of platinum, these coils can be an ongoing source of inflammation within the aneurysm after implantation. The latter group reported that after multiple years, bare platinum coils are still not completely endothelialized at the aneurysm and parent artery interface; and therefore, the aneurysm is not optimally stabilized.[88] Coils have a tendency to have low filling volume as compared to total aneurysm volume[68,43,50] and may compact over time

[40], allowing aneurysm recanalization.[38,30,64,75, 89] This results in re-exposure of the aneurysm wall and subsequent rupture or re-rupture or can potentially result in formation of aneurysms adjacent to the original aneurysm.[40] Recanalization may require additional treatment, thus adding to the overall cost of treatment and increasing risk to the patient. Other efficacy issues surrounding these coils involve migration of coils into the parent vessel[57,91,] difficulty in treating wide necked aneurysms[20], and potential rupture of the aneurysm during coil delivery[26], often with devastating results.

Another material used for endovascular treatment of aneurysms is a liquid ethylene-vinyl copolymer (Onyx HD- 500, ev3, Irvine, CA). This entails placing a balloon catheter in the parent artery over the neck of the aneurysm, temporarily halting blood flow, while the polymer is injected into the aneurysm via a second microcatheter. The material polymerizes in situ. This technique does not guarantee a seal at the balloon–artery interface and can potentially lead to the occlusion of the parent artery or of distal arteries. Also, complications can arise if the material migrates into the parent artery.[24, 61]

2.2.3 Proposed treatment of intracranial aneurysms by shape memory polymer foams

Previously, polymer coils and foams have been proposed as an alternative filling material for treatment of cerebral aneurysms.[60, 64, 68, 39, 77] Polymer coated platinum coils have also been used for aneurysm treatment and have been shown to have favorable results in vivo. However, despite encouraging animal studies[50, 88], the benefits have not been borne out clinically, likely due to the relatively rapid biodegradability.[73, 21] It has also been shown that polyurethane foams have favorable biocompatibility in vivo for

larger aortic aneurysm animal models.[76] In this research, we focus on the biocompatibility of polyurethane-based shape memory polymer (SMP) foams as an aneurysm filling material. We sought to observe the tissue response after implantation of a SMP foam device in a swine aneurysm model. The swine vein pouch aneurysm model, reported by Guglielmi et al.[36, 71] in 1994, was chosen due to its relatively low cost, large arteries, and veins within the neck and similar fibrinolytic and coagulation system to humans. This model is also significant due to the similarity in the achievable dimensions of aneurysm sacs that can be made during the process of attaching the vein pouch to the artery. Similarities in dimension and blood interactions between the device and the in vivo environment within the swine model, facilitate extrapolation of the pathological data acquired from this study to the potential reaction to the implant within humans.[36]

SMPs are materials that have the ability to be made into a primary shape, and upon an increase in the bulk temperature of the material above its transition temperature, can be deformed and programmed into a temporary shape. Programming of these materials occurs when the temperature of the material is brought below its transition temperature while maintaining the deformation, for our device a crimped temporary shape would be desirable [Fig. 1(A)]. A device made from these materials would remain in this programmed shape until it encounters an additional stimulus that raises the material's temperature above its transition temperature, at which point it would recover to its primary shape, for our device an expanded shape to fill the aneurysm sac would be desirable [Fig. 1(B, C)]. This ability to change from one shape to another via the application of a stimulus has made these materials attractive for medical device

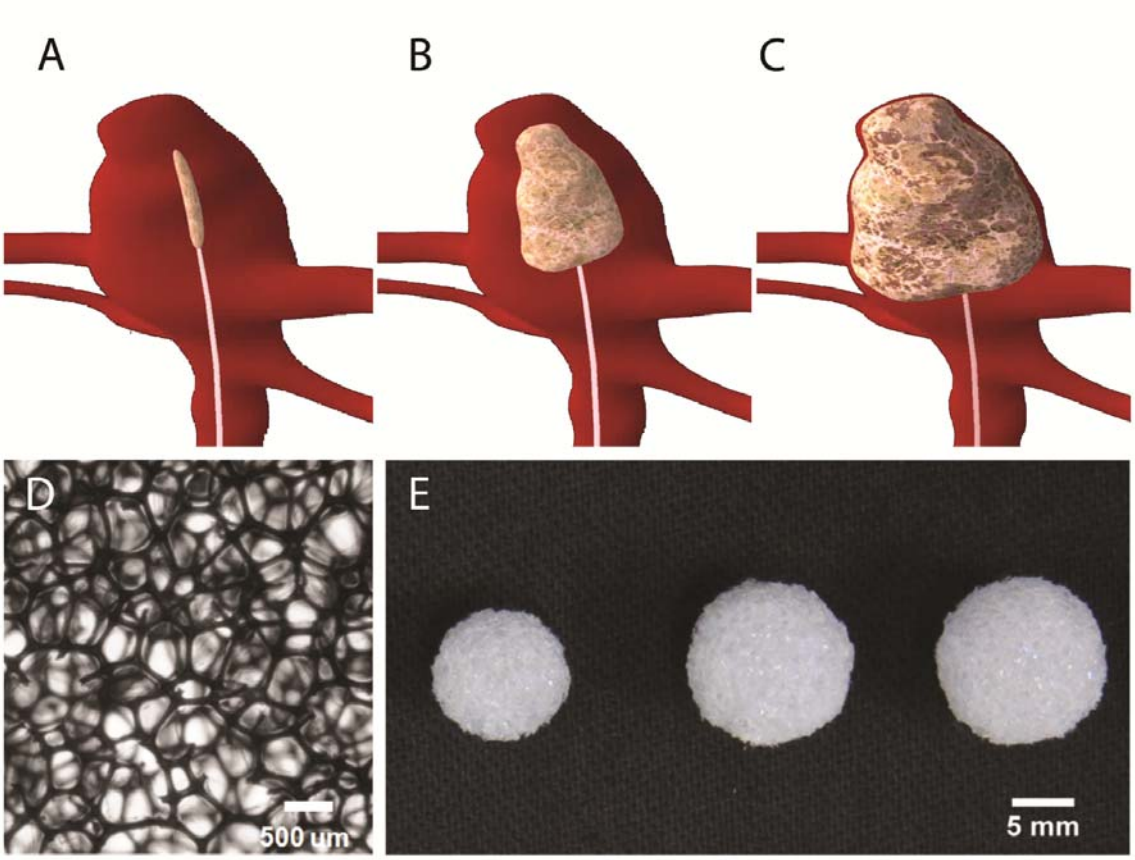

Figure 1: Proposed SMP foam devices for aneurysm filling. (a) crimped (temporary shape) SMP foam device delivered to the aneurysm via catheter, (b) intermediate image of the foam expanding within the aneurysm, as it recovers to its permanent shape via stimuli, (c) treated aneurysm with fully expanded foam, (d) a detail of the foam, scale bar is 500 mm, and (e) foam devices (scale bar is 5 mm).

development.[39] These polymers possess characteristics similar to other polymeric materials, including the ability to be molded or foamed into an open celled architecture.

Due to these favorable characteristics, we have developed polyurethane-based SMP foam for the treatment of intracranial aneurysms.[84] These low-density foams have an expansion force less than that which would pose risk of aneurysm rupture.[46] Both the foams and neat materials have demonstrated biocompatibility in vitro.[36, 84] Biocompatibility of the foams also has been demonstrated in vivo.[77] To further verify biocompatibility in vivo, we have implanted these foams in a porcine vein pouch aneurysm model[36] for 0 (<1 h contact with the circulation before sacrifice), 30, and 90 days. Gross evaluation, low-vacuum scanning electron microscopy (LV-SEM), and histology were performed to assess the tissue response induced by the implanted foams. Inflammation induced by the U.S. Food and Drug Administration approved silk and polypropylene sutures (7-0 Prolene™; Ethicon, San Angelo, TX) used to create the experimental aneurysms was also quantified for comparison.

2.3 Materials and methods

2.3.1 SMP fabrication

Filling devices were fabricated out of polyurethane SMP foams based on the H60 chemistry reported by Singhal et al.[84] An isocyanate prepolymer was prepared by mixing 38% of the total equivalents of hexamethylene diisocyanate (TCI America, Portland, OR) with the hydroxyl monomers N,N,N',N'-tetrakis(hydroxypropyl)ethylenediamine (HPED; Sigma-Aldrich, St. Louis, MO) and triethanolamine (Sigma- Aldrich) at which a

single phase was formed. This prepolymer was allowed to cure at room temperature for 2 days before foaming. At the point of foam fabrication, the balance of hydroxyl monomers to isocyanate monomers, had a net isocyanate index of 105. These monomers were then added to the prepolymer. Subsequent addition of catalysts, surfactants, water (chemical blowing agent), and Enovate (Honeywell, Morristown, NJ; Physical blowing agent), were added and mixed to achieve a homogeneous solution.[32] This solution was then put in the oven at 90 º C where it rose. The foam was then heat cured for 20 min in the oven, followed by a room temperature cure for at least 2 days.

2.3.2 Device fabrication

Spherical SMP foam devices were fabricated using a scalpel into dimensions ranging from 8 to 12 mm in diameter [Fig. 1(E)]. Varying sizes of SMP foam devices were fabricated to allow the vascular surgeon to select the appropriate size to fill the aneurysm.

2.3.3 Cleaning

Removal of surfactants and catalysts from the devices were achieved by cleaning via 0.1 M hydrochloric acid (BDH Chemicals, West Chester, PA) and detergent, Contrad VR 70 solution (Decon Laboratories, King of Prussia, PA). The devices were initially submerged in 0.1 N hydrochloric acid in glass vials, and placed in a sonication bath for 2 h. This step was followed by rinsing the samples in deionized water, and changing the acidic solution in the vial to an 80:20 vol percent, deionized water-ContradVR 70 solution. They were then placed into the sonication bath for 15 min. The samples were washed multiple times in deionized water to remove residual detergent (removal of

detergent was determined by an absence of bubble generation upon shaking). After the samples were free of detergent, they submerged in a vial containing deionized water and placed back into the sonication bath for another 15 min. These steps were repeated once more to ensure thorough cleaning and complete removal of residual mobile species. The cleaned samples were then dried in an oven over night, approximately 12 hours, at 50 C under vacuum. The dried samples were visually examined under magnification for any deformation or presence of loose struts on the surface, and a scalpel was used to manually trim loose struts and to restore dimensions and spherical shape.

2.3.4 Sterilization

Each device was individually sealed in a sterilization pouch and sterilized by ethylene oxide (EtO), and allowed to de-gas for 48 h before implantation.

2.3.5 Porcine animal model

All animal experiments were conducted in accordance with policies set by the Texas A&M University Institutional Animal Care and Use Committee, and met all federal requirements, as defined in the Animal Welfare Act, the Public Health Service Policy, and the Humane Care and Use of Laboratory Animals. Additionally, NIH guidelines (or for non- U.S. residents similar national regulations) for the care and use of laboratory animals (NIH Publication #85-23 Rev. 1985) were observed. A porcine vein pouch saccular sidewall aneurysm model was utilized in this study.[36]

Saccular sidewall aneurysms were created in 3 to 4 month old swine weighing approximately 30 to 40 kg. Anesthesia was induced via intramuscular injection of ketamine, xylazine, and acepromazine (20, 2, and 0.2 mg/kg, respectively) with

intubation and use of isoflurane for maintenance of anesthesia. Using sterile technique a 10 cm incision was made in the midline of neck. After reflecting the sternocleidomastoid muscle medially, a 4-cm long segment of the external jugular vein was isolated and excised after a ligature is placed at each end of the segment. This segment of the vein was then divided transversely, yielding two 2 cm open-ended pouches. The carotid arteries were then subsequently exposed and cleaned of adventitia. Vascular clamps were placed at each end of the area of interest on the artery to provide temporary vessel occlusion. A 7 mm arteriotomy was then made, and end-to-side anastomosis of the venous pouch to the carotid artery will be performed using 7-0 Prolene™ (Ethicon) sutures. An aneurysm between 8 and 10 mm in diameter was then created on each carotid artery, which resulted in two aneurysms per animal. After confirmation of hemostasis, the subcutaneous tissues were closed.

Angiography was performed to visualize the integrity of the aneurysm and to assess for any premature thrombosis. An SMP device was soaked in 37 C saline and then placed in each aneurysm by opening the top suture and reclosing after proper placement had been achieved. Aneurysm filling and integrity were assessed via angiography after implantation of the SMP devices. The implanted devices remained in place for 0 (<1 h exposure to blood before euthanization), 30, or 90 days. At the end of each implantation time point the animals were sacrificed. Each of the aneurysms and their parent vessels were isolated, harvested, and preserved with formalin for gross and histological evaluation.

2.3.6 Gross evaluation of healing

The parent vessels were bisected parallel to the direction of blood flow to allow visualization of the aneurysm neck. Each aneurysm was observed at the main artery and graft interface for endothelialization of the lesion *en face*.

2.3.7 Microscopic evaluation of healing

LV-SEM imaging was used to determine the degree of endothelialization at the parent vessel and device interface (i.e., across the neck of the aneurysm). Histology was used to determine the amount of healing and inflammation at the dome of the aneurysm. Multiple stains including hematoxylin and eosin (H&E), Masson's trichrome, and Mallory's phosphotunsic acid hematoxylin (PTAH) were used.

2.3.8 LV-SEM: endothelialization

A major component of aneurysm stabilization and healing is endothelialization at the device and parent vessel interface and restoration of the intima of the parent artery across the aneurysm neck. Presence of neointima and progression of the covering were assessed via LV-SEM at each time point.

2.3.9 Histopathology

Multiple stains were used to characterize the healing in and around the aneurysms and to evaluate the degree of inflammation present. The pathology slides were scanned by an AperioVR ScanScopeVR slide scanner, and the resulting images were evaluated by ImageScopeVR (Aperio Technologies, Vista, CA), a pathology slide viewing software. Magnifications reported in histology figures are based on these scanned images.

H&E is a microatomic stain that provides information about the general pathology of a tissue and was used as a general stain to evaluate inflammation and neovascularization. The nuclei of cells are stained blue/black by hematoxylin.[14] Eosin is an acid dye that stains cytoplasm various shades of red, pink, and orange.[14]

Masson's trichrome is one of two connective tissue stains that were used to evaluate elastin and fibrin. With this stain, collagen and reticular fibers appear blue/green, cytoplasm and red blood cells red, and the nuclei black/gray.[14, 74] Mallory's PTAH is the second connective tissue stain used. This stain was used to determine the amount of residual fibrin at the aneurysm dome. PTAH is also used to determine the amount of collagen and elastin that has been deposited. This stain colors nuclei of cells a deep blue, fibrin fibers a lighter blue, collagen reddish, and coarse elastin fibers bluish.[14]

2.4 Results

2.4.1 Aneurysm embolization

Based on fluoroscopic imaging performed during implantation and LV-SEM and histological evaluation at 0, 30, and 90 days after implantation, all aneurysms showed complete filling with SMP foam at all time points.

2.4.2 Gross evaluation of healing

Gross evaluation of aneurysm healing is summarized in column A and B of Figure 2. For 0 day, the surgical site was clean as expected, and the polymer had visible thrombus throughout the matrix where it had been in contact with blood flow. For the 30-day implants, the outer surface was composed of a white to slightly opaque dense connective tissue, with tan to golden brown patches. In Figure 2(B.30), the carotid artery

was bisected to expose the en face view of the ostium (neck) of the aneurysm sac. The surface of the ostium was white, glistening and appeared to cover the aneurysm neck. However, there appeared to be focal areas where polymer was exposed. For implants that had remained in vivo for 90 days, the external surface of the aneurysms showed multifocal adhesions of dense white connective tissue with tan to golden brown coloration. The carotid artery was bisected to visualize the ostium and it appeared to be white, glistening, intact and with no evidence of exposed polymer Figure 2(B.90).

2.4.3 Microscopic evaluation of healing

2.4.3.1 LV-SEM: endothelialization

Figure 2, columns C and D correspond to the middle lower edge of and middle of the en face regions respectively, and summarize the endothelialization and topography at the foam/parent artery interface with subsequent rows indicating the results of the three time points: 0, 30, and 90 days. At 0 days the LV-SEM micrographs indicate patchy aggregates of fibrin-enmeshed red blood cells on the surface of the polymer implant. After 30 days there was presence of a discontinuous endothelial layer over the polymer struts. En face images of the ostium at 90 days show an endothelial cell layer comprised of cobblestone patterned and spindle-shaped endothelial cells. These endothelial cells aligned parallel with the direction of blood flow in the parent vessel. The first row in Table 1 summarizes the topographical LV-SEM evaluation of all aneurysms. After 90 days, all of the aneurysms were completely covered by endothelial cells.

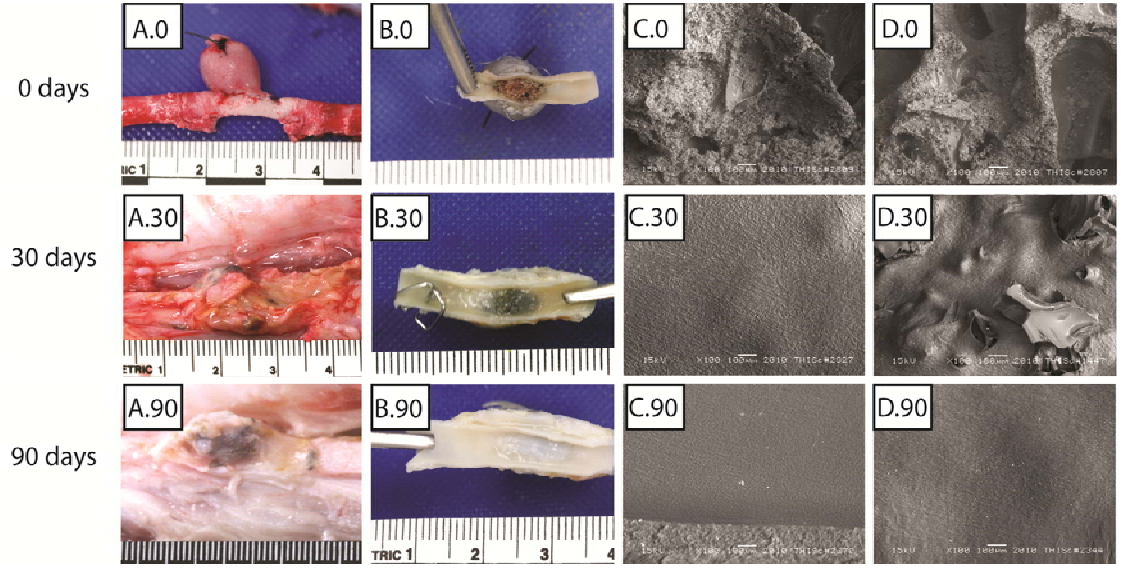

Figure 2: Gross and microscopic figure. Gross and microscopic evaluation of the healing response of the implanted SMP foams: (A.0) 30-min implant of SMP foam in vein pouch model. (B.0) en face view of the aneurysm artery interface after 30 min in vivo. (C.0) LV-SEM shows partial protrusion of foam material into the lumen. (D.0) the porous surface in contact with the vessel lumen has patchy aggregates of fibrin enmeshed erythrocytes attached to the struts of the foam. (A.30) dissected aneurysm in situ after 30 days of implantation. The outer surface of the aneurysm was composed of dense white to slightly opaque connective tissue with patchy tan to golden brown discoloration. (B.30) excised aneurysm with two clips that mark the cranial end. In patchy areas this outer capsule was adherent to adjacent skeletal muscle. The left carotid artery was bisected parallel with the long axis to visualize the ostium of the left aneurysm sac. The cranial end was labeled with two clips. (C.30) most of the ostium shows an imprint of polymer foam beneath the endothelial covering. (D.30) after 30 days of implantation, there is a focal area of disruption and polymer exposed to the lumen. (A.90) the right carotid in situ showed an outer surface of artery and aneurysm with multifocal adhesions of dense white connective tissue. (B.90) the right carotid artery was bisected parallel with the long-axis to visualize the ostium of the left aneurysm sac. The surface covering the ostium was white, glistening and appeared intact. (C.90) the bisected section of artery and en face ostium of aneurysm sac shows an endothelial cell covered surface. (D.90) evidence of proliferating mural thrombosis is not present. The endothelial cell morphology across the ostium is mostly spindle-shaped and parallel with the long axis.

Table 1: Four pathological metrics of healing. (1) condition of endothelium covering, (2) residual thrombus, (3) connective tissue, and (4) lumen narrowing - (1) for characterization of endothelium covering, the ideal condition is defined as 100% endothelium coverage of the aneurysm ostium (score=0). The following conditions are the intermediate gradations between ideal and less than ideal listed in descending order: greater than 95% endothelium coverage (score=1), 90 to 95% endothelium coverage (score=2), and 80 to 89% endothelium coverage (score=3). The less than ideal condition is defined as less than 80% coverage (score=4) determined by LV-SEM. (2) For characterization of thrombus the ideal condition is defined as 0% of SMP foam surface covered by thrombus (score=0). The following conditions are the intermediate gradations between ideal and less than ideal listed in descending order: less than 1% covered by thrombus (score=1), 1 to 4% covered by thrombus (score=2), and 5 to 10% covered by thrombus (score=3). Less than ideal was defined as greater than 10% covered by thrombus (score=4) determined by histology. (3) For characterization of connective tissue the ideal condition is defined as the aneurysm being 100% composed of connective tissue (score=0). The following conditions are the intermediate gradations between ideal and less than ideal listed in descending order: 75% composed of connective tissue (score=1), 50% composed of connective tissue (score=2), and 25% composed of connective tissue (score=3). Less than ideal was defined as 0% (score=4) composed of connective tissue determined by histology. (4) For characterization of lumen narrowing the ideal was defined as a lack of lumen narrowing (score=0). Intermediate gradations between ideal and less than ideal listed in descending order: less than 5% lumen narrowing (score=1), 5 to 20% lumen narrowing (score=2), and 20 to 35% lumen narrowing (score=3). Less than ideal was defined as greater than 35% lumen narrowing (score=4) determined by LV-SEM and histology.

	% of aneurysms scored, 30 days, n=7					% of aneurysms scored, 30 days, n=7				
1. Endothelium covering	0%	25%	50%	25%	0%	0%	0%	0%	0%	100%
2. Residual thrombus	0%	0%	0%	43%	57%	0%	0%	0%	0%	100%
3. Connective tissue	0%	57%	14%	29%	0%	0%	0%	0%	0%	100%
4. Lumen narrowing	0%	0%	29%	70%	0%	0%	0%	0%	0%	100%
	less than ideal →				Ideal	less than ideal →				Ideal

Row 2 of Table 1 summarizes the data regarding mural thrombus at the base of the aneurysms evaluated by LVSEM imaging. There was less than 1% of the surface area of the base of the aneurysm covered with thrombus after 30 days, and no thrombus remaining after 90 days.

2.4.3.2 Histopathology. Connective tissue: Aneurysm composition

Row 3 of Table 1 summarizes the composition of the connective tissue of each aneurysm at the three time points, which includes multinucleated giant cells, macrophages, lymphocytes, and focal aggregates of neutrophils. The amount of connective tissues was determined by pathology, in which a cross-section of the dome was evaluated. It was shown that at 0 days there were no connective tissue present [Fig. 3(A.0,B.0)]. At 30 days there were connective tissues present within the aneurysm dome between 25 and 75% observed throughout all aneurysms [Fig. 3(A.30,B.30,C.30)]. At 90 days there was 75% connective tissue present throughout the aneurysms [Fig. 3(A.90,B.90,C.90)].

2.4.3.3 Remnant fibrin present in aneurysm

Supporting Information Table S1 summarizes the amount of remnant fibrin, or the amount of fibrin that had not been resorbed or fully degraded, throughout the aneurysm domes at each time point observed via pathology. At the 0 day time point (less than 1 h exposure to blood before euthanization), there was between 6 and 10 % fibrin present. After 30 days of implantation, one of seven aneurysms evaluated was composed of more than 50 % fibrin, three of seven between 11 and 25 % fibrin, and the remaining three had 6–10 % residual fibrin [Fig. 4(A.30,B.30,C.30)]. After 90 days, there was one

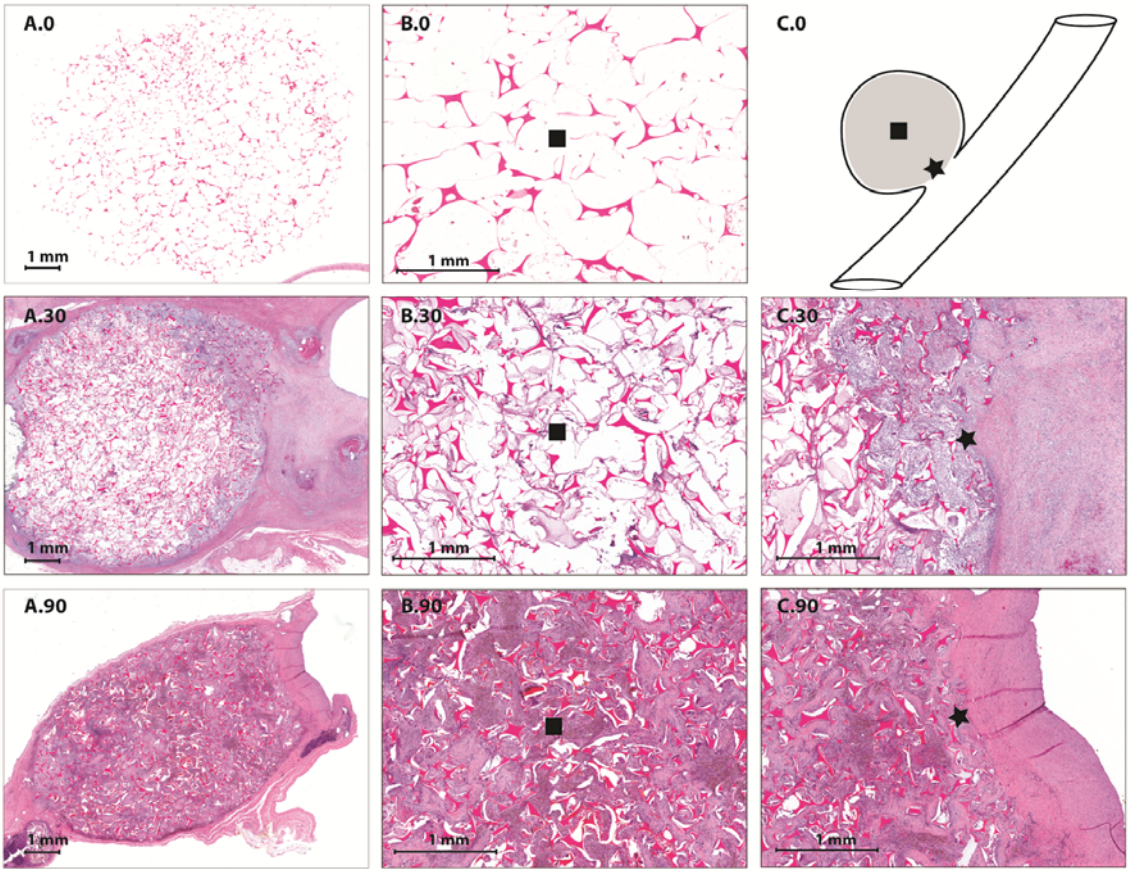

Figure 3: H&E figure. H&E staining (1x and 4x magnification): (A.0) 1x H&E staining of a bisected aneurysm after 30 min of implantation, (B.0) 4x H&E staining of the central core of the bisected aneurysm after 30 min of implantation, (C.0) orientation of SMP foam implant within the aneurysm dome and parent artery, (A.30) 1x H&E staining of a bisected aneurysm after 30 days of implantation, (B.30) 4x H&E staining of the central core of the bisected aneurysm after 30 days of implantation, (C.30) 4x H&E staining of foam and parent artery interface after 30 days of implantation, (A.90) 1x H&E staining of a bisected aneurysm after 30 days of implantation, (B.90) 4x H&E staining of the central core of the bisected aneurysm after 90 days of implantation, and (C.90) 4x H&E staining of foam and parent artery interface after 90 days of implantation.

aneurysm composed of between 11 and 25% fibrin, with the remaining five being composed of less than 5% fibrin [Fig. 4(A.90,B.90,C.90)].

2.4.3.4 Connective tissue within the aneurysm

The first three rows of Table 2 are a summary of the infiltration of dense cellular connective tissue within the aneurysms; it is expressed in the form of a percentage of infiltration of the aneurysms at each time point throughout the volume of the dome. There was no cellular infiltration at 0 days. At 30 days, there was greater than 75% cellular infiltration throughout the aneurysm volume [Fig. 5(A.30,B.30,C.30)]. At 90 days, there was greater than 85% cellular infiltration in all aneurysms [Fig. 5(A.90,B.90,C.90)].

2.4.3.5 Inflammation within and around the aneurysm

The second three rows of Table 2 are a summary of the inflammatory response elicited by the foam within the dome of the aneurysms as measured by the average number of inflammatory cells present per area evaluated at 250x or 0.025 mm^2. Inflammation induced by the presence of foam was evaluated at three locations throughout the volume which included the anastomosis, central core and the apex of the aneurysm. For all areas evaluated at 0 days, there was no significant inflammation due to the short in vivo exposure time. At 30 days, most aneurysms exhibited a mild inflammation score for all three areas, which consisted of between 5 and 10% inflammatory cell infiltrates, which included approximately two to three macrophages or lymphocytes or one neutrophil per area evaluated. At 90 days, most aneurysms exhibited a minimal inflammation score for all three areas, which consisted of between less than

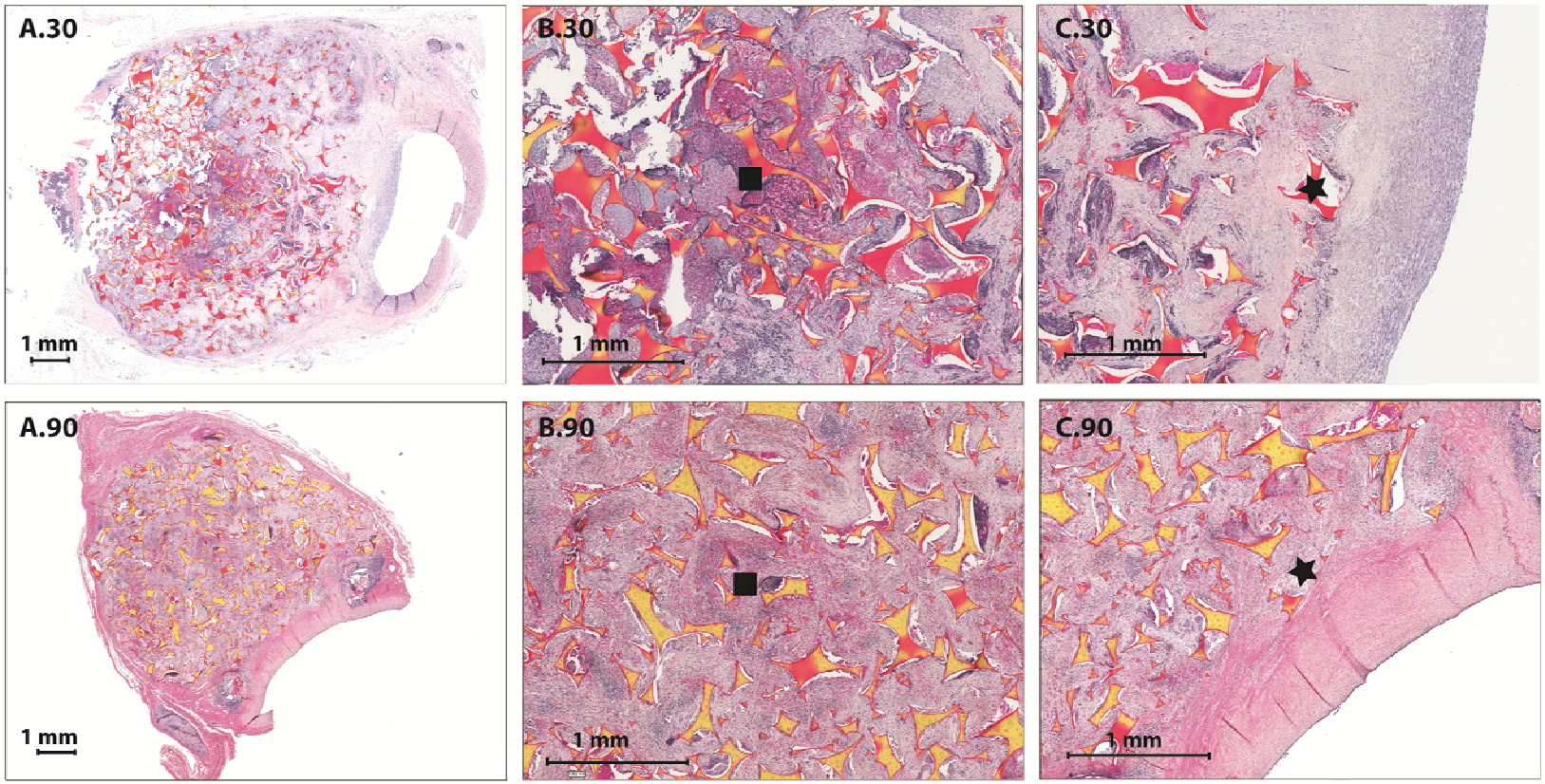

Figure 4: PTAH figure. PTAH staining (1x and 4x magnification): (A.30) 1x PTAH staining of a bisected aneurysm after 30 days of implantation, (B.30) 4x PTAH staining of the central core of the bisected aneurysm after 30 days of implantation, (C.30) 4x PTAH staining of foam and parent artery interface after 30 days of implantation, (A.90) 1x PTAH staining of a bisected aneurysm after 90 days of implantation, (B.90) 4x PTAH staining of the central core of the bisected aneurysm after 90 min of implantation, and (C.90) 4x PTAH staining of foam and parent artery interface after 90 days of implantation.

Table 2: Two metrics of aneurysm composition. (1) percentage of complete infiltration with dense, cellular connective tissue and (2) the amount of inflammatory cells present determined from histology and location within the aneurysm dome (anastomosis interface; inner core; apex) - (1) for dense cellular connective tissue, ideal condition was defined as complete infiltration with dense, cellular connective tissue (score=0). The following conditions are the intermediate gradations between ideal and less than ideal listed in descending order: greater than 95% of the inner core that has been infiltrated with dense cellular connective tissue (score=1), 86 to 95% of the inner core that has been infiltrated with dense cellular connective tissue (score=2), 75 to 85% of the inner core that has been infiltrated with dense cellular connective tissue (score=3). The less than ideal case was defined as less than 75% of the inner core had been infiltrated with dense cellular connective tissue (score=4). (2) For inflammatory cells, ideal condition was defined as a lack of inflammation (score=0). The following conditions are the intermediate gradations between ideal and less than ideal listed in descending order: <less than 5% of the region is infiltrated by inflammatory cells (1 macrophage/lymphocyte per 0.025 mm2) (score=1), between 5 and 10% of the region is infiltrated by inflammatory cells (2–3 macrophages/lymphocytes or 1 neutrophil per 0.025 mm2; score=2), between 10 and 25% of the region is infiltrated by inflammatory cells (4–5 macrophages/lymphocytes or 2 neutrophils per 0.025 mm2; score=3). The less than ideal case was defined as greater than 25% of the region is infiltrated by inflammatory cells (greater than 6 macrophages/lymphocytes or greater than 3 neutrophils per 0.025 mm2; score=4.

	% of aneurysms scored, 30 days, n=7					% of aneurysms scored, 30 days, n=7				
1. Dense cellular connective tissue										
Anastomosis	0%	25%	50%	25%	0%	0%	0%	0%	0%	100%
Inner core	0%	0%	0%	43%	57%	0%	0%	0%	0%	100%
Apex	0%	57%	14%	29%	0%	0%	0%	0%	0%	100%
2. Inflammatory cells										
Anastomosis	0%	25%	50%	25%	0%	0%	0%	0%	0%	100%
Inner core	0%	0%	0%	43%	57%	0%	0%	0%	0%	100%
Apex	0%	57%	14%	29%	0%	0%	0%	0%	0%	100%
	less than ideal →				Ideal	less than ideal →				Ideal

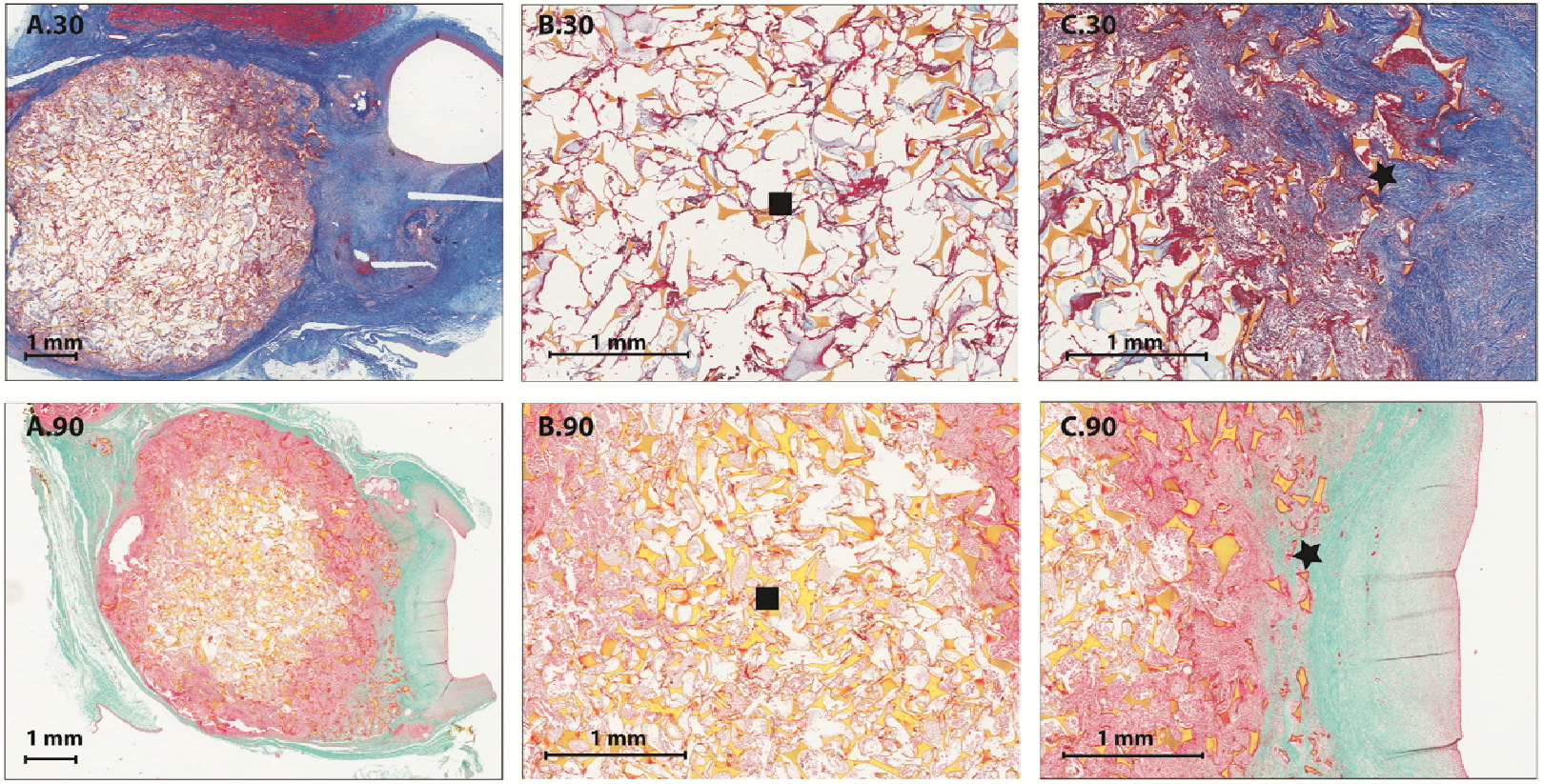

Figure 5: Trichrome figure. Trichrome staining (1x and 4x magnification): (A.30) 1x trichrome staining of a bisected aneurysm after 30 days of implantation, (B.30) 4x trichrome staining of the central core of the bisected aneurysm after 30 days of implantation, (C.30) 4x trichrome staining of foam and parent artery interface after 30 days of implantation, (A.90) 1x trichrome staining of a bisected aneurysm after 30 days of implantation, (B.90) 4x trichrome staining of the central core of the bisected aneurysm after 90 days of implantation, and (C.90) 4x trichrome staining of foam and parent artery interface after 90 days of implantation.

5% inflammatory cell infiltrates, which included approximately one or less macrophage or lymphocytes or one neutrophil per area evaluated.

Figure 6 is a summary of not only the inflammatory response elicited by the foam, but also the inflammation at the suture sites at the periphery of the aneurysms. For the foam, at 0 days the average score for all areas evaluated was approximately 0.5, which corresponded to zero to two leukocytes per area evaluated. At 30 days the foam had an average score of 2.5, which corresponded to three to eight leukocytes per area evaluated. At 90 days the foam had an average score of 3, which corresponded to five to eight leukocytes per area evaluated. For all time points, and all areas observed, the foam elicited an inflammation response, which was slightly higher on the perimeter than within the core.

Suture materials were also evaluated for their inflammation response. At 0 day, polypropylene suture material was the only suture material evaluated do to a lack of silk incorporated into the tissue during histology, and there were three to eight leukocytes per area evaluated. At 30 days, polypropylene suture material induced inflammation reflected by presence of four to eight leukocytes per area evaluated. Silk suture at 30 days elicited eight to 11 leukocytes per area evaluated. At 90 days, there were five to 11 leukocytes per area evaluated for polypropylene sutures and eight to 11 leukocytes per area evaluated for silk. Additionally, focal mineralization was observed in relation to the polypropylene sutures after 30 days and around the silk sutures after 90 days.

Visual comparison of polymer and suture material inflammatory response can be seen in Figure 7(A.30,B.30,C.30,D.30, A.90,B.90,C.90,D.90) for 30- and 90-day time

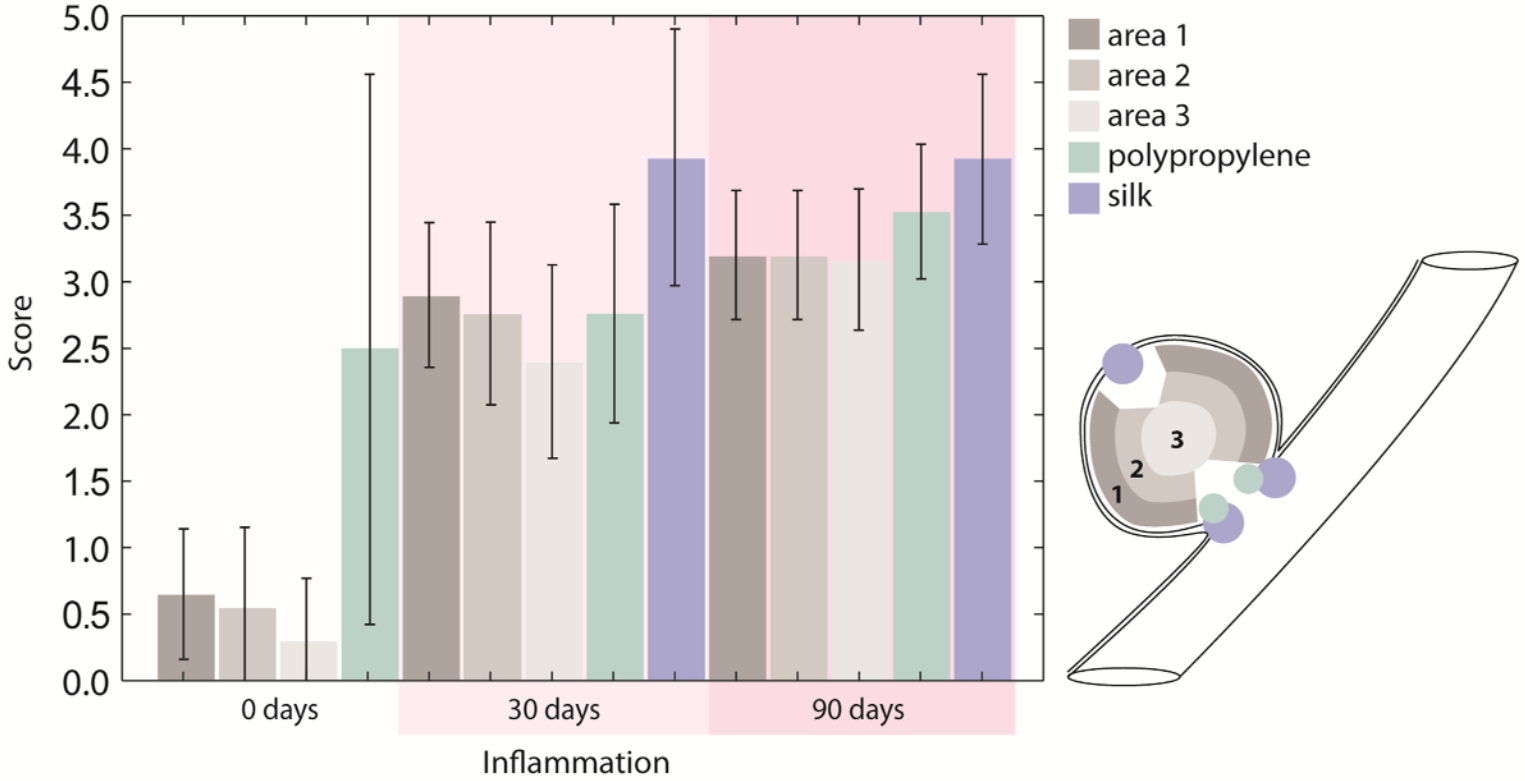

Figure 6: Inflammation figure. Average pathology scoring of inflammation (250x magnification, or 0.025 mm^2, error bars indicate standard deviation): indicated by the amount of leukocytes present throughout the aneurysm dome at 0, 30, and 90 days in areas 1 through 3 and a comparison of the amount of inflammation elicited by suture materials used to create the aneurysm model. Area 1 represents the perimeter of the aneurysm excluding the areas proximal to sutures. Area 2 represents the area between the periphery and the core. Area 3 represents the core, or middle of the aneurysm dome. A score of 0 indicated a lack of leukocytes present in the area evaluated. A score of 1 indicated minimal or one to two leukocytes per area evaluated. A score of 2 indicated three to four leukocytes per area evaluated. A score of 3 indicated five to eight leukocytes per area evaluated. A score of 4 indicated eight to 11 leukocytes per area evaluated. A score of 5 indicated more than 12 leukocytes per area evaluated. Silk was not visible in the 0 day time point.

points. Inflammation around the suture material was evident [Fig. 7(C.30,D.30,C.90,D.90)], reflected by an abundance of multinucleated giant cells when compared to the foam [Fig. 7(B.30,B.90)].

2.4.3.6 Healing throughout the aneurysm dome based on neovascularization

Figure 8 summarizes the amount neovascularization throughout the aneurysm domes by quantifying the amount of neovascularization at three locations from the periphery to the core. It was shown that at 0 days there was no neovascularization, at 30 days there was approximately one neovascular bud per area evaluated (Fig. 8), and at 90 days there was approximately two neovascular buds per area evaluated.

2.4.4 Neointima proliferation at the base of the aneurysms

The fourth row of Table 1 summarizes the amount of neointima proliferation at the neck of the aneurysm as determined via LV-SEM and histology. At 0 day, there is no narrowing of the parent vessel lumen due to a lack of neointima formation [Fig. 2(B.0)]. There was approximately 5% narrowing of the parent vessel at 30 days, and for two aneurysms, there was between 5 and 20% narrowing [Fig. 2(B.30)]. At 90 days, there was <5% narrowing of the parent vessel for all aneurysms [Fig. 2(B.90)].

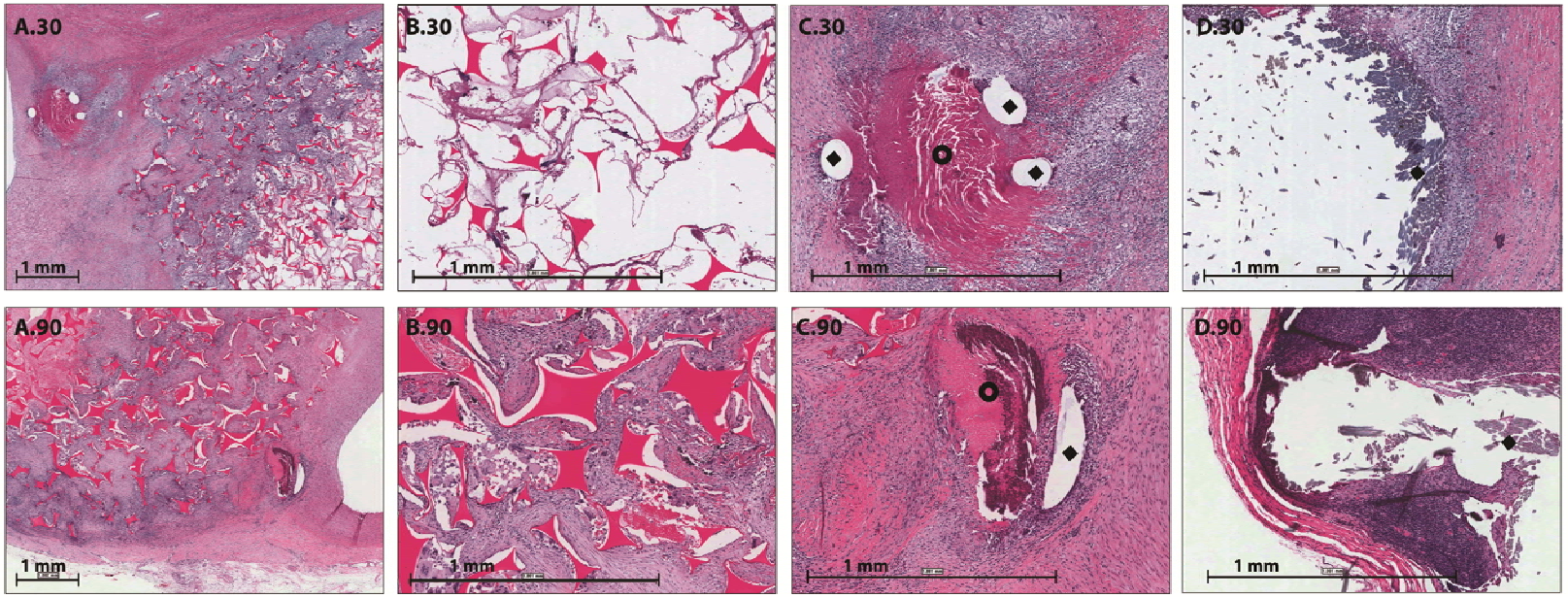

Figure 7: Suture interaction figure. Suture interaction in vivo (2x and 8x magnification): (A.30) 2x H&E staining of a bisected aneurysm exhibiting the foam and suture interaction after 30 days of implantation, (B.30) 8x H&E staining of a middle section of a bisected aneurysm after 30 days of implantation showing the foam-body interaction, (C.30) 8x H&E staining of suture interaction after 30 days of implantation. Diamond indicates polypropylene suture and doughnut indicates focal mineralization adjacent to the polypropylene suture material. (D.30) 8x H&E staining of suture interaction after 30 days of implantation. Diamond indicates silk suture (A.90) 2x H&E staining of a bisected aneurysm after 90 days of implantation, (B.90) 8x H&E staining of a middle section of a bisected aneurysm after 90 days of implantation showing the foam–body interaction, (C.90) 8x H&E staining of suture interaction after 90 days of implantation. Diamond indicates polypropylene suture and doughnut indicates focal mineralization adjacent to the polypropylene suture material, and (D.90) 8x H&E staining of suture interaction after 90 days of implantation. Diamond indicates silk suture.

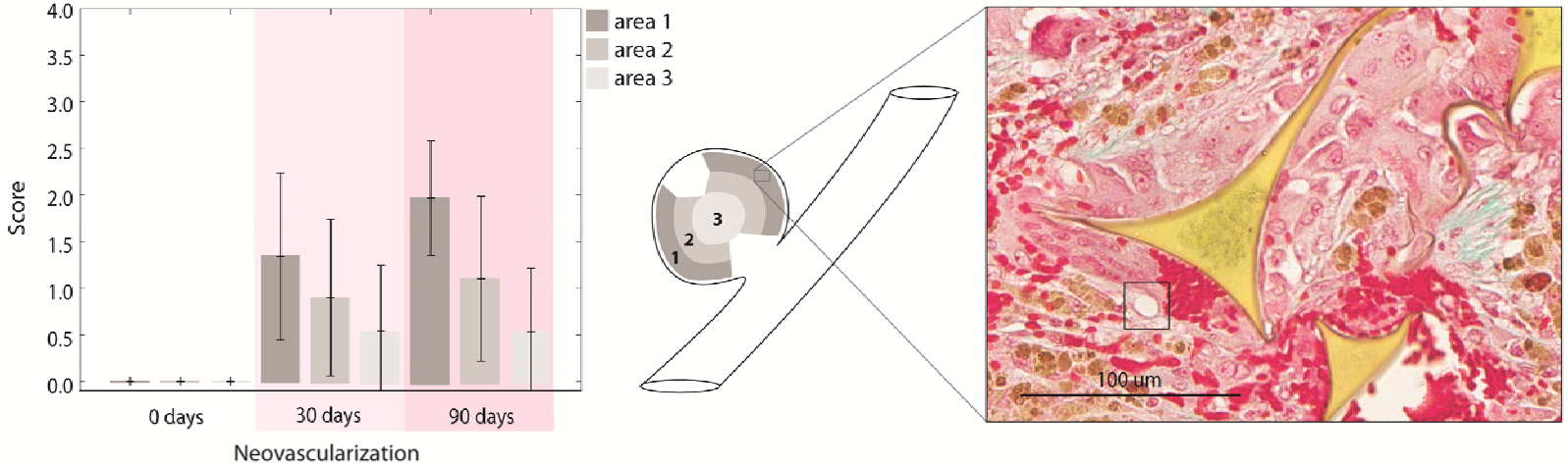

Figure 8: Neovascular bud figure. Average pathology scoring of neovascularization throughout the aneurysm dome at 0, 30, and 90 days in areas 1 through 3 (250x magnification, or 0.025 mm^2, error bars indicate standard deviation): area 1 represents the perimeter of the aneurysm excluding the areas proximal to sutures. Area 2 represents the area between the periphery and the core. Area 3 represents the core, or middle of the aneurysm dome. A score of 0 indicated no neovascular buds present per area evaluated. A score of 1 indicated minimal or one neovascular bud per area evaluated. A score of 2 indicated two to three neovascular buds per area evaluated. A score of 3 indicated four to five neovascular buds per area evaluated. A score of 4 indicated more than five neovascular buds per area evaluated. Black square indicates neovascular bud.

2.5 Discussion

The goals of this research study were twofold: (1) to assess whether polyurethane-based SMP foam is biocompatible in vivo when implanted into a porcine vein pouch aneurysm model and (2) to demonstrate the feasibility of these materials as aneurysm filling devices. These devices were evaluated at three time points, 0, 30, and 90 days. LV-SEM imaging and histology were performed for all aneurysms. Histology verified that the SMP foams are biocompatible and effective at providing a biological scaffold which seems to enhance the healing response as exhibited by presence of a predominantly connective tissue substrate within the foam at 90 days. Healing was also evidenced by neointima formation across the aneurysm neck, permanently excluding the aneurysm from the parent vessel, without compromise of the parent vessel lumen.

We have also shown using an internal control that the SMP foam has a reduced inflammatory response when compared to conventional suture materials (monofilament polypropylene and braided silk). Karaca et al.[52] showed that silk and polypropylene suture promote granulomatous inflammatory response with varying severity. Inflammation noted around these suture materials consisted of a "purulent core surrounded by inflammatory cells and an outer fibrous encapsulation."[52] These results are similar to those of Chu et al.,[19] who noted that in less than 1 month silk and polypropylene elicit a marked and moderate reaction, respectively. When implanted for up to 24 months, silk and polypropylene, such as were used during creation of the aneurysms in the model used for this study, elicit moderate and slight reactions respectively, similar to the findings at 90 days in this study.[19] The fibrous encapsulation

of the foreign material is the hallmark of the end of inflammation induced by a material.[19] This encapsulation isolates the device/material from the surrounding tissues.[19]

When an implanted material induces a minimal or mild inflammatory response the connective tissue capsule is smaller and may even be nonexistent.[19] When directly comparing the SMP foam to the braided silk and to some extent the polypropylene sutures, the perimeter of biological tissues surrounding our SMP foam shows a thinner capsule and showed less inflammation than the suture used in this procedure as an internal control (Fig. 7). The SMP foam induces less chronic-active inflammatory response when compared to silk. Whether or not an implant causes a sustained inflammatory response is dependent upon the host response to the implanted material.[19] For implanted devices, the physical and chemical properties of the device should ideally cause a host inflammatory response that is minimal to mild and of short duration, an indicator of biocompatibility. A chronic or chronic-active inflammatory reaction can lead to impairment of the function of the tissue in which the implant is located.[19] The mild inflammatory response seen with the SMP foam in this study leads to an earlier transition toward healing, evident by the laying down of collagen and elastin throughout the aneurysm and a reduced population of multinucleated giant cells. Transition to healing was also present in the areas where sutures were used, but as compared to the SMP foam, there was a greater cellular inflammatory response.

Granulation tissue (early stage of healing) was present throughout the volume of the SMP foam-filled aneurysm dome. In general, granulation tissue was comprised of collagen, neovascular buds, a small number of macrophages and/or multinucleated giant

cells, and, to a lesser extent, eosinophils and neutrophils,[19] which was seen with these implants. In the later stages of healing, type III collagen is predominant.[19] This fibrous connective tissue substrate with minimal inflammatory cells is the final transition to the host/biomaterial stable state.[19]

Neovascular bud infiltration throughout the SMP foam was also evaluated. The presence of neovascularization indicates an active healing process, or the intermediate step before full encapsulation. In the current study, by 90 days there was an increased number of neovascular buds. Similar results were reported after 6 months in a study of polyglycolic acid/lactic acid copolymer coated platinum aneurysm coils (Matrix coils, Boston Scientific Neurovascular, Fremont, CA; now Stryker Neurovascular).[88] These results suggested that polymers could promote the healing process to a greater degree than bare metal coils when implanted in aneurysms.[88] Another study conducted by Kipshidze et al.,[54] compared a cylindrical reticulated polycarbonate polyurethane based, non-SMP foam (vascular occlusion device; Biomerix, New York, NY), to stainless steel metal coils. They showed that intravascular implantation of the foams resulted in faster and safer aneurysm occlusion.[54] Both of these previous studies support the use of polymers to promote healing, achieve occlusion, and stabilize aneurysms in vivo. A head-to-head comparison of bare platinum coils to these polyurethane SMP foams within an aneurysm model would be required in order to make conclusive statements about biocompatibility, which would include aneurysm occlusion, healing and stabilization.

Compaction of coils within a treated aneurysm is a well documented phenomenon, particularly in the setting of larger aneurysms and lower packing density,

and this compaction results in recanalization of the aneurysm, with varying degrees of filling and potential risk of rupture. There was no visual compaction of foam throughout our study, and within 90 days, neointima formed over the neck of the aneurysm, excluding the aneurysm from the circulation. There was also no gross or microscopic evidence of active thrombogenesis at the endothelialized neck, which implies that the foam is stable and not affected by blood flow. Previously, it has been proposed that aneurysm recurrence[40] is facilitated by compaction of the coils4 within the aneurysm sac due to the constant impingement by arterial blood flow and/or the lack of complete filling during treatment.[68] Compaction of metal coils occurs due to the fact that there has not been neointima formation over the coils at the aneurysm neck or tissue ingrowth from the dome and periphery of the aneurysm; this lack of stabilization and healing is most likely due to the lack of biological activity of the platinum coils.

In conclusion, we achieved both goals introduced in the beginning of the discussion. First, we demonstrated that polyurethane-based SMP foam is a biocompatible aneurysm filling device when implanted into a porcine vein pouch aneurysm model. Second, these initial pathological results demonstrate the feasibility of these materials as aneurysm filling devices for clinical application. This was concluded based on their biocompatibility demonstrated at 90-day pathological results and complete endothelial cap at the base of the aneurysm. Additionally, the ability of these materials to be compressed to dimensions that allow them to be delivered via catheter also demonstrated feasibility as being developed into a clinical aneurysm filling device. While speculative, we believe that aneurysm filling by polyurethane based SMP foams

have the potential to be a superior endovascular aneurysm treatment when compared to bare metal coils based on the positive pathological results demonstrated by this study.

3. OPACIFICATION OF SHAPE MEMORY POLYMER FOAM DESIGNED FOR TREATMENT OF INTRACRANIAL ANEURYSMS*

3.1 Overview

Shape memory polymer (SMP) foam possesses structural and mechanical characteristics that make them very promising as an alternative treatment for intracranial aneurysms. Our SMP foams have low densities, with porosities as high as 98.8%; favorable for catheter delivery and aneurysm filling, but unfavorable for attenuating x-rays. This lack of contrast impedes the progression of this material becoming a viable medical device. This paper reports on increasing radio-opacity by incorporating a high-Z element, tungsten particulate filler to attenuate x-rays, while conserving similar physical properties of the original non-opacified SMP foams. The minimal amount of tungsten for visibility was determined and subsequently incorporated into SMP foams, which were then fabricated into samples of increasing thicknesses. These samples were imaged through a pig's skull to demonstrate radio-opacity in situ. Quantification of the increase in image contrast was performed via image processing methods and standard curves were made for varying concentrations of tungsten doped solid and foam SMP. 4% by volume loading of tungsten incorporated into our SMP foams has proven to be an

---

* Reprinted with permission from "Opacification of shape memory polymer foam designed for treatment of intracranial aneurysms" by Jennifer N. Rodriguez, Ya-Jen Yu, Matthew W. Miller, Thomas S. Wilson, Jonathan Hartman, Fred J. Clubb, Brandon Gentry and Duncan J. Maitland, 2012. Annals of Biomedical Engineering, Volume 40, pages 883-897, Copyright 2012 Springer, License Number: 3345431146003.

effective method for improving radio-opacity of this material while maintaining the mechanical, physical and chemical properties of the original formulation.

3.2 Introduction

Cerebral aneurysms are localized dilations of an artery wall in the vasculature of the brain, are unstable in structure due to thinning of the arterial wall, and are thus prone to rupture.[55] Aneurysm rupture into the subarachnoid space occurs in approximately 10 per 100,000 people in the United States annually[23,56] with the majority of people ending up dead or severely debilitated.[23] Approximately 3–5% of the general population is thought to have cerebral aneurysms.[23,92] Due to the high mortality and morbidity associated with rupture, early and effective treatment of an intracranial aneurysm prior to rupture can increase a person's survival rate and quality of life.[23]

The two most common FDA-approved treatments treating cerebral vascular aneurysms involve isolation of the weakened portion of vessel via surgical clipping[62] and endovascular embolization through the use of flexible platinum coils. Surgical clipping involves a craniotomy, an invasive surgery of the brain, which carries serious inherent risks to the patient. Furthermore, surgical clipping is not always possible due to an inaccessible location of the aneurysm within the brain or the patient being a high risk candidate for surgery due to age or associated medical conditions. As a result of these limitations on surgical clipping, endovascular treatment has become an increasingly attractive option. The coils are introduced to the aneurysm endovascularly via a microcatheter. This filling treatment involves isolation of the weakened area of artery from the rest of the vasculature, ideally resulting in the regrowth of the endothelium, the

innermost layer of the artery over the entry point or ‘‘neck’’ of the aneurysm. Further, this endovascular treatment is not perfect in avoiding aneurysm rupture and subsequent hemorrhage, but they have been shown to be superior to clipping in both ruptured and unruptured aneurysms.[12,41,47,62]

While being the favored treatment for intracranial aneurysms, coils do have drawbacks, such as the possibility of coil compaction and subsequent formation of new side aneurysms adjacent to the original aneurysm,[40,100] low packing volume (less than 50% of the total aneurysm volume[45,49,68] leading to recanalizationor refilling,[38] migration of loose coils into the parent artery,[96] and although uncommon, potential puncture of the aneurysm dome during coil placement.[26] Additionally, coils are not very successful at treating aneurysms with neck diameters greater than 4 mm.[68] In these large neck aneurysms, approximately one-third of coil treated aneurysms either rebleed or recanalize.[30,63,75,89] It has also been shown that endothelialization at the base of the aneurysm is limited due to low endothelial cell adhesion on the platinumsurface.[50] Therefore, although coil treatment is the preferred filling method by interventionalists, there is still room for improvement in terms of the safety and efficacy of these devices.

The drawbacks of the commonly accepted treatments have spurred development of alternative aneurysm filling methods. Some of these technologies include treatment with multiple commercial devices,[42] hydrogel polymer,[38] collagen based coils,[50] hybrid metal and hydrogel coils,[1] shape memory polymer (SMP) coils [39] and polymer foams.[68,86,98,99] Previously, it has been proposed by Hampikian et al.,[39] that radiopaque SMP coils be used to fill aneurysms. This paper focuses on SMP foams as an aneurysm

filling method.[25,68,87] In theory, the foam provides a scaffold for clotting in a large sub-volume of the aneurysm that may have advantages over coils.[3,60] SMP foams are soft, compliant materials that have the ability to be fabricated into essentially any shape. This initial geometry can then be deformed by raising the temperature of the material above its transition temperature and applying a force. Continuing to apply force while cooling below its transition temperature programs the material into a secondary, temporary shape. The SMP foam would remain in its temporary shape until it is again heated above its transition temperature. For the purposes of aneurysm treatment, a foam of a given size and shape matching that of the aneurysm would be crimped onto a delivery device, directed into the aneurysm, and then deployed using either an external energy source or the body temperature of the patient.

These SMP foams are polyurethane based[97] and have favorable biocompatibility.[15] One drawback, however, is that these polymer foams have no inherent radio-opacity and are not visible using conventional patient imaging modalities (e.g., fluoroscopy). This limitation would reduce the likelihood of clinical use as without the ability to visualize it, the material could not be delivered safely.[8] The first aim of this research was to address this lack of radio-opacity, and develop SMP foams that exhibited radio-opaque characteristics using standard imaging and superimposition of bony and soft tissue structures, with the intention of advancing the clinical application of this technology.

To increase the radio-opacity of our SMP foam, tungsten was added to the polymer matrix prior to curing. To minimize the change in the material properties, it was

essential to use the smallest amount of tungsten possible that still provided adequate opacity. Mechanical, chemical and physical properties before and after the addition of contrast agent were compared to determine the effects of adding this opacifying agent to the SMP foam. The properties tested include tensile strength, and glass transition temperature. In addition to mechanical, chemical and physical properties, biocompatibility was also evaluated with a pilot study of one animal consisting of two vein pouch aneurysms with an implantation time of 90 days.

3.3 Materials and methods

3.3.1 Neat shape memory polymer sample preparation: determination of minimal amount of contrast agent necessary for visibility

Solid, otherwise known as neat SMP material, was used to determine the minimum amount of contrast necessary to create a visible change in fluoroscopic imaging of the SMP material. Fine tungsten powder, <1 micometer in diameter based on manufacturer specifications (Alfa Asear, Ward Hill, MA), was added in varying concentrations to neat SMP, and the materials were then cut into samples of increasing thicknesses. These samples were placed on top of a porcine head used to mimic the density of a human skull, and were imaged fluoroscopically to determine the minimum material thickness and the lowest concentration necessary for the polymer to be visible.

3.3.2 Solid polymer fabrication

Neat network polyurethane SMP samples were fabricated based on a variation of a composition specified by Wilson et al.[97] in 2007, using stoichiometric ratios of polyol and diisocyanate monomers. Triethanolamine was added in a 2.0% excess (by mass).

N,N,N',N'-Tetrakis(2-hydroxypropyl)ethylenediamine (HPED, 98%) (TCI America, Portland, OR), triethanolamine (TEA ≥ 99.5%) (Sigma-Aldrich Co., St. Louis, MO) and hexamethylene diisocyanate (HDI, 98%) (TCI America, Portland, OR) were decanted in a precise basic controlled atmosphere glove box (LabConco Corporation, Kansas City, Missouri) under a dry air atmosphere into glass jars and were subsequently sealed. The monomer-containing jars were then removed from the glove box and transferred to a vacuum oven, loosely opened for degassing, and degassed for 36 h at 45 C at 1 Torr. At the end of the degassing cycle, the monomer containers were re-sealed and transferred back to the glove box. The appropriate masses for 0.5, 1.0, 2.0 and 4.0% by volume of tungsten powder (<1 lm particle size, 99.95% purity) (Alpha Aesar, Ward Hill, MA) were measured out and placed into 60 mL maximum volume mixing containers (FlackTek^{TM}, Inc. Landrum, SC) which were then transferred to the glove box. The purge/fill cycle of the glove box was run for at least 5 cycles prior to transferring monomers into their respective containers.

The alcohol monomers, 0.4 mol of HPED and 0.19 mol of TEA, were added to the containers with the appropriate amount of tungsten, sealed tightly and then removed from the glove box. The 1.00 mol of HDI monomer, stored in a desiccator until use, was then added to the containers in the fume hood. After combining all of the monomers and tungsten, the containers were mixed for 2 min at 2400 rpm using the DAC 150 speed mixer (FlackTek ^{TM}, Inc. Landrum, SC).

A volume of 3 mL of the mixture was transferred to 5 mL lurelock syringes. This volume was chosen such that the stoppers had ample room to move during degassing

without separating from the syringe. The syringes, with a cap tightly secured on the tip, were put into a sonicator for 1.5 min. The exterior of the syringes were dried, the caps loosened, and then they were placed in a bell jar for 1.5 min under vacuum. The samples were removed from the bell jar, caps retightened, and the sonication step was repeated for 1.5 min. After sonication, the syringe caps were punctured with a needle and placed back into the bell jar for another 20 min under vacuum. The samples were initially held at room temperature for 2 h, and then the temperature was increased at a rate of 30 º C/h 120 º C was reached, at which point the temperature was held constant for 1 h prior to slow cooling to room temperature.

3.3.3 Solid sample preparation

Use of 5 mL syringes as casting molds resulted in 12.3 mm diameter cylinders of polymer doped with the varying amounts of tungsten (0.5, 1.0, 2.0 and 4.0%). These cylinders were then cut to thicknesses of 0.25, 0.5, 1.0, 1.5, 2.0, 2.5, 3.0, 3.5, 4.0, 4.5, 5.0, 6.0, 7.0, 8.0, 9.0 and 10.0 mm by an IsoMet 11-1280-160 saw (Buehler, Lake Bluff, Illinois). One control of 0% tungsten SMP polymer was cut into a 10.0 mm sample.

3.3.4 Multiple samples mounted in one holder: preliminary imaging

Samples of increasing thicknesses of 0.5, 1.0, 2.0 and 4.0% tungsten-doped SMP were mounted in and acrylic holder, one for each concentration, etched by a LS100 laser cutter (Gravograph, Duluth, GA) to allow for ease of imaging in one frame (Fig. 9).

3.3.4 Samples mounted separately: quantitative imaging

Neat samples of all concentrations and increasing thicknesses were individually mounted into acrylic holders that were laser etched by a LS100 laser cutter. Each acrylic

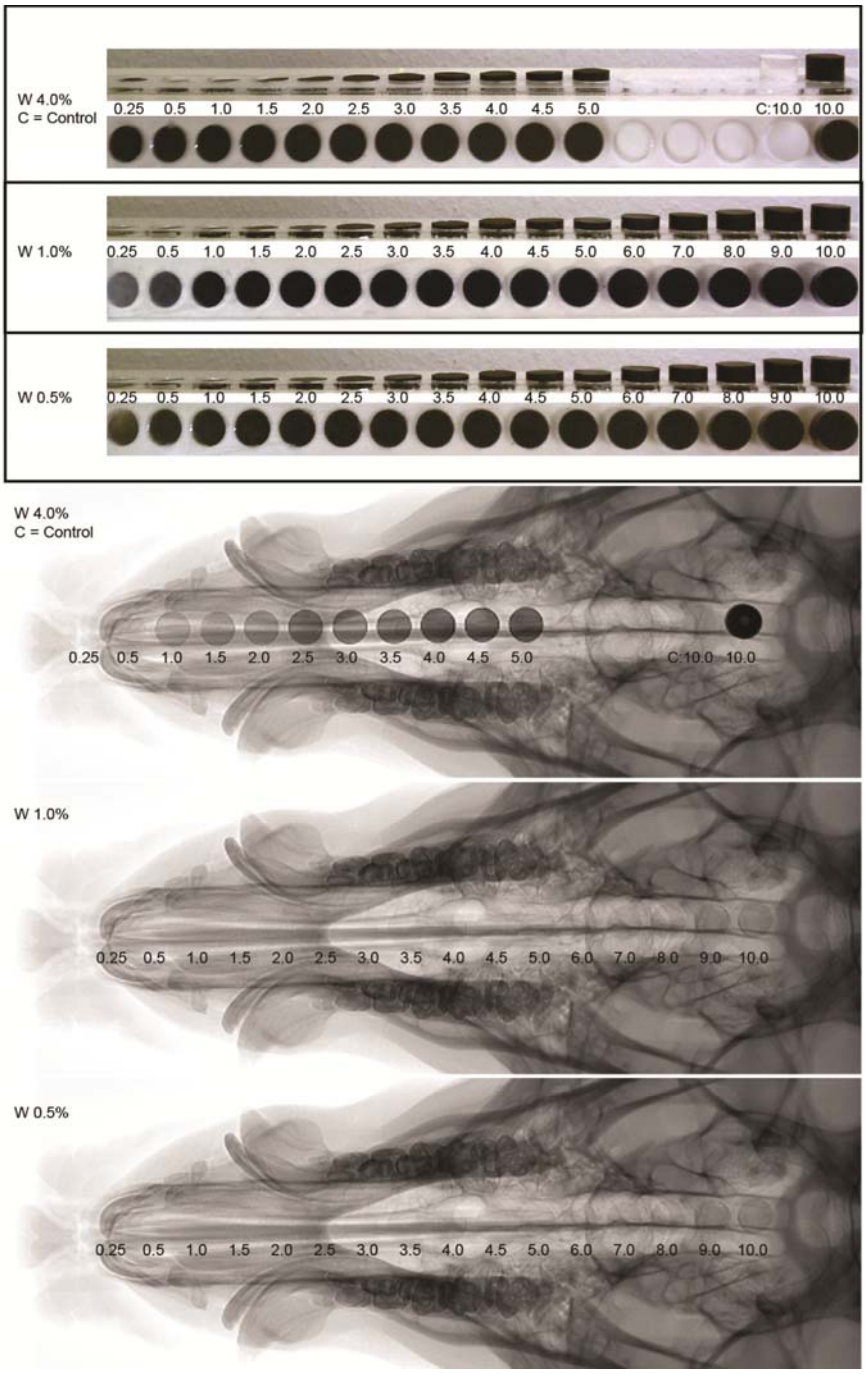

Figure 9: Increasing thicknesses of 0.5, 1.0, and 4.0% tungsten doped neat polymer samples mounted in an acrylic holder, samples imaged via fluoroscopy at TIPS.

sample holder was identified by radio-opaque markers that indicated concentration and sample height (Fig. 10b).

3.3.5 Determination of minimal polymer loading by fluoroscopic imaging

The neat polymer samples with a pig (Fig. 9) were imaged at the Texas Institute for Preclinical Studies (TIPS) at Texas A&M University, using an AlluraXper FD20 (Philips Healthcare, Andover, MA) fixed fluoroscope. Single image plane images were acquired at a rate of 3 frames per second, with an exposure of 22 mAs, using Allura Xper 7.2.1 software, with the voltage potential set to 70 kV. The source to detector, and source to sample distances were set to 1195 and 810 mm respectively for all samples. All samples were imaged using these power settings for the remaining imaging sessions of this paper. Each of the samples, mounted in their respective holder, was imaged to show the relative increase in contrast observed for each set of samples for each concentration.

3.3.6 Qualitative radio-opacity of SMP foam preparation

Polyurethane SMP foam samples were prepared with the same monomers as the neat polymer samples, using HDI, HPED and TEA. These monomers were premixed forming an isocyanate prepolymer and stored in a desiccator for 42 h prior to being mixed with the alcohol premix, catalysts and surfactants. The isocyanate prepolymers were foamed by adding alcohol premix (TEA), catalysts and surfactants (DC-5179, DC-I990, T131, BL-22 (Air Products and Chemicals, Inc, Allentown, PA)) and blowing agents (DI water and Enovate (Honeywell International Inc., Morristown, NJ)), and then

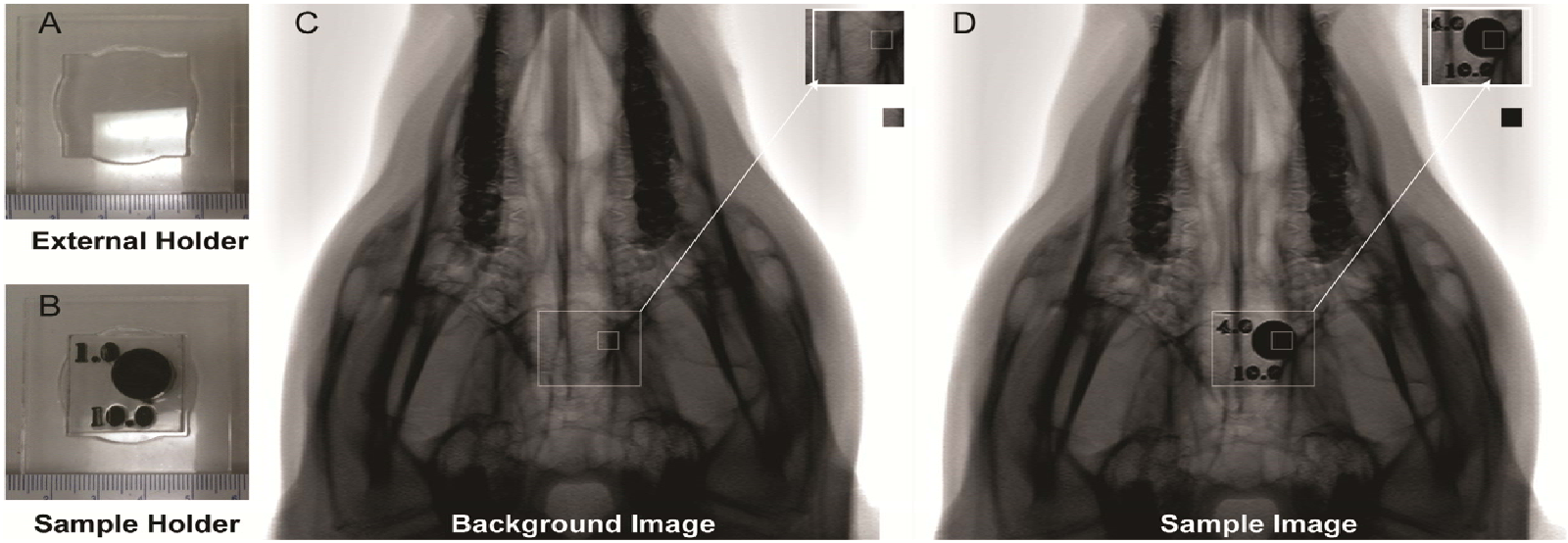

Figure 10: Controlled sample positioning imaging setup. (a) external holder to secure the sample to the pig's head in the same position in all images, (b) sample holder mounted inside of the external holder, top number is the concentration of tungsten, and the bottom number is the thickness in mm, (c) background image consisting of the pig's skull and the external holder, (d) sample image consisting of the pig's skull, external holder and sample.

mixed by a DAC 150 speed mixer for 15 s at 3400 rpm. An overall NCO/OH ratio of 1.05 was used for foaming. The foams were cured at 90 C under vacuum for 12 h.

Both the SMP foam and tungsten-doped SMP foam were made in a similar manner. The 4% by volume tungsten foam was made by adding 28.978 g of tungsten to the isocyanate premix and mixed for 30 s in the DAC 150 speed mixer at 3400 rpm. The alcohol premix was then added, and mixed for another 15 s at 3400 rpm. A volume of 3 mL of blowing agent (Enovate) was added to the mixture, and was allowed to vent while mixed for another 15 s at 3400 rpm. While the foam began to raise it was then allowed to sit at room temperature for 5 min prior to being placed in a 90 º C preheated oven. To support the cell structure as it cured, a vacuum was gradually pulled. After 1 h, the temperature was allowed to gradually decrease to room temperature; however, the vacuum remained on while the foam cured overnight.

3.3.7 Foam sample preparation

Cylinders of foam, 12 mm in diameter, were cut using biopsy punches. Samples of 0 and 4% tungsten doped foams were cut to be eight times the sample height of the neat polymer samples, which resulted in cylinders with heights of 2, 4, 8, 12, 16, 20, 24, 28, 32, 36, and 40 mm (Fig. 11a).

3.3.8 Multiple foam samples mounted in one holder: preliminary imaging

Foam cylinders of increasing heights, made of both the 0 and 4% tungsten foams, were mounted in acrylic holders similar to the solid samples (Fig. 11a), that were laser etched by a LS100 laser cutter.

3.3.9 Foam samples mounted separately: quantitative imaging

Samples of the same concentration and heights used in the preliminary imaging step were also individually mounted into acrylic holders that were laser etched by a LS100 laser cutter and individually identified by radio-opaque tags that indicated concentration and sample height (Fig. 10b).

3.3.10 Qualitative determination of radio-opacity of SMP foams via fluoroscopic imaging

The samples of 0 and 4% tungsten foams that were mounted in their respective acrylic holder were imaged using via fluoroscope, using the same settings as before, both with a pig's skull thickness (Figs. 11b, 11c) and alone next to a radiographic standard (Figs. 11d–3f).

3.3.11 Radio-opacity of crimped SMP foams

Multiple diameters of biopsy punches, 6, 8, 10 and 12 mm, were used to make cylindrical tungsten-doped samples of foam. These samples were crimped radially, parallel to the central axis, to their minimum diameter with a ST150-42 stent crimper (Machine Solutions Inc.TM, Flagstaff, Arizona), at 100 degrees C, and allowed to cool to room temperature for 2 h. Crimped samples were imaged through the crimped cylinder thickness using a fluoroscope, with a pig's skull and tissue, next to a microcatheter to observe their relative radio-opacity (Figs. 12a–12b).

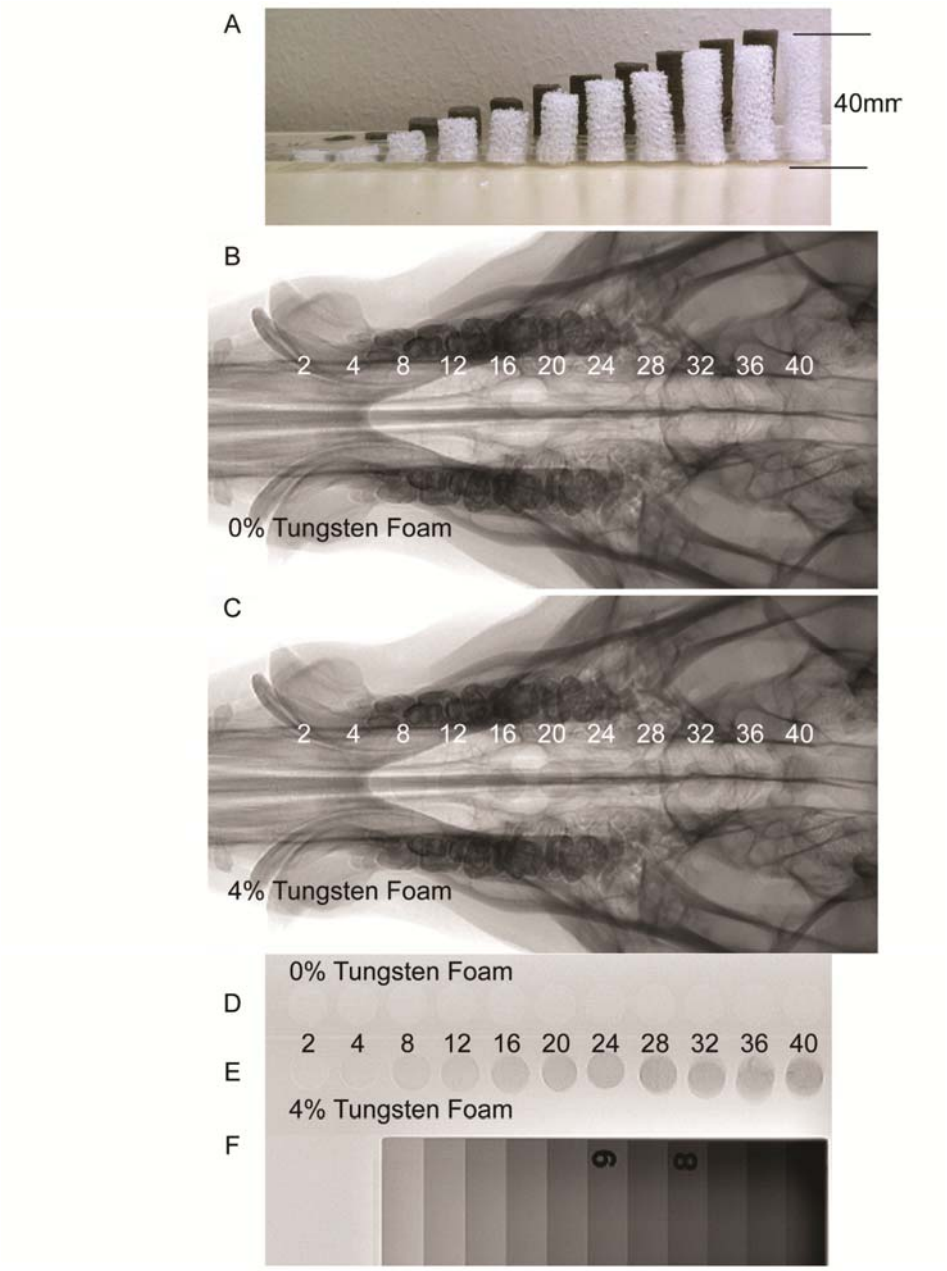

Figure 11: Fluoroscopic imaging of SMP foam with pig skull thickness. (a) profile view of 0 and 4% tungsten-doped SMP foam samples, (b) control 0% tungsten-doped SMP foam device with increasing thicknesses from 2 to 40 mm imaged via fluoroscopy with a pig's skull thickness, (c) 4% tungstendoped SMP foam device with increasing thicknesses from 2 to 40 mm imaged via fluoroscopy with a pig's skull thickness, (d) control 0% tungsten-doped SMP foam device with increasing thicknesses from 2 to 40 mm imaged via fluoroscopy, (e) 4% tungsten-doped SMP foam device with increasing thicknesses from 2 to 40 mm imaged via fluoroscopy, (f) aluminum standard.

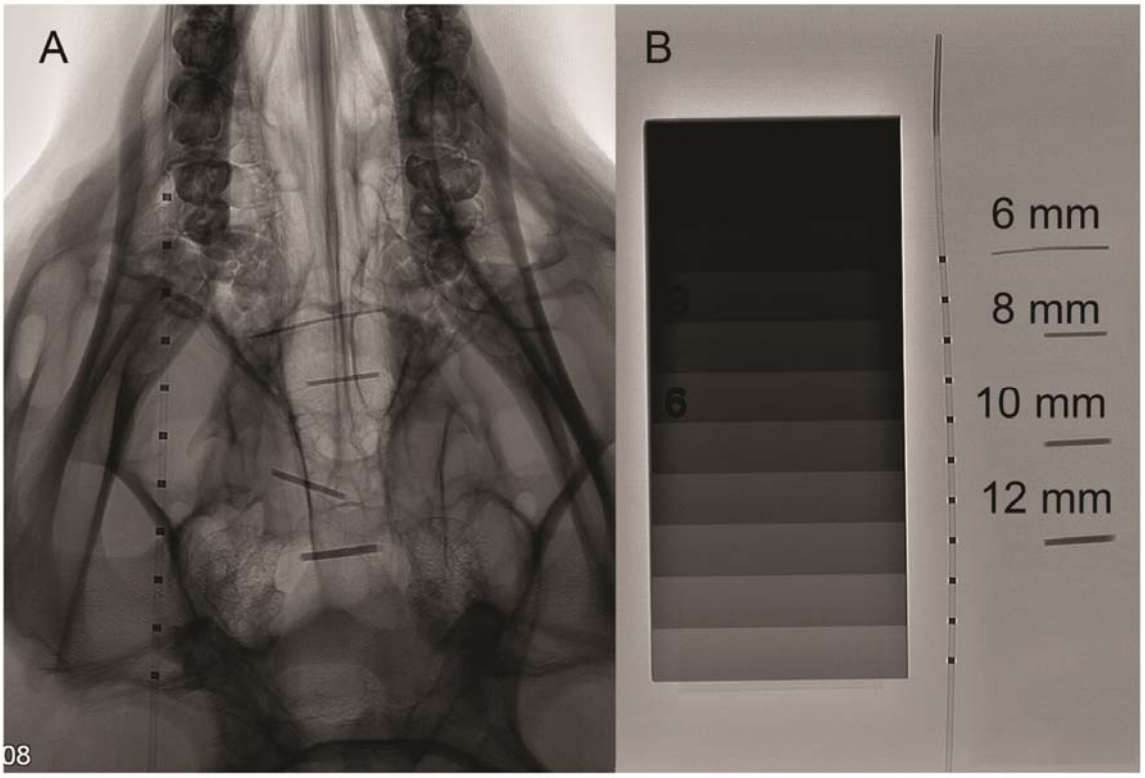

Figure 12: Fluoroscopic imaging of crimped SMP foam. (a) mechanically crimped 4% tungsten-doped SMP foam imaged via fluoroscopy, original diameters: 6, 8, 10 and 12 mm with a pig's skull thickness next to a catheter with radio-opaque platinum bands, (b) mechanically crimped 4% tungsten doped SMP foam imaged via fluoroscopy, original diameters: 6, 8, 10 and 12 mm next to the same catheter as in 4A. Thicknesses from 2 to 40 mm imaged via fluoroscopy, (e) 4% tungsten-doped SMP foam device with increasing thicknesses from 2 to 40 mm imaged via fluoroscopy, (f) aluminum standard.

3.3.12 Quantification of image contrast of solid SMP and foams

A stationary external acrylic mount was laser etched by a LS100 laser cutter to ensure proper positioning of the individually mounted samples while being imaged (Fig. 10a). The individually mounted samples of solid SMP and foam were imaged using a fluoroscope by securing the external holder to the pig's head, and imaging each sample down the center of its cylindrical geometry, as seen in Fig. 10d, to quantify the increase in image contrast as material thickness increased. Additionally, images with the external holder secured to the head without a sample were obtained as the background images; the background image representing the contrast obtained from a pig's head (Fig. 10c).

The original fluoroscopic images acquired were converted from Digital Imaging and Communications in Medicine (DICOM) to 8 bit Tagged Image File Format (TIFF) format and imported into Matlab R2008a (MathWorks, Natick, MA), where they were processed using the Image Processing Toolbox. Each image, originally 512 x 512 pixels in dimension, with a resolution of 0.439 mm/pixel, including an averaged background image, were cropped to a 15 x 15 pixel, equivalent to 6.6 mm x 6.6 mm image (Figs. 10c– 10d)—a region well within the area (120 mm^2 for neat samples and 110 mm^2 for foam samples) of the sample portion within the image. Using the cropped images, the sample images were subtracted from the background image. The difference in contrast was determined for each pixel from the 15 x 15 pixel images.

3.3.13 Differential scanning calorimetry

Differential Scanning Calorimetry was performed on all samples using a Q200 (TA Instruments, New Castle, DE), using a heat-cool-heat cycle (an initial ramp of 20 º

C/min up to 150 º C, held isothermal for 2 min, then ramped down to 240 º C at a rate of 20 º C/min, held isothermal for 2 min, and then ramped back up to 150 º C at a rate of 20 º C/min) detailed by Wilson et al.[97] Six samples were run at each concentration for all neat SMP and foam concentrations.

3.3.14 Mechanical testing

Stress/strain behavior of the 0 and 4% by volume tungsten-doped foams were determined via strain to failure experiments using an Insight 30 material tester (Materials Testing Solutions MTS Systems Corporation, Eden Prairie, MN). Due to fabrication methods of our foams, sample size was limited to 60 mm x 15 mm x 6 mm. Following the ASTM D638-Standard Test Method for Tensile Properties, ten samples of each concentration were tested utilizing a speed for non-rigid samples at a constant strain rate of 50 mm/ min at room temperature.[2]

3.3.15 Scanning electron microscopy

Foam samples were dried in an oven preheated to 90 C for12 h under vacuum. SEM analysis was carried out on foam blocks of 5 mm x 5 mm x 5 mm in dimension. The foam samples were secured to the holder using double-sided carbon tape that were then sputter-coated with gold and palladium to increase the conductivity and to prevent charge build-up of the electrons absorbed by the specimen. The morphology of the foam samples were analyzed using a Quanta 600 field emission scanning electron microscope (FEI, Hillsboro, Oregon).

3.3.16 Porcine implants of 4% tungsten-doped foams

4% tungsten-doped SMP block of foam was machined into two 12 mm spherical samples using a MDX-540 Roland 3D Mill (Roland DGA Corporation, Irvine, California). These samples were cleaned and sterilized via ethylene oxide to prepare them for implantation. A porcine animal model previously reported by Guglielmi in 1994,[36] was utilized to simulate in vivo aneurysm conditions for histological evaluation and healing of 4% tungsten-doped SMP foam. This model is constructed by the use of a harvested vein segment, in which one end of the segment is sewn onto an opening created on the carotid artery, with the opposite end tied off at the apex to create a pouch.[36] These samples were implanted into the aneurysms located on both the left and right carotids. The implanted materials remained 90 days within the aneurysms prior to sacrifice.

Vessels were harvested, fixed via formalin, and both pathology and SEM were performed to analyze healing. Histology of the vessels included embedding of tissues in paraffin, and serial sectioning of the aneurysm domes. For microatomic histological evaluation, or presence of cells associated with inflammation, hematoxylin and eosin (H&E) was used to stain the tissues; this staining elucidates the nuclear structures by staining them blue, and all other eosinophilic structures pink or orange. Masson's trichrome and Phosphotungstic acid haematoxylin (PTAH) was used to evaluate connective tissues, such as fibrin and collagen. Trichrome dyes erythrocytes orange, cell cytoplasm red and collagen fibers blue. PTAH stains collagen fibers reddish pink and fibrin fibers blue. Three serial sections of the aneurysms were evaluated: proximal to the

aneurysm orifice, middle aneurysm dome and apex of the dome. Overall healing for all areas was reported; magnifications evaluated were 3.5, 4, 10 and 20x. The initial gross results demonstrated in Fig. 10b, and the morphology of the lesion were verified and evaluated by SEM imaging of the same area (Fig. 10c).

This work was approved by and performed in accordance with guidelines of the Texas Institute for Preclinical Studies, and Texas A&M University's (Institutional Animal Use and Care Committee, IACUC), and that it adheres to the Guide in the Care and Use of Laboratory Animals established by the US National Academy of Sciences (or guidelines that insure equivalent or higher standards of care).

3.4 Results

3.4.1 Determination of minimal tungsten loading of polymer via fluoroscopy imaging

Thicknesses of solid SMP samples mounted in acrylic holders were imaged fluoroscopically superimposed on a pig head to determine minimal percentage of tungsten loading that could be seen in thin samples (~1 mm). Neat polymer samples cut from all concentrations (0.5, 1.0, 2.0 and 4.0%) tungsten were imaged, as seen in Fig. 9. This set of images indicated 4% tungsten samples were able to produce clearly defined regions of contrast, and poorly defined regions of increased contrast were observed by samples made from the lower concentrations. It was determined that 4% tungsten by volume loading would be sufficient for the doped foam samples for the remainder of the experiment.

3.4.2 Qualitative determination of radio-opacity of SMP foams via fluoroscopic imaging

3.4.2.1 Expanded foams

All of the 0% tungsten foams (Figs. 11b, 11d) were not visible when imaged via fluoroscopy, both superimposed with a pig's skull and alone, next to the radiographic standard. The 4% tungsten-doped aneurysm foams imaged (Figs. 11c, 11e) were visible at thicknesses greater than 8 mm when superimposed with a pig's skull. When imaged without being superimposed with a pig's skull, the 4% tungsten foams of all thicknesses greater than 2 mm were visible when imaged next to the radiographic standard. The image contrast obtained by 40 mm of 4% tungsten-doped foam was measured to be equivalent to 1 cm thickness of aluminum (Figs. 11e, 11f).

3.4.2.2 Crimped foams

Crimped 4% tungsten-doped SMP foams (6, 8, 10 and 12 mm original diameter) were made and imaged via fluoroscopy with a pig and next to a catheter and a radiographic standard (Figs. 12a–12b). When imaged without the pig's skull thickness, the crimped samples (6, 8, 10 and 12 mm original diameter) exhibit contrast levels similar to aluminum between 2 and 4 cm thicknesses respectively, when compared to the radiographic standard (Fig. 12b). The crimped foams were superimposed on the pig skull (Fig. 12a), demonstrating visibility for devices with an original thickness of at least 6 mm and increasing visibility with increasing original diameter, or material thickness.

3.4.2.3 Quantification of image contrast of solid SMP and foams

Samples from 0.5, 1.0, 2.0 and 4.0% tungsten-doped neat polymer, 0 and 4% tungsten-doped SMP foam were imaged using fluoroscopy in the same position, positioned by the external stationary holder (Fig. 10a) secured to the top of a pig's skull as seen in Fig. 10d. Raw data was acquired in DICOM format, converted to TIFF format where each individual sample image was subtracted from a background image, and data was plotted as difference in contrast vs. polymer thickness, as seen in Fig. 13 for solid polymer samples, Fig. 14 for foam samples. Figure 13 quantifies the increased contrast obtained from the solid polymer samples superimposed on the pig's head. The observed increase in contrast obtained from all thicknesses of control SMP foams as seen in Fig. 11b is not visible to the human eye. As seen in Fig. 11c, foams greater than 8 mm show up on fluoroscopic images; indicating that increase in contrast obtained by these samples are visible to the eye. Figure 14 compares the percentage of increase in image contrast vs. sample thickness for 0 and 4% tungsten-doped foams.

3.4.3 Differential scanning calorimetry

The differential scanning calorimetry data for all materials observed in this study is summarized in Fig. 16, where inflection point data for six samples per concentration is reported. The 0 and 4% tungsten foam samples had average glass transition temperatures of 83.4 and 83.4 º C, high glass transition temperatures of 85.3 and 85.7 º C and low glass transition temperatures of 81.1 and 82.2 º C, respectively. Solid polymer samples exhibited an average glass transition of 62.5 º C, and an overall range of glass transitions within 11.5 º C for all samples measured (Fig. 16).

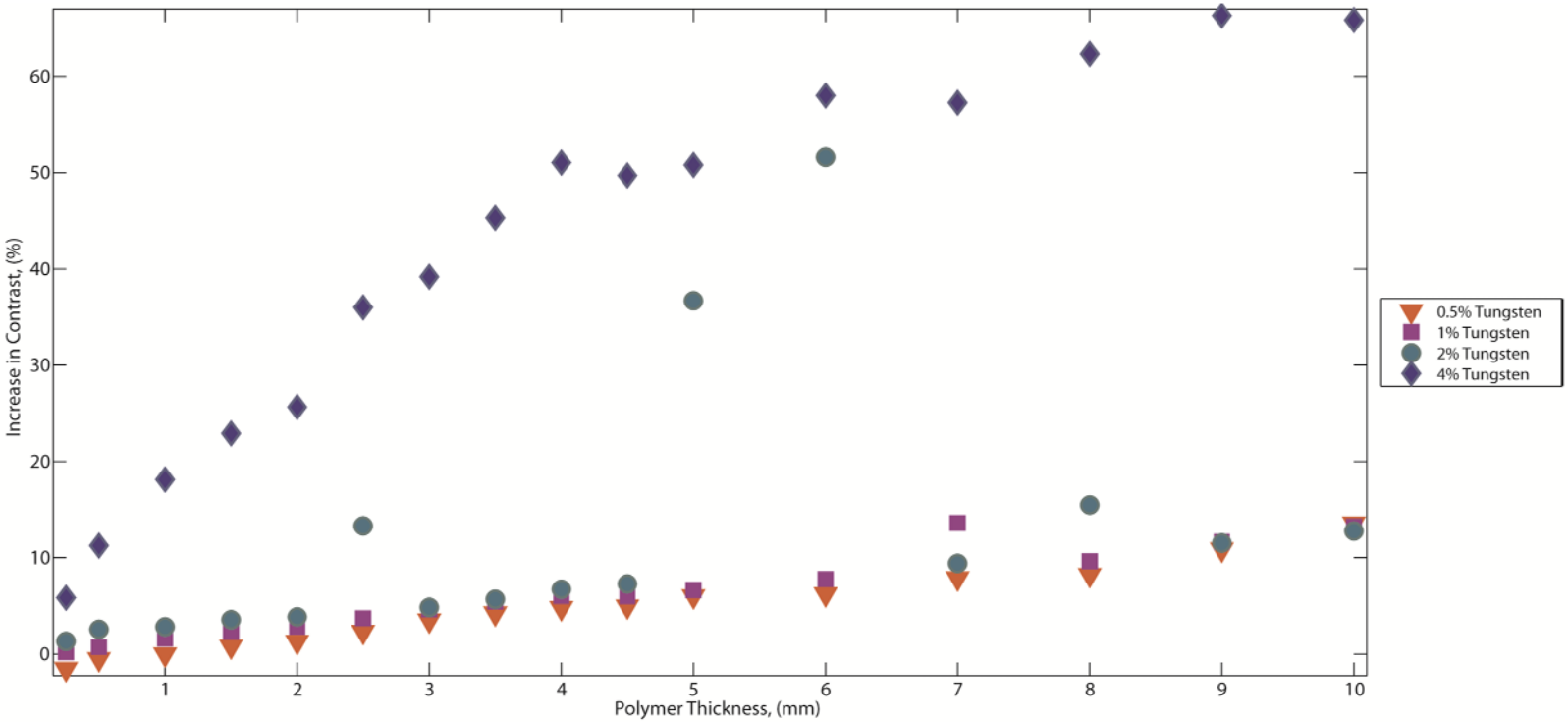

Figure 13: Percentage of increase in contrast obtained by neat polymer samples.

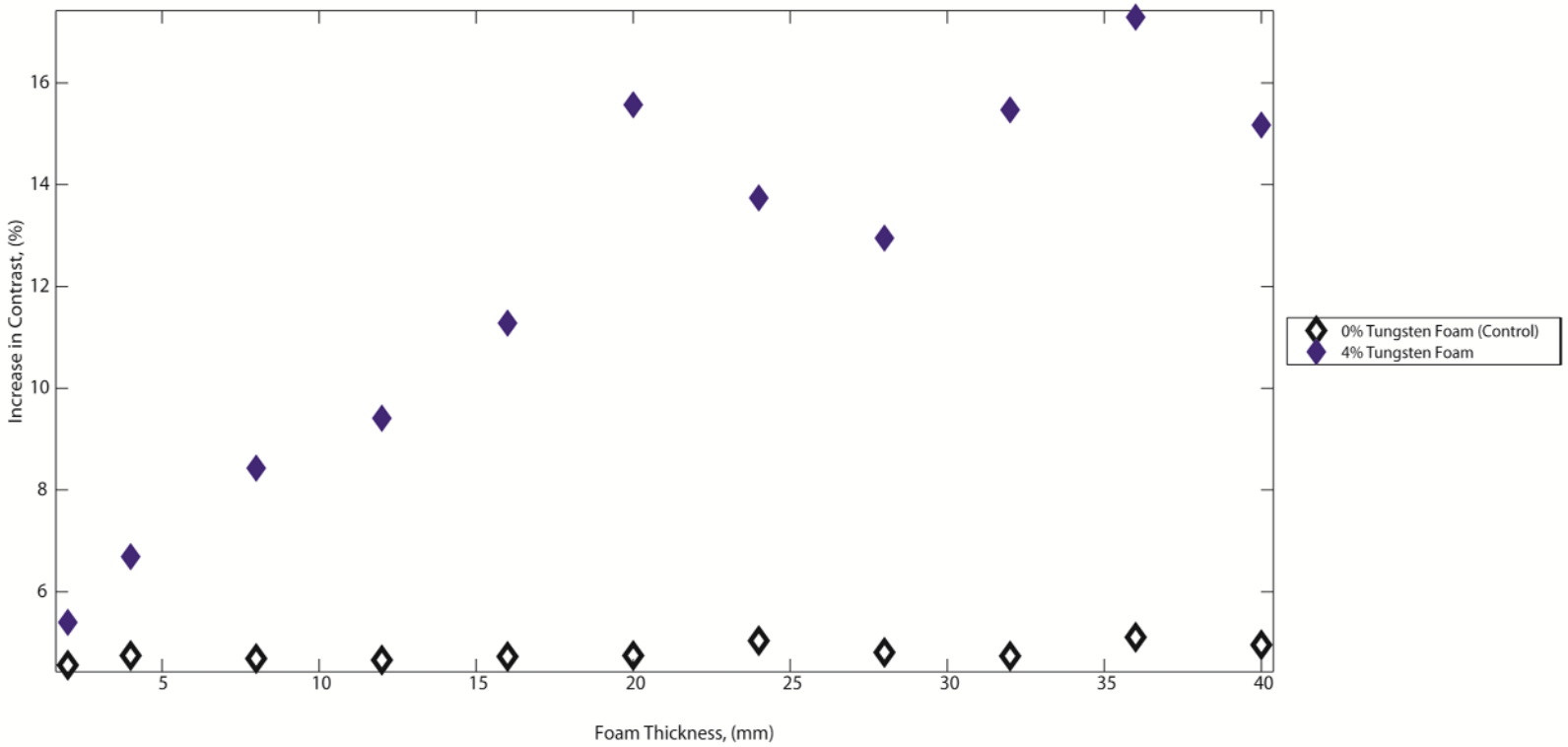

Figure 14: Percentage of increase in contrast obtained by SMP foam samples.

3.4.4 Mechanical testing

A summary of the mechanical results were tabulated in Table 3. Breaking tensile strength increased in the 4% tungsten-doped foams when compared to the 0% tungsten foams. Breaking strain increased in the 4% doped tungsten foams when compared to the control (0% tungsten foams). On average, the doped foams exhibited an increase in Young's moduli; the 4% tungsten-doped foams exhibited a Young's modulus of 1670 ± 548, and the 0% tungsten, or control foams, exhibited a Young's modulus of 1170 ± 406. Figure 15 is a representative stress strain curve for 0 and 4% tungsten-doped foams. The elastic behavior of these materials is represented by the linear region exhibited at strains less than 5%. There was an average increase in the modulus by 43% of the 4% tungsten-doped foams compared to the control foams.

3.4.5 Scanning electron microscopy

Figures 17a–17c are Scanning Electron Microscopy (SEM) images of 0 and 4% SMP foams. Figure 17a is a 40x magnification SEM image of the control (0% tungsten) SMP foam showing pore cell diameters roughly around 600 micrometers. In Fig. 17b, 4% tungsten doped foam is shown at 40x magnification, and in this image, pore cells are shown to be heterogeneous, roughly ranging from 250 to 800 micrometers in diameter. Figure 17c is a 250x magnification SEM image of a 4% tungsten-doped foam sample, which exhibited the <1 micrometer diameter tungsten particles dispersed within the polymer matrix.

Table 3: Summary of mechanical property results.

	Breaking Tensile Strength (kPa)	Breaking Strain (%)	Young's Modulus (MPa)
Control SMP Foam	78 ± 30	10 ± 3	0.8 ± 0.4
4% Tungsten Foam	130 ± 25	16 ± 4	0.8 ± 0.2

± One Standard Deviation, n = 10 per concentration

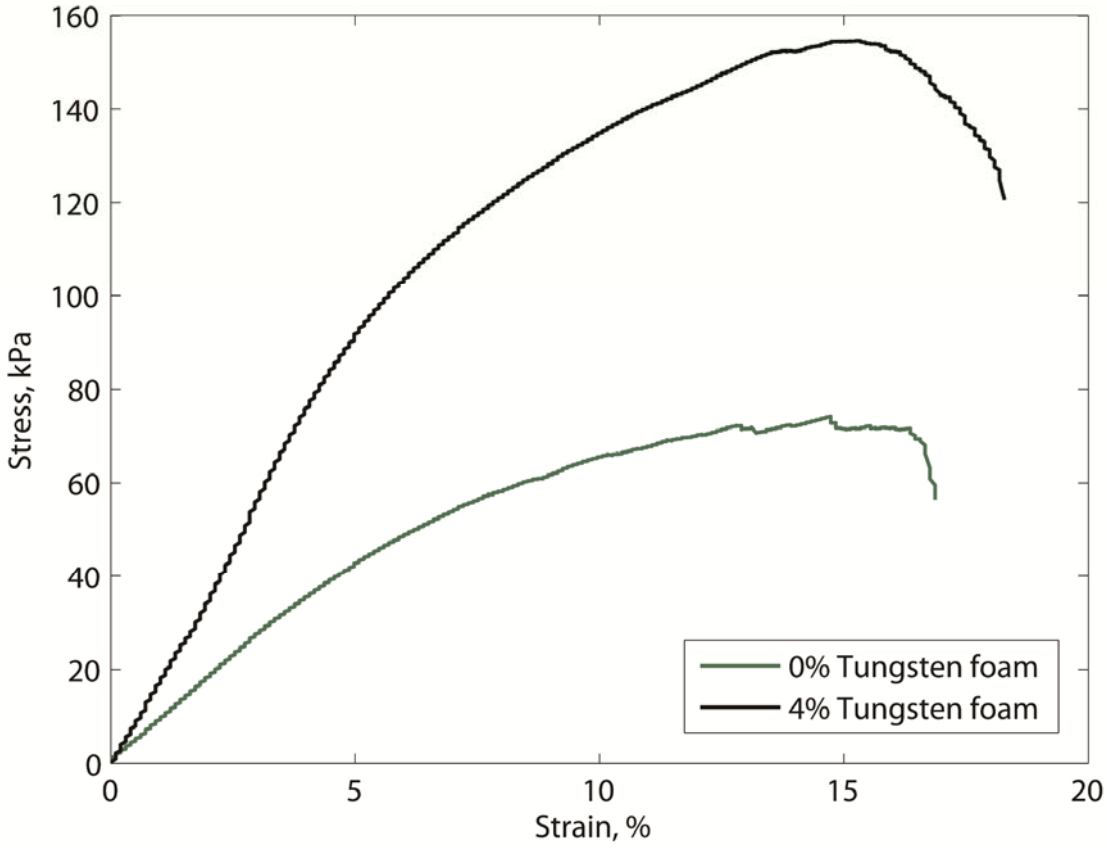

Figure 15: Representative stress strain curve of tensile testing of 0 and 4% tungsten foams.

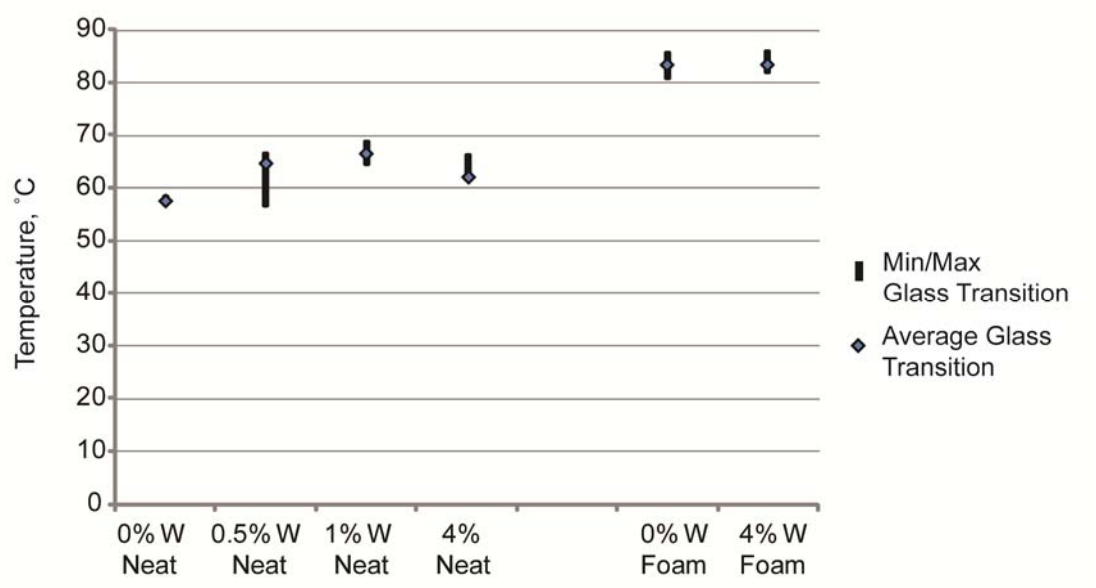

Figure 16: Glass transition data for solid SMP and SMP foam, n = 6 per concentration.

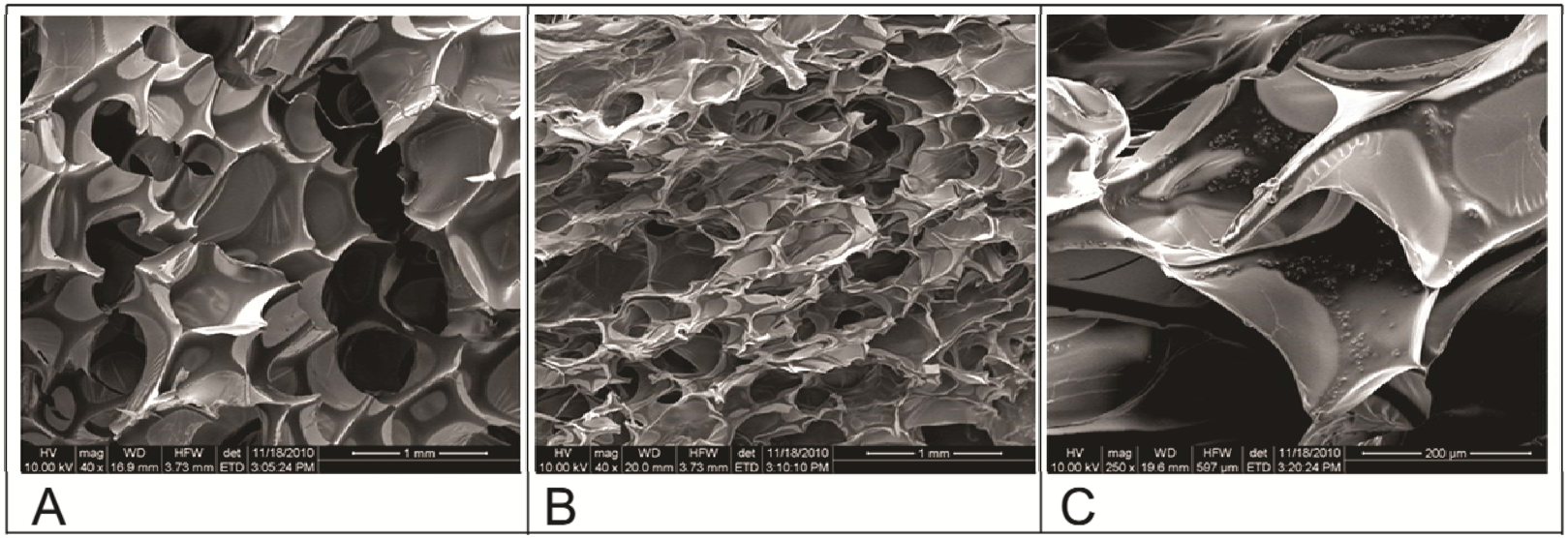

Figure 17: Scanning electron microscopy of control and 4% tungsten foams. (a) SEM micrograph of control SMP foam (40x magnification), (b) SEM micrograph of 4% tungsten SMP foam (40x magnification), and (c) SEM micrograph of 4% tungsten SMP foam (250x magnification).

3.4.6 Porcine implants of 4% tungsten-doped foams

3.4.6.1 SEM of lumen of artery at foam artery interface

Figure 18 summarizes the SEM and pathological results from implanting 4% tungsten foams within a vein pouch porcine aneurysm model for 90 days. Figures 18a, 10b and 10c are representative of the healing response at the gross and microscopic scales. The left carotid aneurysm model failed due to vasospasm during implantation, which caused the artery to collapse on itself, and thereby eliminating patency of the parent artery. Due to a lack of blood flow interaction with the parent vessel, SEM imaging was not performed on the left carotid aneurysm. The right carotid remained patent throughout the 90 days of implantation, and the aneurysm/artery interface was imaged via SEM at 100x magnification at 15 kV. SEM imaging of the right carotid showed that there was complete covering of the exposed foam with endothelial cells aligned parallel to the arterial blood flow, the surface exhibited a lack of mural thrombi, and complete healing of the aneurysm lesion was observed. Macroscopically there is an evident presence of endothelial cells at the aneurysm and artery interface after 90 days (Fig. 18b). Additionally in Fig. 18c, the endothelial cells were mature and aligned to blood flow.

3.4.6.2 Pathology

Both carotid aneurysms were evaluated via histology. The left and right aneurysms were both composed of 75% connective tissue, and had minimal lumen narrowing (<5%) with respect to the neointima proliferation. More than 95% of the inner core of the aneurysms had been infiltrated by dense cellular connective tissue with

regards to the healing that took place at the anastomosis interface, central core, and outer distal edge of the aneurysm dome. Inflammation of the central core and outer edge was minimal for both of the aneurysms; having less than 5% of the regions infiltrated by inflammatory cells.

Figure 18d is a hematoxylin and eosin stain (H&E) cross-section of bisected artery and aneurysm sac (4x magnification). The presence of blue stained nuclei helped determine the amount of multinucleated giant cells; an abundance of such cells indicates inflammation. However, as is shown in Fig. 18d, there are minimal amounts of multinucleated giant cells surrounding polymer struts, indicating a contained healing response within the dome of the aneurysm. For both aneurysms, less than 5% of the volume was filled with fibrin, and there was greater than 90% of collagen throughout the aneurysm (Fig. 18e). Additionally, in Fig. 18e, is a Trichrome cross-section of bisected aneurysm sac (4x magnification). It is shown in Fig. 18e that significant healing has occurred within 90 days, represented by blue stained collagen throughout the dome of the aneurysm, and minimal presence of red blood cell residuals. Figure 18f is a Phosphotungstic acid–hematoxylin (PTAH) cross-section of bisected artery and aneurysm sac (3.5x magnification). It is shown in Fig. 18f that there is more than 90% deposition of collagen, and less than 5% residual fibrin throughout the dome of the aneurysm. Figures 18h and 18i are histological details of the amount of inflammation present around suture materials, polypropylene and silk respectively. There were multifocal areas of mild chronic inflammatory cells proximal to the areas of suture material (Figs. 18h, 18i). These areas show a granulomatous inflammatory cell response

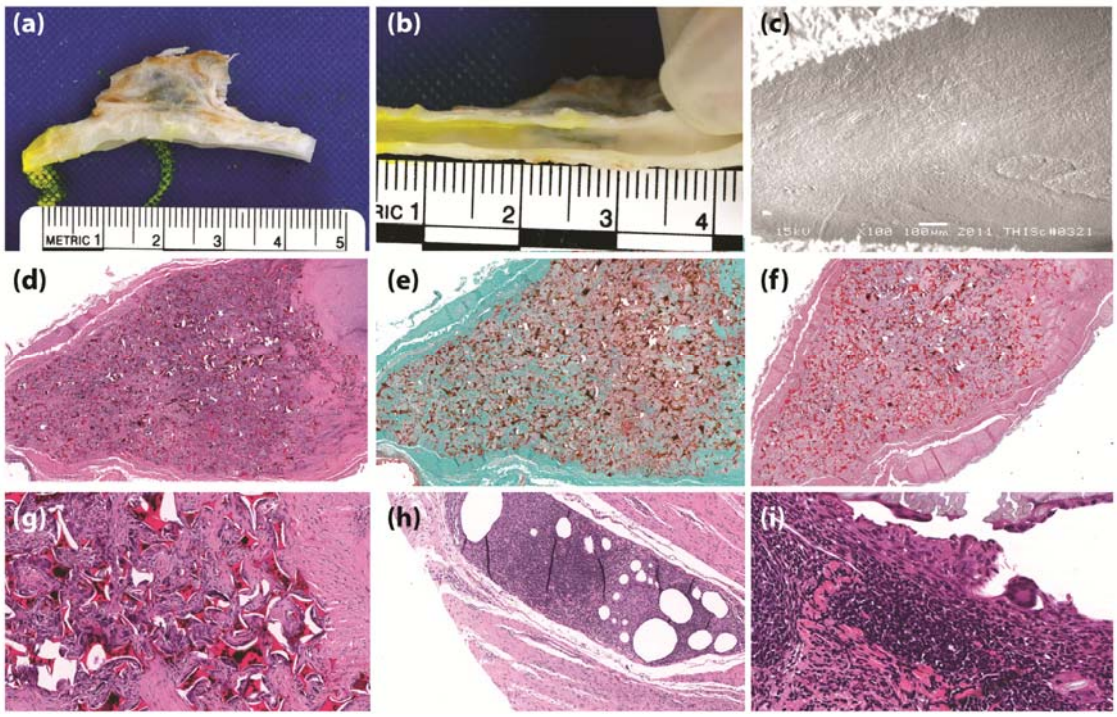

Figure 18: SEM and pathology results of implanted foams. (a) gross picture of dissected aneurysm and parent vessel, (b) gross picture of healing that took place between aneurysm and parent artery intersection (en face), (c) SEM of endothelial cell morphology across the ostium (100x magnification), (d) H&E cross-section of bisected artery and aneurysm sac (4x magnification), (e) trichrome cross section of bisected aneurysm sac (4x magnification), (f) PTAH cross-section of bisected artery and aneurysm sac (3.5x magnification), (g) H&E Cross-section of bisected artery and aneurysm sac (20x magnification), (h) H&E detail of the FDA approved suture material, polypropylene, indicated by the black arrow (10x magnification), and (i) H&E detail of the FDA approved suture material, silk, indicated by the black arrow (40x magnification).

to the suture materials represented by densely packed cells indicated by purple stained nuclei (Figs. 18h, 18i). When comparing the 4% tungsten-doped foam (Fig. 18g) to the silk and polypropylene suture materials, there is significantly less inflammation around the implanted polymer material (Figs. 18h, 18i).

3.5 Discussion

The goal of this research was to determine the minimal amount of tungsten necessary to make SMP foam visible when imaged via standard clinical imaging methods. Creating cylindrical neat polymer samples doped with increasing concentrations (0.5, 1, 2 and 4% by volume) cut into samples of increasing thicknesses facilitated the plotting of a standard curve for each concentration to be made. Visibility of the 4% tungsten neat samples at 1 mm thickness demonstrated the feasibility of achieving clinically practical radio-opacity in the 4% tungsten-doped foams. This assumption was based on an expected 80x expansion ratio of neat polymer to foam, and the subsequent conclusion that approximately 1 mm thickness of tungsten doped neat polymer and 8 mm thickness of 4% tungsten-doped SMP foam contained relatively the same amount of tungsten. In previous research performed by Hampikian et al.[39], 3% by volume doping of tantalum in SMP was successful at qualitatively creating visible X-ray contrast via fluoroscopy imaging at material thicknesses of down to 0.088 mm through water, which is consistent of our results. However, they did not perform imaging through bone and soft tissues, nor did they quantify the amount of contrast they achieved with 3% doping of their SMP.[39]

In order to quantify the degree of contrast at different concentrations of tungsten for both neat and foam SMP samples, the difference in pixel intensity from the background image was calculated for each of the samples. It was observed that when a sample of sufficient thickness increased image contrast, or darkened the image, by approximately 8% (Weber contrast) for an 8-Bit image, they were visible through the skull and associated soft tissues. The 0% tungsten (control) SMP foam of all heights was determined to increase the contrast by approximately 5% (Weber contrast[95]) over background in both the images taken with the skull thickness and when imaged alone, remained unidentifiable by visual inspection. By doping the SMP foam with 4% by volume of tungsten powder, it was determined that foam was visible at a thickness greater than 8 mm when superimposed with the skull and tissues, which was the case when there was an increase in the contrast by more than 8% by the sample (Weber contrast[95]).

Our proposed SMP aneurysm filling device consists of foam that would be crimped to its minimum diameter for delivery, and remain in this temporary state until it had been navigated into an aneurysm, at which point it would be actuated by heat to fill the sac. It was demonstrated that visibility of a crimped 4% tungsten-doped foam, original diameter of 6 mm (Fig. 12) was accomplished, and the increase in contrast observed by all of the crimped samples were approximately equal to 2–4 cm of aluminum when compared to the radio-opaque standard (Fig. 12b). The crimped samples exhibited a 25, 30, 33 and 37% increase in contrast for 6, 8, 10 and 12 mm original diameter samples respectively (Figs. 12a, 12b). Creating contrast by crimped foams of

these diameters was a significant step toward clinical application, as the average size of berry aneurysms is approximately 8 mm in diameter, and the imaging used in this study was the same as would be employed in a clinical setting. Although the 4% tungsten doped 6 mm SMP foam was visible in the crimped state, the sample may not be visible when expanded in vivo. Clinically, this may not be an issue due to the similarities to the current clinical situation during endovascular treatment of aneurysms, in which the unsatisfactory or satisfactory nature of the embolization is defined by the presence or absence of filling of the aneurysm by blood (injected contrast dye), rather than by the appearance of the coils themselves.

An additional goal of this research was to determine if the addition of tungsten powder to the matrix of the polymer would greatly alter the transition temperature of our foams. For all the 24 neat polymer samples the average glass transition was 62.5 ± 3.9 degrees C (Avg ± Std. Dev.). Among the 12 foam samples measured the average was 83.6 degrees C, and the standard deviation was 1.3 degrees C. The addition of particulate tungsten powder at a concentration of 4% by volume did not significantly alter the glass transition of the foam material, and therefore, acted as an inert filler material. These results coincide with the previously published study by Cui et al.[22], in which they demonstrated that the addition of particulate BaSO4 up to 40% by weight into polyurethane based SMP did not greatly affect the polymer matrix. Differential scanning calorimetry data showed that there was more variation of the glass transition temperatures among the neat polymer samples however; all samples in all concentrations

and polymer forms were within approximately 10 degrees C of each other, indicating that the tungsten filler had little effect on the polymer matrix during fabrication.

The mechanical properties of the ten samples tested of each 0% (control) and 4% tungsten-doped SMP foams are summarized in Table 3. The addition of 4% tungsten to the SMP foam increased its breaking tensile strength, breaking strain, and Young's modulus by 67, 60, and 43%, respectively. Previously, it has been shown by Gibson and Goods that there is a relationship between increases in cell density and an increase in the modulus of foam material,[34,35] which may have been the case with the 4% tungsten-doped foams in our study. It was observed that the 4% tungsten-doped foams exhibited greater cell density than the 0% tungsten non-doped foams. Additionally, in 2002 and 2004, Gall et al.[31,32] have demonstrated that the addition of a filler into SMP can increase modulus, and strength. More specifically related to foam materials, Saha,[82] reported that the addition of nanoparticle filler materials to polyurethane foams increased the tensile strength and the modulus. Our material, also being based off of polyurethane chemistry, may be exhibiting similar mechanical behaviors.

Figures 17b and 17c are SEM images of the two concentrations of SMP foams tested. These figures are examples of the cell structures in both concentrations. From the SEM images, it is evident that the cell size and cell density of 0 and 4% tungsten-doped SMP foams are different. The 4% tungsten foam sample exhibited a higher cell density and appeared to be more heterogeneous in pore cell size, including smaller pore cell sizes than that of 0% tungsten SMP foams, which suggests that the <1 micrometer dispersed tungsten particles act as heterogeneous nucleation sites during cell

formation.[16,66,82] Figure 17c shows the tungsten particles dispersed into the matrix of the polymer. These particles are potentially acting as points of stabilization throughout the material, thereby increasing the toughness of the foam, which is also exhibited by the mechanical testing (Fig. 15). Heterogeneity was seen in the tungsten-doped foams by the increased range in pore cell sizes exhibited in the SEM images.

Pathological results show that there was minimal inflammation (<5% fibrin deposition and less than 5% inflammatory cell infiltration) within the aneurysm dome. These results are all indicative that the tungsten doped SMP is a biocompatible filling material for the treatment of aneurysms.

Relative to the addition of tungsten to the SMP, the risk of tungsten toxicity for tungsten coils has been addressed. Peuster et al.[72] showed that slow degradation of tungsten coils emit small amounts (29 microgram/day) of tungsten in the vasculature and is not toxic in vitro which has been validated clinically by the lack of toxicity to tungsten coils in patients. Note that we use much less tungsten in our foams (0.2 g for typical 8 mm foam sphere) than the average coils used by Kampmann et al.[51] and Saatci et al.[81] (12 g per coil, for a 0.25 mm DIA and 12.5 mm length of mechanically detachable spiral tungsten coils (MDSs)) and an average of 5 coils inserted per aneurysm. In Fig. 18g, a 20x magnification detail of the aneurysm dome, it is shown that the tungsten particulate is encapsulated within SMP, preventing it from leaching out at a fast rate in vivo. If leaching is present, it should be at such a slow rate that it would not be toxic to the patient, given that the material has remained intact for a time frame of 90 days in vivo. This previous research performed by Peuster et al.[72] and this research support tungsten

doped polyurethane based SMP foams as a viable alternative filling material for treating intracranial aneurysms.

This research sought to accomplish multiple goals in the process of the development of a SMP foam aneurysm-filling device. The first requirement addressed was the opacification of the SMP foam which would allow for visualization during endovascular treatments using standard imaging (fluoroscopy) while being superimposed with bony and soft tissue structures (imaging through a pig head), and we have demonstrated this. The second requirement addressed was that the mechanical properties of the opacified foam be similar, or better when compared to the original formulation of SMP foam. This second requirement was met when the foam was doped with 4% by volume tungsten particulate. The tungsten-doped foam not only maintained its integrity, but also exhibited an increase in its modulus based on the results of the stress to failure mechanical testing. The third requirement addressed related to the chemical properties of the material, which required that the addition of tungsten particulate not significantly change the transition temperature, for this material the glass transition temperature. The tight grouping of glass transition temperatures exhibited by the 0% (control) and 4% tungsten foams supports the success of this goal. The fourth requirement was that the 4% tungsten-doped SMP materials should not have a significantly higher inflammatory response in vivo when compared to FDA approved materials. This fourth requirement was met by the almost complete healing of the aneurysm site after 90 days, and the lack of inflammation when compared to the suture material. These results provide a significant advancement for these materials to be

developed into aneurysms filling devices for clinical use. Further study is warranted; including more thorough biocompatibility tests of the 4% tungsten-doped SMP material in vivo and eventually clinical trials. This research serves as a foundation to support these future endeavors.

4. RETICULATION OF LOW DENSITY SHAPE MEMORY POLYMER FOAM FOR VASCULAR OCCLUSION

4.1 Overview

Predominantly closed-cell low-density shape memory polymer (SMP) foam was recently reported to be an effective aneurysm-filling device in a porcine model (Rodriguez et al., Journal of Biomedical Materials Research Part A 2013: (http://dx.doi.org/10.1002/jbm.a.34782)). Because healing involved blood clotting and cell migration throughout the foam volume, a more open-cell structure may further enhance the healing response. This research sought to develop a non-destructive reticulation process for this SMP foam to disrupt the membranes between pore cells. Non-destructive mechanical reticulation was achieved using a gravity-driven floating nitinol pin array coupled with vibratory agitation of the foam and supplemental chemical etching. Reticulation resulted in a reduced elastic modulus, but did not impede shape memory behavior. Reticulated foams were capable of achieving rapid vascular occlusion in an in vivo porcine model.

4.2 Introduction

An intracranial aneurysm, or abnormal bulging of an artery wall within the brain, is susceptible to rupture, having a great potential to result in mental debilitation or death.[7] Rupture of an aneurysm, or sub-arachnoid hemorrhage, results in bleeding out into the spaces of the brain. The cause of aneurysm growth and rupture is not fully known, but is thought to be due to abnormal blood flow patterns, local shear stresses and

the weakened state of the arterial wall.[17] Due to the inability to predict the occurrence of a rupture of such a malformation, and its potential to have a mortal or harmful outcome, it is advantageous for the patient to be treated as early in the disease progression as possible.

In the past couple of decades, endovascular treatment has become the preferred treatment versus surgical methods. This is mainly due to the significantly less invasive nature of endovascular treatments, which includes reduced recovery time and cost when compared to surgical craniotomy. Previously, it has been shown that polyurethane based shape memory polymer (SMP) foam is a biocompatible material for the purpose of aneurysm filling[77, 79] in a porcine animal model. Additionally, other non-shape memory polymeric polyurethane and polycarbonate foams have been explored for the purpose of vascular[54] and abdominal aortic aneurysm[76] occlusion with promising results. In this research we sought to develop a self-actuating vascular occlusion device (VOD) made of SMP foam to be delivered via endovascular methods.

It has been shown by Singhal, et al., in 2012, that polyurethane based SMP formulations can be tailored to be blown into foams with various actuation temperatures, densities and pore cell sizes.[85] These ultra-low density SMP materials have the ability to be temporarily programmed to a secondary compressed shape and maintain that shape until the material's temperature is elevated above its transition temperature. Around the transition temperature, the material regains its original shape. This ability to maintain a compressed shape until exposed to an increase in temperature above its transition temperature makes these materials excellent candidates for endovascular applications.

Given their shape memory capability, tunable pore cell size, tunable actuation temperature and proven biocompatibility[77], we desire to develop these materials as an endovascularly delivered VOD.

These foams possess a predominantly closed cell microstructure, which may not be optimal for aneurysm occlusion and subsequent healing. Post processing to reticulate the foam, or remove/puncture the thin membranes between pore cells while leaving the net-like foam backbone intact[33], will likely enable blood flow to more easily permeate throughout the foam, and allow for a forming clot to stabilize the device within the aneurysm. This permeation of blood throughout the material also enables the desired cellular components necessary to induce healing to more easily migrate into the volume of foam after clotting has occurred.

Reticulation has been achieved by multiple post-processing methods within industry, including caustic leaching[33] via exposure of the foam to a caustic bath for a specific amount of time, temperature and speed, thermal reticulation via a controlled burning of the membranes with the ignition of hydrogen and oxygen gases within a vessel housing the foam, or cyclic loading and unloading of the material. The act of reticulation changes the overall physical properties of foam. In general, it has been shown that with the removal of membranes there is a decrease in the resistance to mechanical compression.[9] There is also an increase in tensile properties, such as elongation and tearing strength.[9] When developing a reticulation procedure for SMP foam, care must be taken to avoid damaging the foam struts to preserve shape memory behavior and minimize the impact on its mechanical properties.

This research sought to develop a methodology for reticulation of membranes between the pores of SMP foam without damaging the native structure[9] or shape memory ability, with the intent of using these processed materials as a VOD. A viable non-destructive method of reticulation was developed involving mechanical membrane puncture and supplemental chemical etching, and the effect of reticulation on the mechanical properties of the foam was determined. To demonstrate proof of concept for these materials as a VOD, the occlusion time was determined via catheter implantation of reticulated foam devices within the vasculature of a porcine animal model. This research may accelerate the process of development of these materials as VODs for aneurysm treatment or other vascular applications aimed at achieving hemostasis.

4.3 Materials and methods

4.3.1 Foam synthesis

Two versions of SMP foam were fabricated by the method described by Singhal et al., in 2012 and 2013.[84,85] One version contained 100% Hexamethylene diisocyanate (HDI) and the other contained 20% HDI and 80% Trimethyl-1,6-Hexamethylene diisocyanate (TMHDI) for the isocyanate monomer in the polyurethane reaction. The less hydrophobic 100% HDI foam was made specifically for vessel implantation studies to allow for immediate self-actuation of the VOD in vivo without the need for external heating. The foam actuates at body temperature after exposure to moisture in the blood which causes a drop in the material's transition temperature. The other formulation was used for development of the reticulation system and mechanical testing. Both foams were reticulated and chemically post-processed in the same manner. Aside from their

different hydrophobicities, these two foams share very similar mechanical properties and shape memory characteristics.[84] During the foaming process, the material is constrained by the side walls of the container and unconstrained from above as it rises. Due to these conditions and their ultra-low densities[9], the foams have an anisotropic morphology as demonstrated in Figure 19.

4.3.2 Nitinol wire characterization

Nitinol wire pins were chosen as the means of mechanically reticulating the foam. Straight drawn nitinol wire (0.008" diameter) was purchased from Nitinol Devices & Components, Inc. (Fremont, CA), and was tested via strain to failure according to ASTM F2516 – 07 Standard Test Method for Tension Testing of Nickel-Titanium Superelastic Materials. Tests were performed on six samples using an Instron 5965 load frame (Instron©, Norwood, MA) equipped with a 500 N load cell. The Young's modulus and buckling load (critical load at which a column bows outward) of the nitinol wire were calculated. Young's modulus was calculated as the ratio of true stress to true strain at low strain. The buckling load was determined from the Euler column formula

$$F_{cr} = (\pi^2 EI)/(KL)^2$$

where F_{cr} is the minimal buckling load, K accounts for the end conditions, E is the Young's modulus, L is the length of the column and I is the area moment of inertia for the cross section of a cylindrical column, a circle, given by

$$I = (\pi/4)R^4$$

where R is the radius of the column. The end conditions, K, are determined as follows: both ends fixed: K = 0.5, one end fixed, one end pivots: K =0.707, both ends pivot: K =

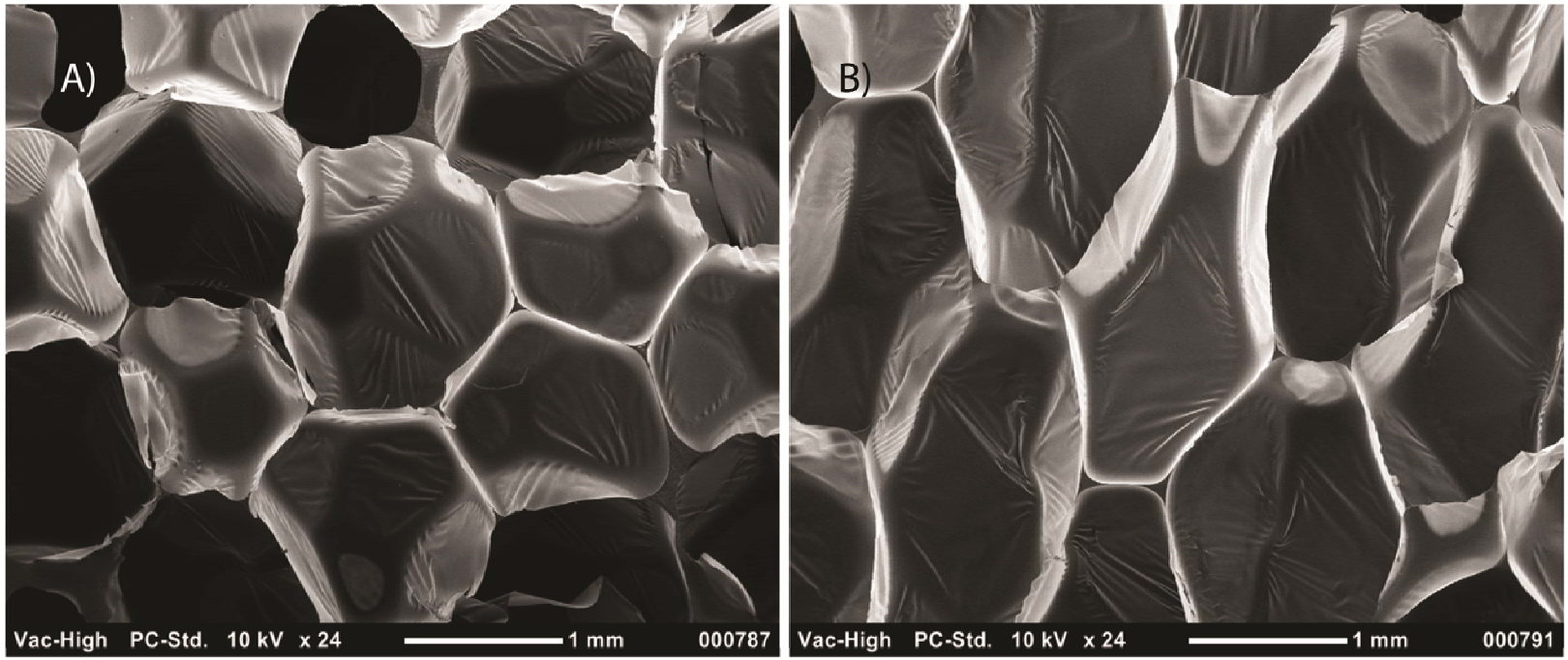

Figure 19: SEM cross-section images of native SMP foam in (a) horizontal (x-y) and (b) vertical (x-z) planes. The cells are elongated in the direction of the foam rise (z, vertical). The membranes between cells are evident.

1, one end fixed, one end free: K = 2. Since the end of the nitinol pin is free to move laterally when interacting with the foam surfaces, K was taken to be 2.

4.3.3 Mechanical reticulation system

The mechanical reticulation system consisted of two main components: (1) a gravity-driven floating nitinol pin array and (2) a vertically oscillating vibratory shaker upon which the foam was mounted for reticulation (Figure 20A). Each pin was made by casting a nitinol wire in a 1 ml syringe filled with EpoxAcast® 690 (Smooth-On, Inc., Easton, PA) doped with < 1 μm tungsten particulate (Alfa Aesar, Ward Hill, MA). A 50-mm length of nitinol protruded from the cast polymer cylinder (Figure 20B). The pins were loaded perpendicular to the top surface of the foam in individual channels drilled in a delrin block. The low-friction channels allowed unrestricted vertical motion of the pins. The pins were spaced 7 mm apart in a radial pattern. With the free ends of the floating nitinol pins in contact with the foam, the foam was agitated (0.25 mm amplitude) by the vertically oscillating shaker (Fritsch, Analysette 3 Spartan pulverisette 0), allowing for gravity-driven downward movement of the pins. Agitation continued until the pins penetrated the full thickness of the foam. The delrin block, which was chucked into a Bridgeport milling machine (Hardinge Inc., Elmira, NY) for controlled step wise movement, was then translated horizontally (pins removed) for further reticulation of the foam sample. Samples were punched in a raster manner every 500 μm. The samples were punched in one axis (uni-axial) or three axes (tri-axial). Uni-axial reticulated samples were punched along the direction of foam rise only (z-axis).

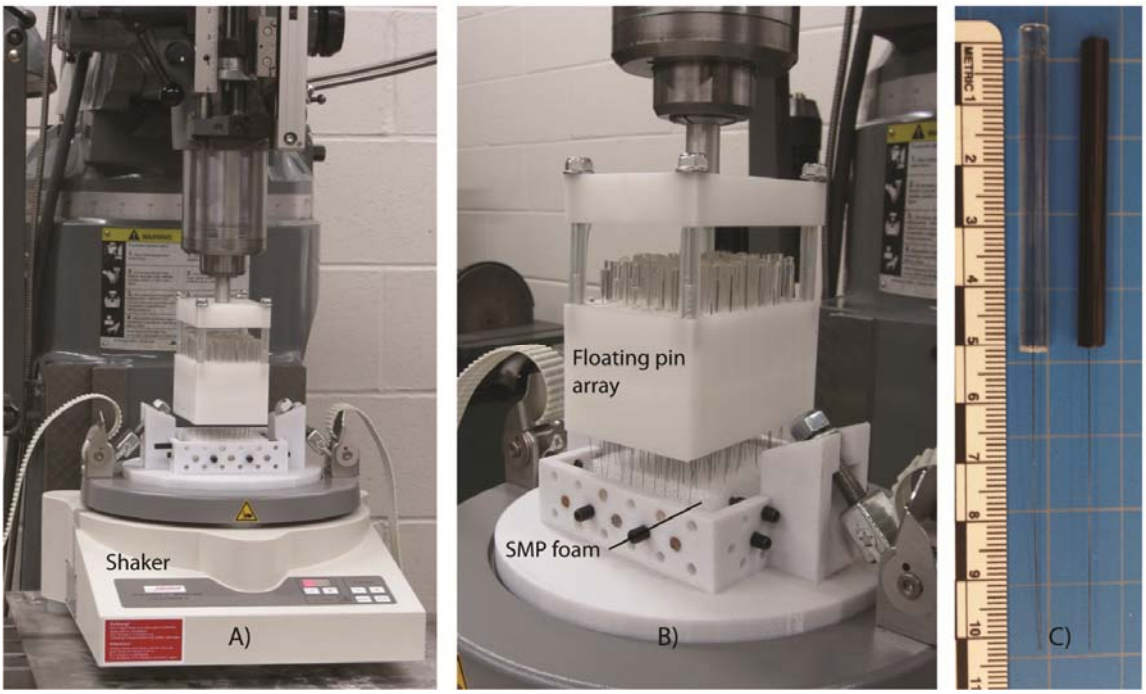

Figure 20: Mechanical reticulation system setup. (a) mechanical reticulation system including the floating nitinol pin array and vibratory foam shaker. (b) close up of the array punching the foam. (c) nitinol pins cast in non-doped (left pin) and tungsten-doped polymer (right pin).

Tri-axial reticulated samples were punched along the x-, y-, and z-axes by punching along one axis, re-orienting the foam, and punching along a different axis.

4.3.4 Preliminary mechanical reticulation testing

To determine the pin mass necessary to puncture a 30-mm-thick foam sample using the mechanical reticulation system, pins of variable mass were made by varying the amount of tungsten in the cast pins. Pins were made with masses of 0.25, 0.5, 0.75, 1.0, 1.5, 2.0, 2.5 and 3.0 grams. Uni-axial reticulation was performed to assess the effect of pin mass.

In addition to the method of varying the pin mass using the reticulation system, the membrane strength (minimal force necessary to puncture a membrane) and the friction of a wire passing through the foam were determined via mechanical testing using the Instron load frame equipped with a 50 N load cell. Agitation of the foam was not employed in these tests. A custom grip incorporating a pin vise was used to hold the 0.008" nitinol wire perpendicular to the foam sample. The wire extended 50 mm beyond the grip. All measurements were taken at ambient temperature. The force necessary to puncture a single membrane was determined in both the axial (foam rise) and trans-axial (orthogonal to foam rise) directions to assess potential differences due to the anisotropic foam cell structure. The force necessary to puncture a membrane was determined as the first spike in force prior to a sharp decrease in force encountered within the first 2 mm of foam. This distance was chosen due to the average pore cell size being roughly 1 mm in diameter. Force spikes greater than 10 g were likely caused by direct interaction with a strut, not a membrane, and were ignored. One hundred and fifty four (154)

measurements in the axial direction and 153 measurements in the trans-axial direction were made. For measurement of friction between the nitinol wire and the foam as it penetrated through the 30-mm-thick foam, the crosshead was translated at a rate of 1 mm/min while the load was recorded. Two separate measurements were made. The friction is reported as the slope of the load vs. extension data, excluding the spikes where the nitinol wire tip directly contacted a membrane or strut.

4.3.5 Chemical etching and final cleaning

In specified cases mechanical reticulation was supplemented by chemical etching to assess the effect of more thorough membrane removal as opposed to membrane puncture. To attempt to remove residual membranes after mechanical reticulation the foams were immersed into a 5N NaOH solution for 30 minutes while sonicated using a 5510R-DTH and 3510R-DTH ultrasonic cleaner (Branson® Ultrasonics Corp., Danbury, CT). The samples were then repeatedly rinsed with RO water to neutralize the samples. All samples (etched or not) were finally cleaned using the protocol outlined by Rodriguez et al. in 2013.[78] The samples were then dried for approximately three hours under vacuum at 90 ºC.

4.3.6 Imaging foam microstructure

Dried foam samples were sputter coated with gold using a Cressington 108 sputter coater, model 6002-8 (Ted Pella, Inc., Redding, CA) for 60 seconds at a distance of 3 cm. Imaging of the SMP foam was done before and after reticulation via low vacuum scanning electron microscopy (LV-SEM) using a NeoScope JCM-5000 (Jeol USA, Inc., Peabody, MA).

4.3.7 Mechanical characterization of foam

Mechanical testing of SMP foam was performed in compression mode according to ASTM D1621 – 10 Standard Test Method for Compressive Properties of Rigid Cellular Plastics using the Instron load frame with a 500N load cell. Cylindrical samples 25.4 mm in diameter by 25.4 mm tall of both the non-reticulated and reticulated (chemically etched or not etched) foams were prepared. These samples were frozen in a -80 ºC freezer overnight and subsequently lyophilized for 24 hours prior to mechanical testing. To assess the effects of pin mass, uni-axial vs. tri-axial reticulation, and chemical etching, nine different reticulation schemes (including a non-reticulated control) were investigated as outlined in Table 4. Five (5) samples were tested for each scheme.

4.3.8 In vivo *vascular occlusion assessment*

Uni-axial and tri-axial reticulated SMP foam samples were cut into 20-30 mm long cylindrical samples using a 10mm diameter biopsy punch. The samples were pre-conditioned by radially compressing to 1 mm diameter using a SC250 stent crimper (Machine Solutions Inc®, Flagstaff, AZ) at 97 °C and heated to expand to their original shape. The SMP foam cylinders were then chemically etched, rinsed, and cleaned. The samples were dried in vacuum and stored in an air-tight container with desiccant. The cylindrical samples were cut to 8 mm diameter using fine-tip scissors and 10 mm long using a razor blade. Samples were then radially compressed to the minimum diameter of approximately 1 mm using the stent crimper at 97 °C, cooled under compression to maintain the compressed shape, and stored in an air-tight container with desiccant until implantation in vivo.

Six (6) devices (3 uni-axial and 3 tri-axial reticulated using 1 g pins) were successfully deployed into multiple hind limb vessels of a three month old, 25 kg pig. Angiography performed prior to implantation of the VODs indicated the diameters of the vessels were on average 2.6 mm in diameter, which was smaller than the 8-mm diameter of the uncompressed VODs; therefore, the devices were able to expand to approximately 33% of their original diameter. A 5F catheter, 0.055" inner diameter, was navigated to the implant site using a 0.035" guidewire. The compressed foam VOD was submerged in room temperature saline for 2-5 minutes and then submerged in 32 °C saline for 3-5 seconds. The device was placed inside the catheter for 5 minutes to allow the foam to begin expanding and then pushed out of the catheter using the 0.035" guidewire (Figure 21A-C). This procedure resulted in expansion of the foam immediately as it emerged out of the catheter as shown in a preliminary bench top in vitro demonstration (Figure 21D-F). Contrast enhanced fluoroscopy was used to determine when the device had been deployed, by observing the location of the guide wire and if possible a lack of contrast agent in the vessel. After delivery into the vessel, the device expanded to its primary shape and subsequently blocked the vessel. We defined vessel occlusion time as the time after device delivery until injected contrast agent ceased to flow through or past the device; at that point clotting is likely to have occurred. Vessel occlusion time was determined via iodinated contrast injections visualized with angiography 45 seconds after deployment and then at 30 second intervals thereafter.[54]Average occlusion times were reported.

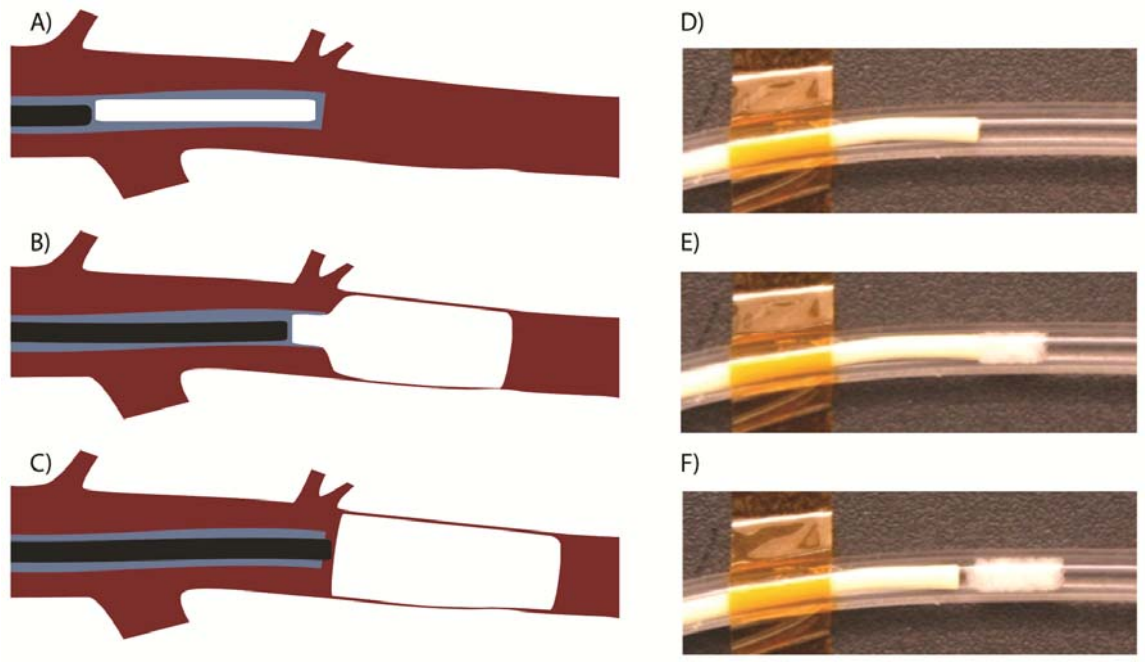

Figure 21: Schematic diagram of endovascular deployment of the SMP foam VOD. (a) the device is pushed near the 5F catheter tip by the guidewire, (b) the guidewire pushes the self-actuating device out of the catheter, and (c) the deployed device fills the vessel lumen. (d-f) in vitro demonstration of VOD deployment showing immediate expansion of the VOD in 37°C (body temperature) water in a silicone tube (3.5 mm inner diameter).

4.4 Results

4.4.1 Nitinol pin properties

From the six samples tested it was determined that the average Young's modulus of the nitinol wire was 58.62 ± 0.93 GPa. From this data, the buckling load for different pin lengths was calculated (Figure 22). The buckling load for the 50-mm-long nitinol pins is estimated to be 0.5 g.

4.4.2 Mechanical reticulation

Results of varying the mass of the pins showed that there is a range of masses that increase the number of punctured membranes throughout the foam thickness as seen in Figure 23. This range is between 0.75- 2 grams when reticulated in the axial direction of the foam.

The average and median mechanical force to puncture a single membrane was determined to be 2.07 ± 2.23 grams and 1.27 grams in the axial direction and 1.13 ± 1.09 grams and 0.80 grams in the trans-axial direction respectively (Figure 24A). Due to the range of measurements, large standard deviation and overlapping data a Wilcoxon Mann test was used to evaluate the difference between the two data sets. The Wilcoxon Mann test resulted in a P_TwoTail value of 0.00252858, which indicated that the two data sets were not the same. Buckling of the nitinol pins may occur based on these measurements, which could influence the reticulation path (and, hence, the number of punctured membranes) as they penetrate through the foam. Friction during penetration though the

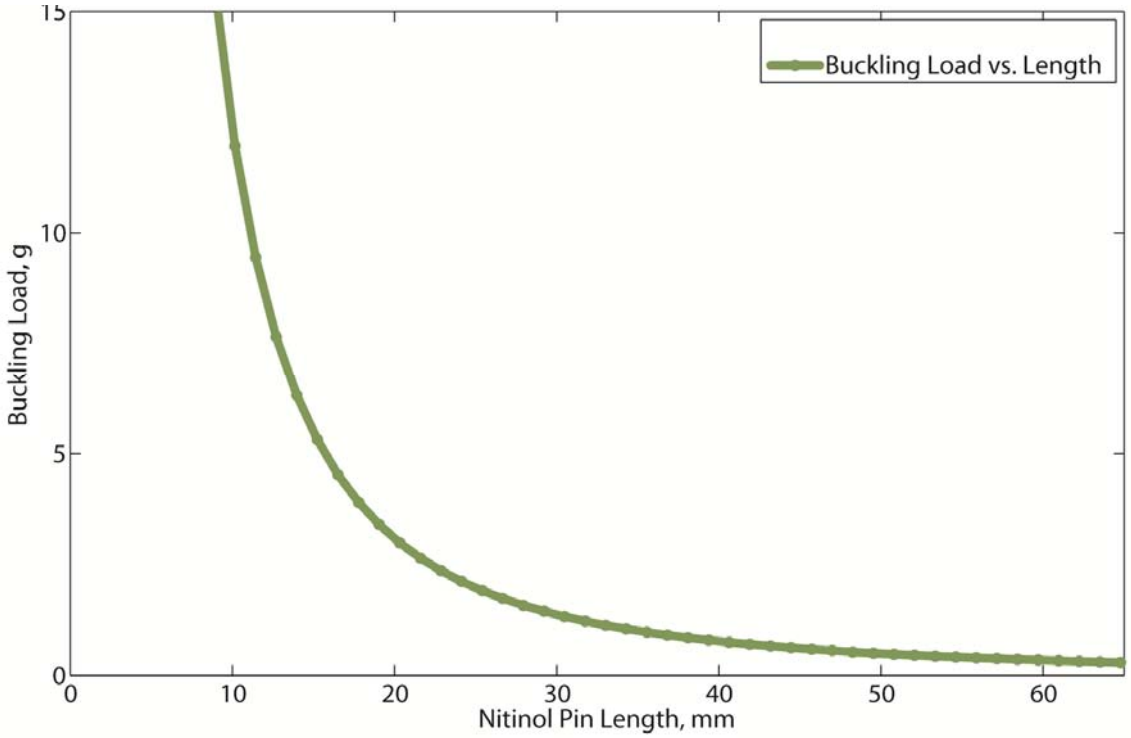

Figure 22: Calculated buckling load of 0.008" diameter nitinol wire.

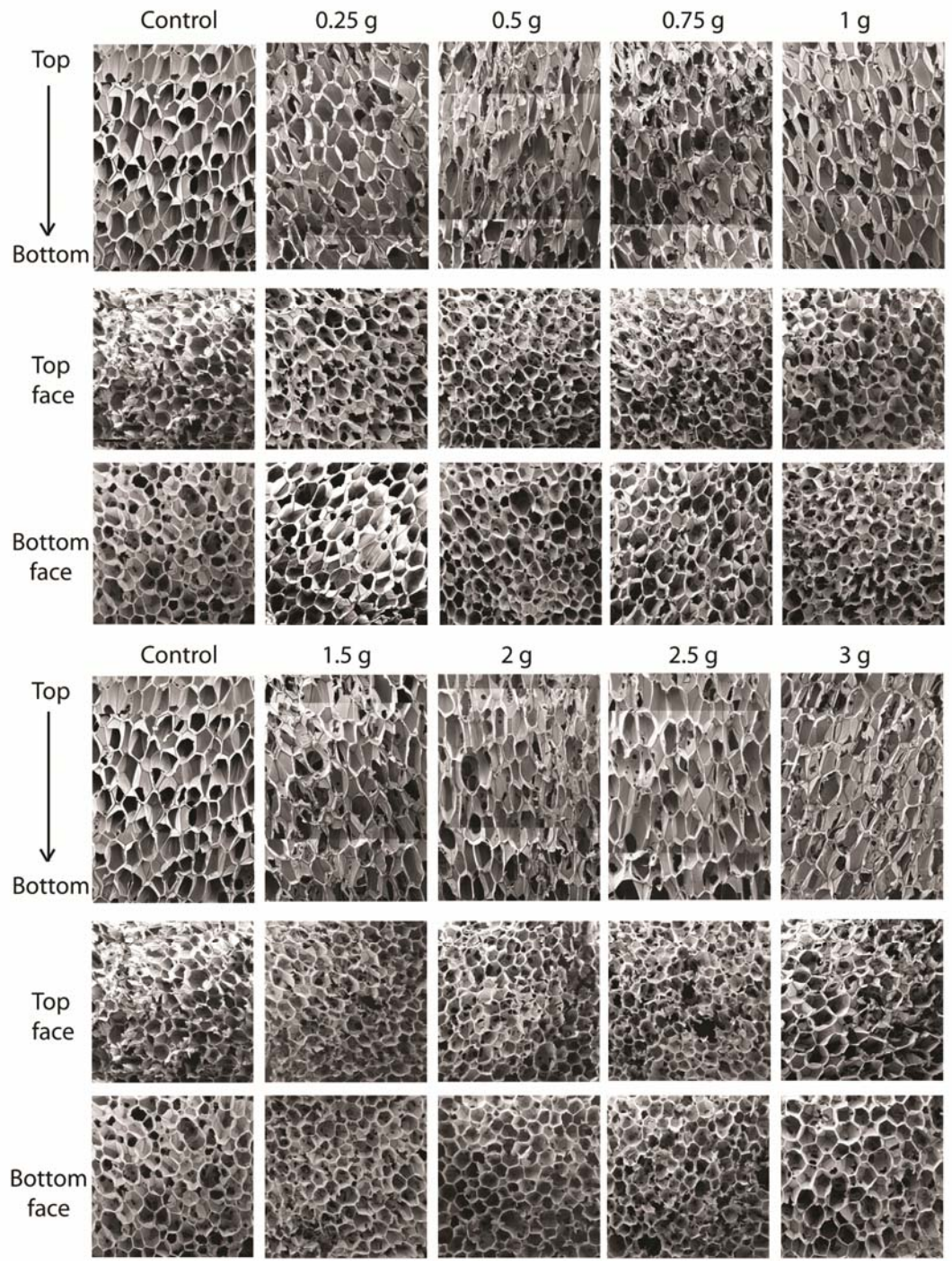

Figure 23: Results of axial reticulation through 30 mm of SMP foam using pins with different masses. An increase in reticulation was observed for pin masses of 0.75-2 grams.

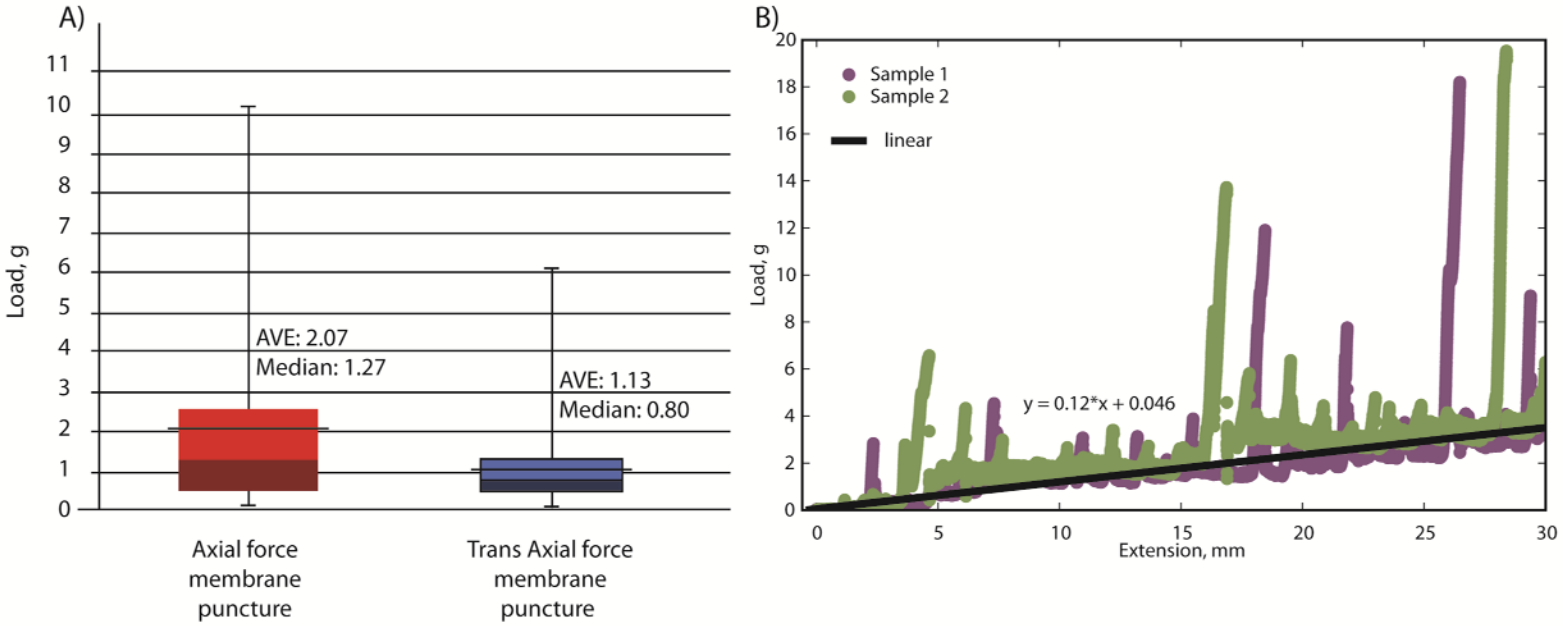

Figure 24: Membrane strength and friction interaction. (a) membrane strength for the axial and trans axial orientations and (b) frictional force experienced between the nitinol wire and SMP foam as it penetrated through a 30 mm thickness of foam in the axial direction.

foam was estimated to be 0.12 g/mm (Figure 24B). The spikes in the data are interactions between the nitinol tip and either a membrane or a strut of the SMP foam, and were intentionally ignored for the friction estimate. However, the spikes generally exceeded the estimated buckling load of the nitinol pins, further suggesting that buckling can occur during reticulation.

4.4.3 Effect of reticulation of foam mechanical properties

The foams reticulated according to Table 4 are shown in Figure 25. As shown in Figure 26, the non-reticulated control foam had an average elastic modulus of approximately 2.65 X 10^5 Pa. Reticulation reduced the modulus, with the tri-axial reticulated foams having the lowest moduli. The more extensive disruption of the cell membranes caused by reticulation in multiple axes resulted in higher reduction of the modulus. Closer inspection of the data shows that chemical etching of the uni-axial reticulated foam increased the modulus, while the tri-axial reticulated foams showed a slight decrease in modulus after chemical etching. In both the axial and tri-axial cases, the modulus was higher when 2 gram pins were used for axial reticulation compared to the use of 1 g pins. Figure 27 is a summary of the average stress versus strain curves for the 5 samples tested per case. Following the trend in modulus, the non-reticulated foam had the highest stress plateau before densification, followed by the uni-axial and finally the tri-axial reticulated foams.

Table 4: Reticulation schemes employed for mechanical testing of foams.

	Nitinol Pin Mass	Chemical Etch?	Number of Samples Tested
Uni-axial	1 g	no	5
	1 g	yes	5
	2 g	no	5
	2 g	yes	5
Tri-axial	1 g axial, 1 g trans-axial	no	5
	1 g axial, 1 g trans-axial	yes	5
	2 g axial, 1 g trans-axial	no	5
	2 g axial, 1 g trans-axial	yes	5
Non-reticulated control	not applicable	no	5

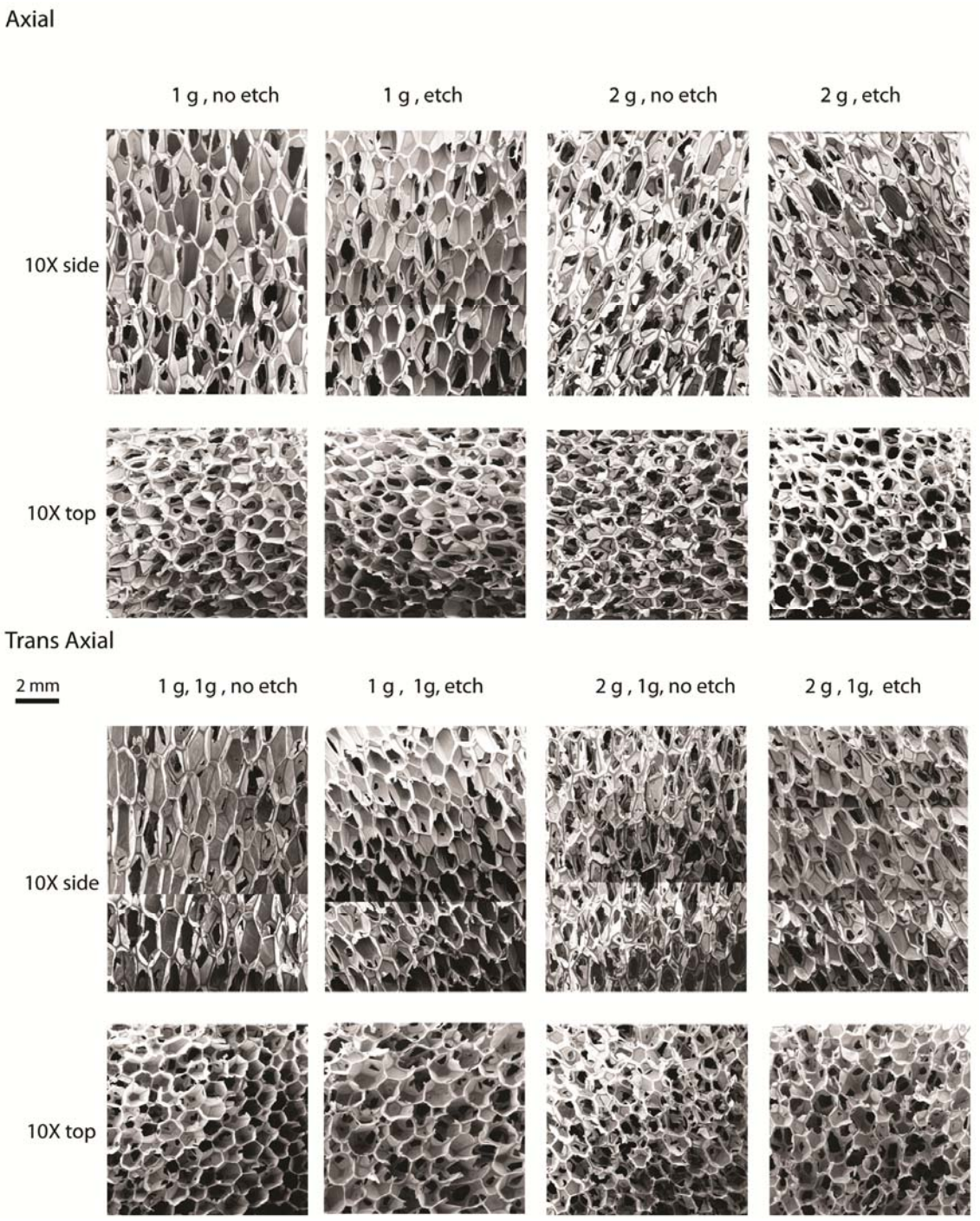

Figure 25: Scanning electron microscopy (10X magnification, scale bar = 2 mm) of reticulated foam samples that were later mechanically tested. The cases are summarized in table 1.

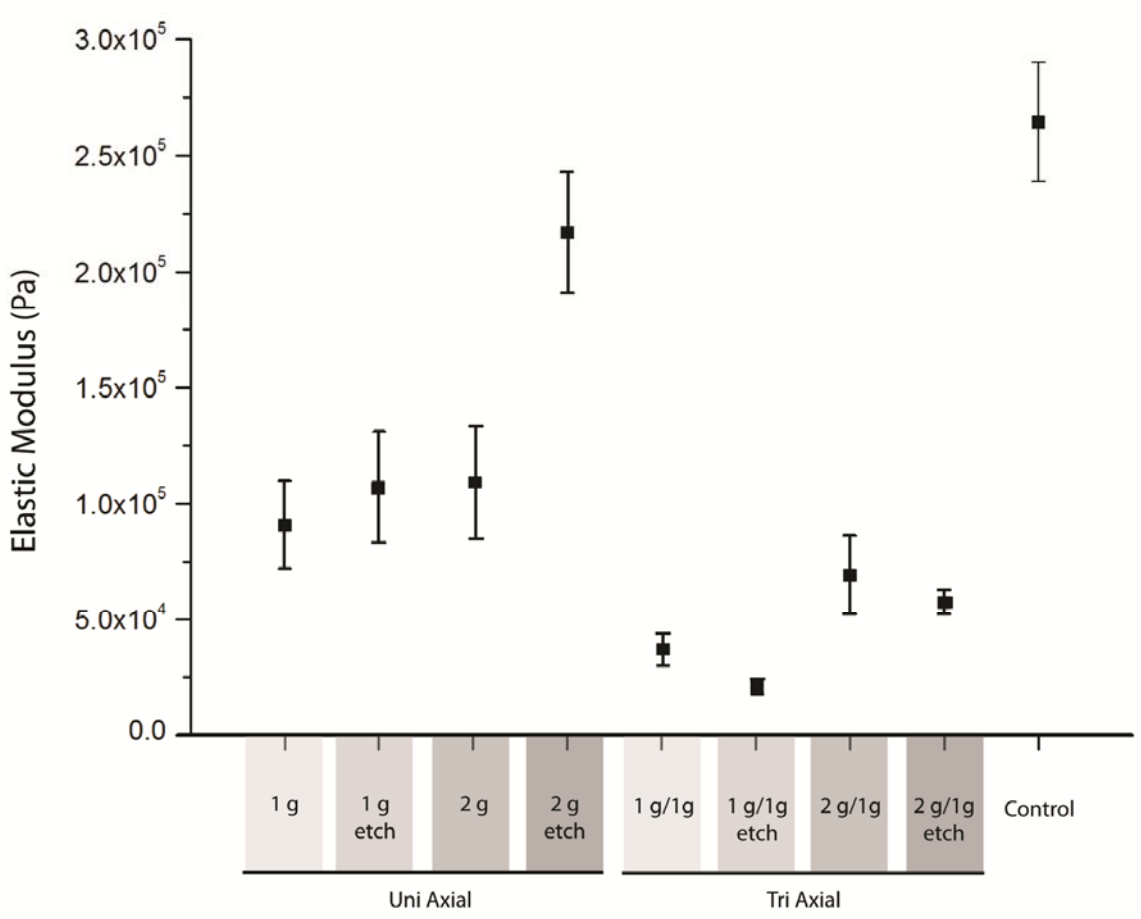

Figure 26: Elastic moduli for the foams reticulated according to table 1.

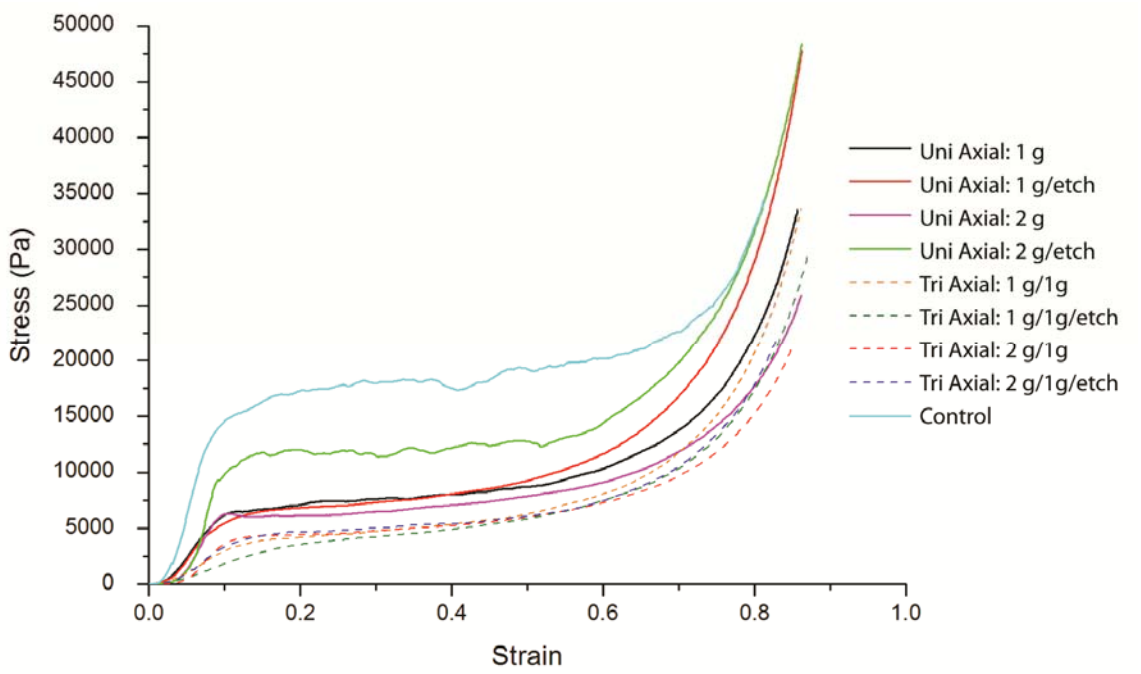

Figure 27: Average compressive engineering stress vs. engineering strain for the foams reticulated according to table 1.

4.4.4 In vivo *vascular occlusion*

The uni-axial reticulated foam had an average occlusion time of 90 ± 11s and the tri-axial reticulated foam had an average occlusion time of 128 ± 77s. Figure 28 illustrates VOD deployment and subsequent vascular occlusion of a tri-axially reticulated VOD. Figure 29 shows angiograms of all treated vessels before VOD implantation and after vessel occlusion. On average the uni-axial reticulated foam induced faster occlusion that the tri-axial reticulated foam. This result is not unexpected since blood flow is likely impeded more by the less reticulated foam, potentially resulting in more rapid clotting. However, the large deviation of the occlusion time for the tri-axial reticulated foams, as well as the 30-s interval between contrast injections, prevents reaching a definitive conclusion on the effect of extent of reticulation on occlusion time; further study is required.

4.5 Discussion

Previously we have demonstrated that our SMP foams are biocompatible in vivo, when implanted into a porcine aneurysm model.[77] Though excellent healing was observed, these foams possessed a predominantly closed-cell structure, which likely limits the amount of blood flow allowed to percolate through the material and may delay or inhibit optimal healing in vivo. Reticulation may enhance application of these materials as an aneurysm filling or other vascular occlusion device.

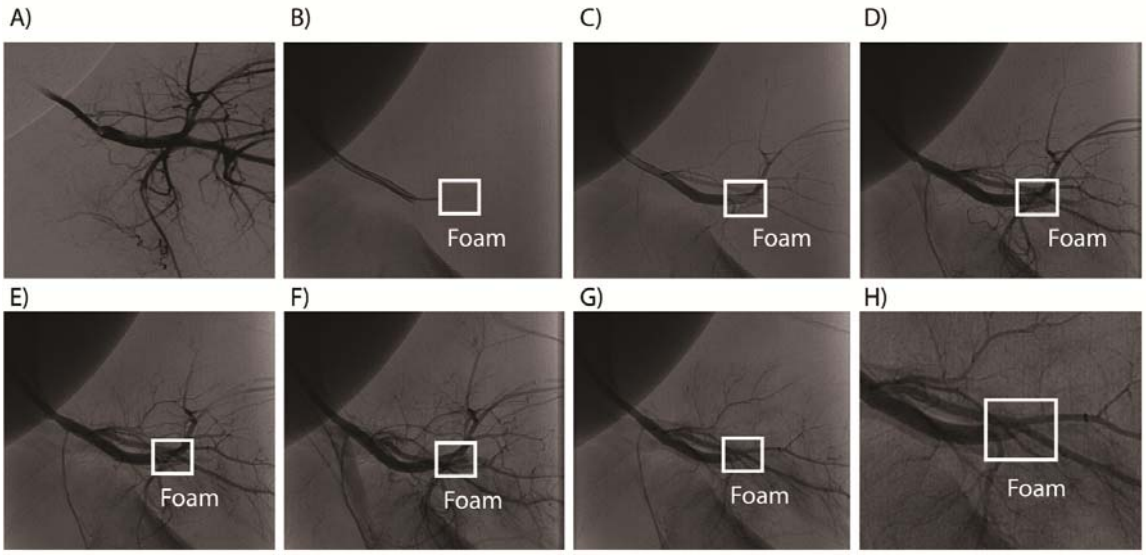

Figure 28: In vivo deployment of a tri-axial reticulated foam. a) pre-deployment contrast enhanced angiography, b) guidewire ejection of the foam from the catheter (no contrast used), c-g) contrast enhanced angiograms acquired after deployment at 30-s intervals, h) close up view of the fifth contrast enhanced angiography performed after deployment. Occlusion is evident in (g) and (h), 165 s after delivery.

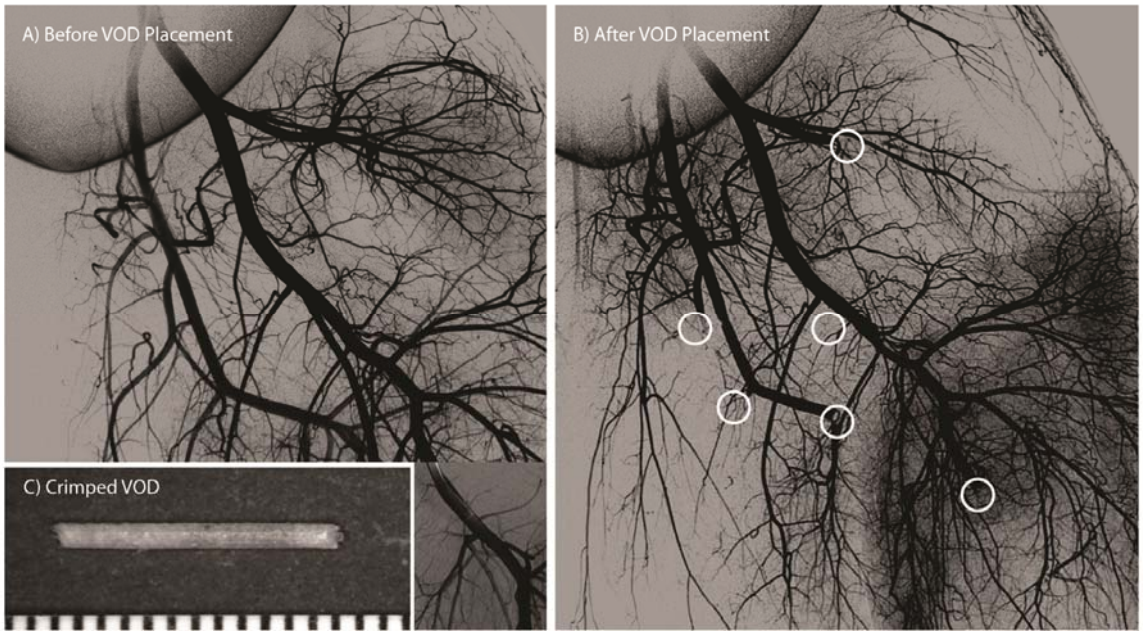

Figure 29: Angiograms acquired (a) before implantation of the SMP foam VODs and (b) after vessel occlusion occurred. A separate angiogram showing the distal portion of one of the treated vessels is overlaid in (a). White circles indicate the locations of the SMP foam VODs in (b). (c) Compressed vascular occlusion device (scale divisions in mm).

We developed a method for non-destructive mechanical reticulation of ultra-low density SMP foam by using a gravity-driven floating nitinol pin array coupled with vibratory agitation of the foam. Appropriate pin masses and agitation amplitude were identified to enable the desired level of reticulation. We focused on mechanical reticulation in different axes, versus changing the pin density of the array, to adjust the level of reticulation, and investigated chemical etching of the materials post reticulation.

Overall, mechanical reticulation resulted in a reduced elastic modulus, but did not impede shape memory behavior as demonstrated by the in vitro delivery and in vivo occlusion tests. The modulus was lower for foams reticulated in multiple axes compared to a single axis. Supplemental chemical etching was not mechanically detrimental and for the axial cases tended to slightly increase the elastic modulus.

The reticulated VODs were capable of achieving rapid vascular occlusion in an in vivo porcine model, indicating that SMP foam could be used as a device not only to fill aneurysms, but to also occlude patent vessels under arterial pressure. It was shown that on average the less reticulated the VOD, the faster the occlusion time. However, further study is needed to definitively conclude that occlusion time is affected by level of reticulation. While we hypothesize that predominantly open-cell foams may enhance the aneurysm healing response compared to predominantly closed-cell foams due to the increased pathways for blood flow and cell migration, further work must be done to assess the healing response of reticulated foams.

5. 4D FLOW VISUALIZATION AND POROUS MEDIA PROPERTIES OF MECHANICALLY RETICULATED SHAPE MEMORY POLYMER FOAM

5.1 Overview

Intracranial aneurysms, an unstable dilation of an artery within the brain that are prone to rupture. Upon rupture they have debilitating or mortal consequences to the patient. We have proposed an alternate endovascular filling method to the currently used platinum coils; based on shape memory polyurethane polymeric foams. Promising pathological results have resulted from the implants of these materials *in vivo* at ninety days within a porcine animal model. These blown foams are natively closed cell, which is not advantageous for proper healing *in vivo* or for fluid dynamics characterizations. In an effort to increase permeability of this porous media we previously developed a mechanical reticulation system to disrupt the membranes. These advances in material processing and previously reported promising pathological results have increased the desire to determine the fluid and foam structure interactions. We have used mechanical reticulation and chemical etching to vary the permeability of these materials and characterized them. We have estimated the structure of the blown foams to determine surface area, porosity and aspect ratio based on location within the batch. We have further imaged flow patterns, via MRI imaging, and have measured the porous media properties of these foams in an effort to further understand the physics of the fluid and foam. This research is an initial step toward understanding the foam and fluid

interactions *in vivo* and provides a better understanding of the structure of these heterogeneous materials.

5.2 Introduction

5.2.1 Cerebral aneurysms and subarachnoid hemorrhage

5.2.1.1 Current treatments and limitations

The current treatment for intracranial aneurysms involves either platinum clipping of the sac or endovascular filling involving mostly platinum coils. Surgical clipping involves an invasive craniotomy, with inherent risks of its own, and therefore endovascular methods have become the favored option for treatment. Treatment with platinum coils involves filling the aneurysm sac via the aide of fluoroscopic imaging. Platinum coils are implanted until there is a lack of contrast agent present within the dome after an injection is made to the site. This methodology usually results in low packing of the dome, but thus far is the standard for implantation. Along with low packing density of the aneurysm dome, there are other drawbacks with the use of platinum coils to treat these malformations within the brain.

Platinum coils have the tendency to compact or migrate from the site of implantation. These two complications can result in the reformation of sidewall aneurysms, recanalization of the original aneurysm, or potential blockage of the parent vessel. There also remains the possibility that the platinum coils can puncture the unstable dome either during or after treatment, resulting in a catastrophic event. In addition to the previously mentioned drawbacks, aneurysms that remain treated also have the tendency to remain in constant state of inflammation which never results in

healing; such a state would be indicated by a constant cycle of breaking down and reforming of an unstable fibrin layer on the platinum coils. With the limitations of the currently available treatment methods, we have proposed a polymeric based alternative method for filling the aneurysms. Of note, there are other polymer based and hybrid devices that are either on the market or are being developed for the treatment of aneurysms, however this paper will focus on a polymer based foam treatment.

5.2.1.2 Proposed treatment of intracranial aneurysms by SMP foams

We have proposed to treat intracranial aneurysms with shape memory polymer foams. These materials are based on polyurethane chemistry, previously reported by Singhal, et al.[85] They are blown foams that are foamed into closed cell morphology. With the aid of mechanical reticulation and caustic etching[78], the pores can be interconnected for the passage of fluids, such as blood. After processing the material is said to be in its permanent shape. These materials have the ability to be programmed into a different shape other than their permanent shape, a temporary shape, and remain in this condition until they are exposed to a stimulus, which raises their bulk temperature above their transition temperature. Programming involves raising the temperature of the material above its transition temperature, and then deforming the material by application of a force. To finish the programming process the material is constrained in a temporary shape while cooling the material below its transition temperature. Once the temperature is below the transition temperature the material will remain in this shape. These properties along with demonstrated in vivo biocompatibility[77]at ninety days, make these materials ideal for the development of an endovascular aneurysm filling method.

5.2.2 Necessity of characterization of SMP foam for prediction of fluid interaction in vivo

The previous implantations of these materials within the porcine aneurysm model has demonstrated that these materials induce favorable conditions for healing[77] and that they promote clotting within minutes of exposure to blood *in vivo.*[78] Therefore, further characterizations of these materials through a thorough study of their *in vitro* fluid interactions are advantageous for further understanding of the occlusion process. There are multiple factors that may be initiating the clotting process *in vivo*. By studying the fluid interaction with these porous media, we hope to better elucidate some of the processes and form some general knowledge of what is occurring *in vivo*. For example, dwelling time within the foam and shear rates have been shown to affect the clotting cascade in vivo. Understanding the porous media properties and fluid dynamics of these materials at varying amounts of reticulation may help in the future design of these materials as occlusion devices.

Previously, it has been shown that within an artery of a patient having a basilar artery aneurysm, the mean blood velocity in the parent vessel is between 20 and 50 cm/s to 10 to 30 cm/s.[53] In 2013, Ortega et al., has performed CFD simulations within SMP foam treated aneurysms and has shown that velocities within the foam are much lower than the previously values reported.[70] Due to these findings, we find it necessary to quantify permeability and average velocity flows in lower velocity ranges from 0 to 7 cm/s to better help validate our previous work on simulations. Further validation of observing low velocities via permeability and magnetic resonance velocimetry (MRV)

comes from previous work performed by Small et al. in 2009. It was shown that the velocity of the fluid within the foam increased and was significantly decreased distal to the foam when observed via MRV.[86]

5.2.3 Permeability

The previously reported method for mechanical reticulation involved the use of individual nitinol pins that were able to penetrate the foam via agitation and gravity. These pins were patterned in a matrix that had a set distance of pins, which was used in a raster manner to reticulate in one or three axes of the foam. This method enabled the amount of reticulation of these foams to be varied. The pin punching density can tune the resultant amount of fluid allowed to pass through. This ability for fluids to pass through a porous material is called permeability or the pressure drop across the material, which can be measured experimentally by varying the velocity of the fluid. Further analysis of these foams can estimate the viscous and inertial losses of the pressure drop via the Forchheimer-Hazen-Dupuit-Darcy (FHDD) equation:

$$\frac{-\partial P}{\partial x} = \frac{\mu}{K} v_o + \rho C {v_o}^2$$

where the pressure gradient, $\frac{-\partial P}{\partial x}$, along the sample in the direction of flow (Pa/m), μ is the dynamic viscosity of the fluid (Pa · s), K is the intrinsic permeability of the sample (m^2), v_o is the Darcy velocity (flow rate, Q, divided by cross-sectional area of the sample) (m/s), ρ is the density of the fluid (kg/m3), and C is the form factor of the sample (m^{-1}). When the velocities of the flow are low, at Reynolds numbers less than 1, the FHDD equation reduces to the Darcy equation.[4]

The Reynolds number can be estimated from the previous equation as:

$$\mathrm{Re} = \frac{\rho \nu_o KC}{\mu}$$

which is a ratio of the forces contributed via inertial losses to the losses from the viscous forces.

The friction factor can be determined via non-dimensionalization of the FHDD equation by $C\rho v_o^2$.[65]

$$\frac{-dp/dx}{C\rho v_o^2} = f = \frac{1}{\mathrm{Re}} + 1$$

in which the left hand side of the equation are the calculated terms based off of measured values and the right hand side of the equation is the theoretical model for the friction factor. Via the Reynolds number and friction factor, data from the experimental results of this study can be compared to previous or future data. In addition to the porous media properties determined from permeability measurements, it is also possible to visualize the flow within these reticulated foams via magnetic resonance imaging (MRI) or more specifically magnetic resonance velocimetry (MRV).

5.2.4 MRV measurements

Magnetic resonance velocimetry (MRV) is a non-invasive and non-destructive method for measuring three dimensional mean velocity components within an object via traditional MRI or nuclear magnetic resonance (NMR). These imaging methods can be used on complex and opaque models, making this method potentially superior to the traditional particle image velocimetry (PIV) method. MRV can be used to measure a

one, two or three-dimensional space within a model at a range between 10^1 and 10^3 μm.[28] In addition to mean velocities, MRI can be used to measure temperature[86], velocities of turbulent flow, Reynolds stresses, diffusion coefficients, chemical species, and the presence of multiple phases.[28] MRV is capable of measuring velocities between 10 m/s to 1 cm/day, or 1.2 x 10^{-7} m/s.[28] Imaging of one dimensional images takes mere minutes to measure, while three dimensional volumes can take a couple of hours, with conventional scanners able to image sub millimeter resolution having a diameter of 30 cm.[28]

Previously, MRV imaging was used to measure temperature and mean velocity flows within an SMP foam device while it was actuated via laser light heating.[86] However, this data was to observe the actuation of a slightly oversized device (~ 4 mm) in small diameter tubing of 2.5 mm for the testing and optimization of medical device design using similar materials. In this paper, we propose to use MRV to further characterize SMP foams that have had differing amounts of mechanical reticulation. We would like to determine if MRV is a way to visualize and quantify the average velocity vectors within SMP foams that are of different formulations and morphology of SMP foam as a way to optimize these materials.

Velocity encoding involves utilizing the local spin magnetization, a vector quantity, as a way to measure flow. By obtaining magnitude and phase data from velocity encoding gradient acquired MRI imaging, the velocity of a fluid may be determined by subtracting the two set of phase images while the magnitude data can be used as a mask. Two sets of phase data are acquired during the application of inverted

gradients, the usual method for encoding velocity, which results in two image sets with different first moments, ΔM_1, or $M_1^{(1)}$-$M_1^{(2)}$, that are proportional to the amplitude and timing of the gradient. Subtraction of the two phase images results in phase differences $\Delta\Phi$ that are proportional to the velocity of the fluid. By Fourier reconstruction the MRV signal is resolved into phase and intensity data as a function of location. The spatial velocities are determined by dividing the pixel intensities in the phase difference images by $\boldsymbol{\gamma\Delta}$M, where the velocity sensitivity, or venc, is the maximum velocity.[58] The average velocity of the fluid is calculated through the following equations:

$$v = \Delta\Phi/(\Upsilon\Delta M_1) = (\Delta\Phi/\pi)*\text{venc}$$

$$\text{venc} = \pi/(\Upsilon\Delta M_1)$$

$$\Delta\Phi = \pm\pi$$

where v is the velocity (m/s), $\Delta\Phi$ is the phase difference, ΔM_1 is the difference in the first moments, venc is the maximum velocity in m/s and γ is the gyrometric ratio. Imaging flow within the foam via clinical imaging methods can be achieved is a pulse sequence, 4D Flow, which acquires the difference in phase in X, Y, Z.[59]

5.2.5 Significance of these characterizations

Four samples of SMP foam measurements are capable of acquiring data about the fluid flow within a complex model; it provides limited information about pressure.[29] Therefore, permeability measurements via traditional methods are necessary in order to determine the form factor (C) and permeability (K) values of a material. Additionally, MRV measurements could potentially be used to validate computational fluid dynamics (CFD) predictions and the measured permeability along with surface area results can be

used to fine tune the current models used to simulate fluid flow through SMP foam.[67, 69, 70]

5.3 Materials and methods

5.3.1 SMP fabrication

The foams used for this study were based off of 80TM SMP chemistry reported by Singhal, et al., in 2013.[84] This foam was mechanically reticulated in a similar manner as reported by Rodriguez et al., in 2014[78], which had a hole punching density of approximately 13% per face punched, (12.9717mm²/100 mm^2). There were nine cases of foam that were made for this study based on different levels of reticulation, or removal of membranes between individual pore cells, which are summarized in Table 5.

5.3.2 Permeability and imaging foam sample fabrication

These samples were core punched into cylindrical samples that were approximately 17 mm in diameter and 20 mm in length parallel to the axis of foaming. After mechanical reticulation these samples were affixed into acrylic sample holders that were 19 mm OD, 16 mm ID and 30 mm in length, with UV cured medical grade epoxy (Dymax Corporation, Torrington, CT). The foam was lined up with the proximal end of the sample holder to leave 1 cm open on the distal end and were compressed by approximately 9.1% within the sample holder. The acrylic sample holders were fashioned with custom silicone gaskets on both ends to ensure flow through the sample during measurements. These gaskets were made of 0.015” thick soft silicone rubber with

Table 5: Samples prepared for the study. Axial cases gram weight indicates the mass used to reticulate in the Z-axis. Tri axial cases list gram weight of the Z-axis reticulation first and the Z-X and Z-Y axes second.

Designation:	Mechanical Reticulation:		Chemical Processing:
Case #	Axial Mass	Trans Axial Mass	10% vol. NaOH Etch
1	1g	n/a	No
2	1g	n/a	Yes
3	1g	1g	No
4	1g	1g	Yes
5	2g	n/a	No
6	2g	n/a	Yes
7	2g	1g	No
8	2g	1g	Yes
9	n/a	n/a	No
	Axial Punching		
	Tri Axial Punching		
	Control, no mechanical reticulation		

a durometer hardness of 20A that were cut to size with a Gravograph LS100, CO^2 laser etcher (Gravograph, La Chapelle-Saint-Luc, France). These gaskets were then adhered to the ends of the sample holders with silicone adhesive.

Samples were then either cleaned or base etched and cleaned. Cleaning was achieved with soap solution consisting of (80:20) RO water and Contrad 70 solution, (Decon Labs, Inc., King of Prussia, PA), and agitated via sonication for 30 minutes. Base etching was achieved via 5N NaOH solution for 30 minutes with sonication.[78] These different cases are called case 1-9 for the remainder of this paper (Table 5), with case 9 being the control group. After processing the samples were then placed in water and evacuated in a bell jar eight hours to remove bubbles from the samples.

5.3.2.1 Foam characterization

After mechanical reticulation and etching the samples were characterized via multiple imaging methods and their porosity, relative density, major diameter, minor diameter, aspect ratio, surface are and expansion ratio were estimated based on their location within the foam. The nine cases of foam that were characterized in this paper were imaged via scanning electron microscopy on a NeoScope JCM-5000 (Jeol USA, Inc., Peabody, MA) after the samples were sputter coated with gold using a Cressington 108 sputter coater, model 6002-8 (Ted Pella, Inc., Redding, CA) for 60 seconds at a distance of 3 cm. SEM imaging of the foams allowed for visualization of the amount of membrane removal for the nine cases. Micro computed tomographic (μ-CT) imaging was performed using an Xradia scanner, using a 4X objective, set at 50kV, and 5W, and

reconstructed by the Xradia Reconstructor having a 5.96 μm/voxel for 800 slices on two foam samples.

Additional characteristics of the foam were also calculated from the density of the neat polymer (1.1 g/cm^3) and measurements from microscopy images.[84] The relative density of the foam (ρ_{porous}) was calculated from the mass of a known volume of foam. The porosity, Θ, of the foam, or void space within the foam, was measured and determined via the equation:

$$\Theta = (\rho_{neat} - \rho_{porous})/ \rho_{neat}$$

The volume expansion of the foam, or how much the foam can be compressed, was determined via the equation:

$$VE = \rho_{neat}/ \rho_{porous}$$

The aspect ratio was determined via the equation:

$$AR = D_{major}/D_{minor}$$

where D_{major} is the larger diameter and D_{minor} is the smaller diameter. Aspect ratio was determined after measurements were made from pore cells in different areas of the foam via microscopy. These values were used to determine the approximate surface area from 3 dimensional 12 faced pentagonal and 14 faced hexagonal models. From these 3D models surface area and volume of one pore was determined.

Surface area of the foam was approximated using the following relationships:

$$\Theta = (\rho_{neat} - \rho_{porous})/ \rho_{neat} = (V_{total} - V_{foam})/V_{total}$$

where Θ is the porosity, V_{total} is the total volume and was assumed to be 1 cm^3 and V_{foam} is the volume taken up by the struts and membranes of the foam. V_{foam} was

approximated using the following equation:

$$V_{foam} = V_{total} - (N_{pores} * V_{pore})$$

where N_{pores} is the number of pores within 1 cm^3 and V_{pore} is the volume of one pore estimated from the 3D models. N_{pores} was approximated using the following equation:

$$N_{pores} = (\Theta / V_{total}) / V_{pore}$$

Which resulted in the following equation for surface area:

$$SA_{foam} = SA_{pore} (\Phi / V_{pore})$$

where SA_{foam} is the surface area of the foam and SA_{pore} is the surface area of one pore. Characterization of the structure of the foam by the previous mentioned methods allowed for the surface area of the foam based off of location within a batch to be estimated. These estimates along with permeability measurements further elucidate the foam and fluid interaction necessary for CFD validation and refinement.

5.3.3 Permeability flow loop

The nine cases of samples (n = 3 per case) having varying densities were evacuated overnight to remove air bubbles from the samples and were then placed within the pressure chamber in the flow loop, diagramed in Figure 30. The pressure drop across the foam was measured by an increase in flow rates to determine the permeability. The flow rates measured ranged from 0 to 850 ml/min, or Darcy velocities between 0 to 0.071 m/s for each of the samples. Three types of pressure transducers were used for these measurements: 1) 0-10 inches of water differential pressure transducer (model #

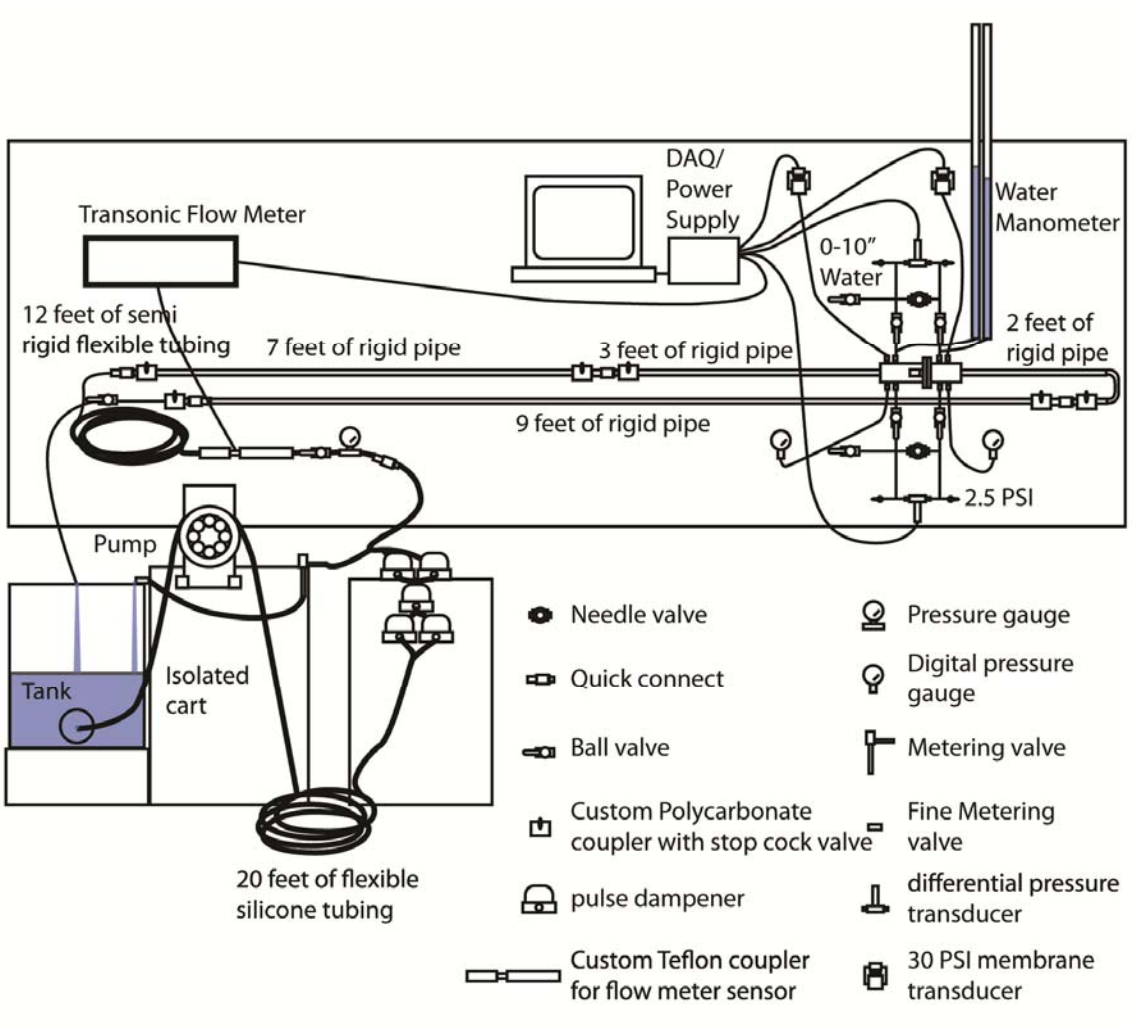

Figure 30: Diagram of the permeability setup.

PX409-10WDWUV) 0.08% of range accuracy (Omega Engineering, Inc., Stamford, Connecticut), 2) 2.5 PSI differential pressure transducer (model # PX409-2.5WDWUV) 0.08% of range accuracy, (Omega Engineering, Inc., Stamford, Connecticut) and 3) 30 PSI absolute membrane pressure transducer (model PXM42MG7-400MBARGV) 0.25% of range accuracy (Omega Engineering, Inc., Stamford, Connecticut). In addition to the pressure transducers, a set of two rigid tubes were fashioned as a water manometer and a set of digital 30 PSI pressure gauges (Dwyer Instruments, Michigan City, IN) (Model: DPGWB-06) with 0.01 of range resolution, were used to determine the maximum pressure differential of the highest flow prior to measurement with the transducers (Figure 31).

The pump consisted of a Verderflex® Smart, (Verderflex, England, U.K.) L20 series, peristaltic pump equipped with a non-standard six head roller on an isolated cart, for reduction of pulse within the system. In addition to the six head roller, 20 feet of large diameter (12.7 mm ID and 15.875 mm OD) flexible silicone tubing was placed after the pump just before five pulse dampeners. After the pulse dampeners, there was an additional 12 feet of semi-rigid flexible tubing (12.7 mm ID and 19.1 mm OD) and subsequently ten feet of rigid tubing (15.875 mm ID and 19.05 mm OD) before the pressure chamber. A flow meter probe, attached to a small animal blood flow meter (model number T206) (Transonic Inc., Ithaca, NY) was placed after the five pulse dampeners to quantify the pulse within the system and for flow rate measurements. In an effort to further reduce the pulse of the system seen by the sample, the tank was also isolated on its own cart.

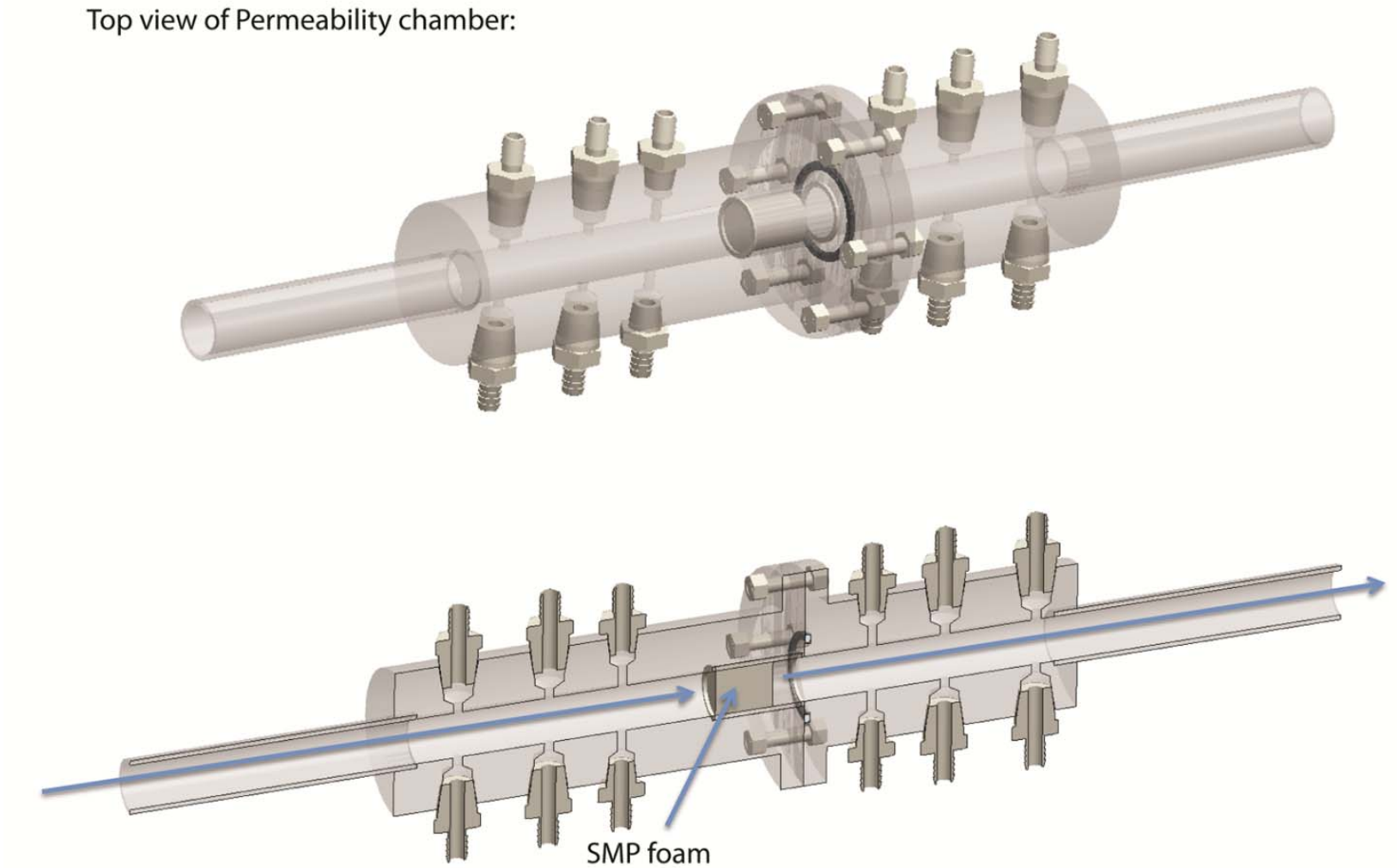

Figure 31: Close up of the permeability measurement chamber and sample holder.

5.3.4 MRI Flow loop

The MRI flow loop was similar to the permeability setup, as far as length of tubing in the system prior to and after the sample holders (Figure 32). However, the MRI setup consisted of rigid tubing after the flow meter and just before the tank and the chamber was different. All magnetic components were at least twenty feet from the bore of the MRI. All other materials less than 20 feet from the system were composed of polymer, nylon, rubber, silicone or fiberglass to ensure compatibility with the MRI (Figure 33). The sample chamber (Figure 34), allowed for the same samples that were measured via permeability to be imaged.

5.3.5 MRI imaging

MRI phase contrast imaging was performed on a MAGNETOM Verio 3T (Siemens, Malvern, PA) clinical imaging scanner, using the 4D Flow pulse sequence [59], written by Markl, et al. This sequence is based off of a FLASH sequence and a modified ICE reconstruction program. Scan parameters were: TE 6.445 ms, TR 37.6 ms, and a flip angle of 15˚. In plane VENC 0.30 m/s, Through-plane VENC 0.30 m/s, Echo Spacing of 9.40 ms, min rise time of 10 ms, FOV 70 mm, Resolution of 0.5 x 0.5 x 0.5 mm^3, a Bandwidth of 450 hz/pixel, one slab with 72 slices and a scan time of 1 hour and 52 minutes and a distance factor of 20%, and 32 averages per scan. A solution of water and copper sulfate 1% by volume was used to increase contrast of the images. The images were based off of T1 contrast due to a short TR and short TE of the scan. Two additional samples were imaged using the same parameters as stated with a larger of slab thickness of 120 slices equivalent to 6 cm.

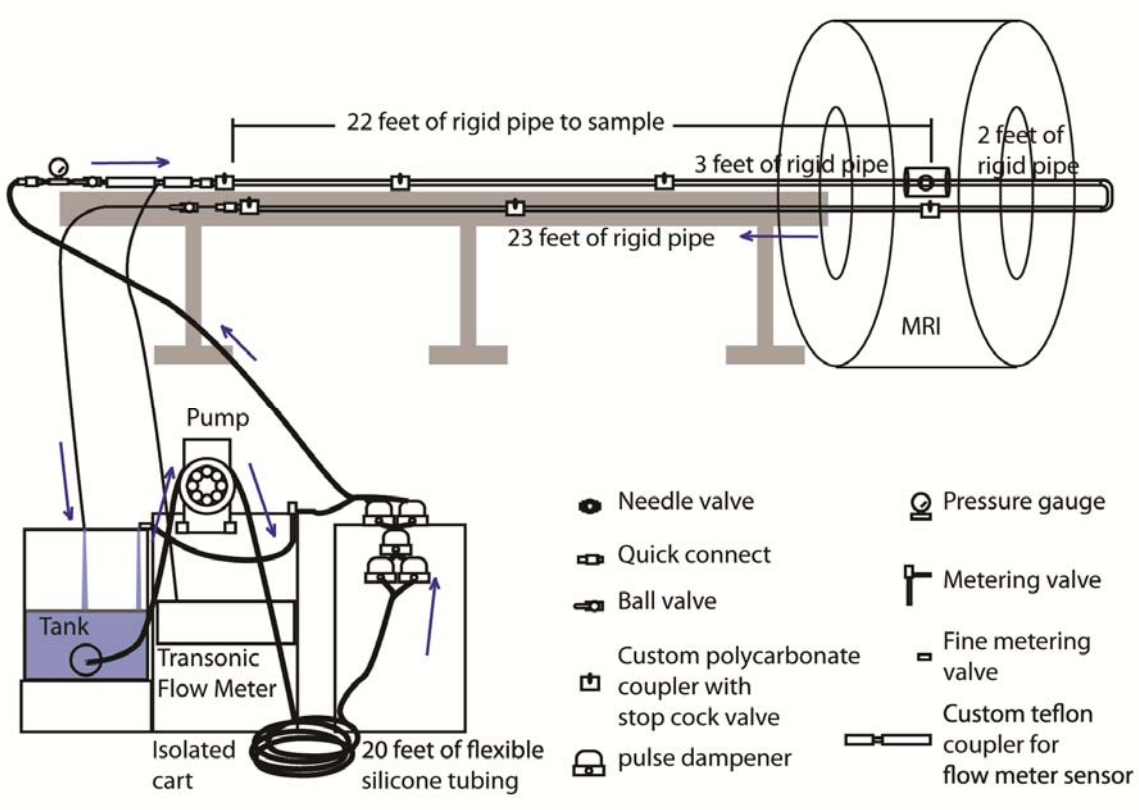

Figure 32: MRI flow loop.

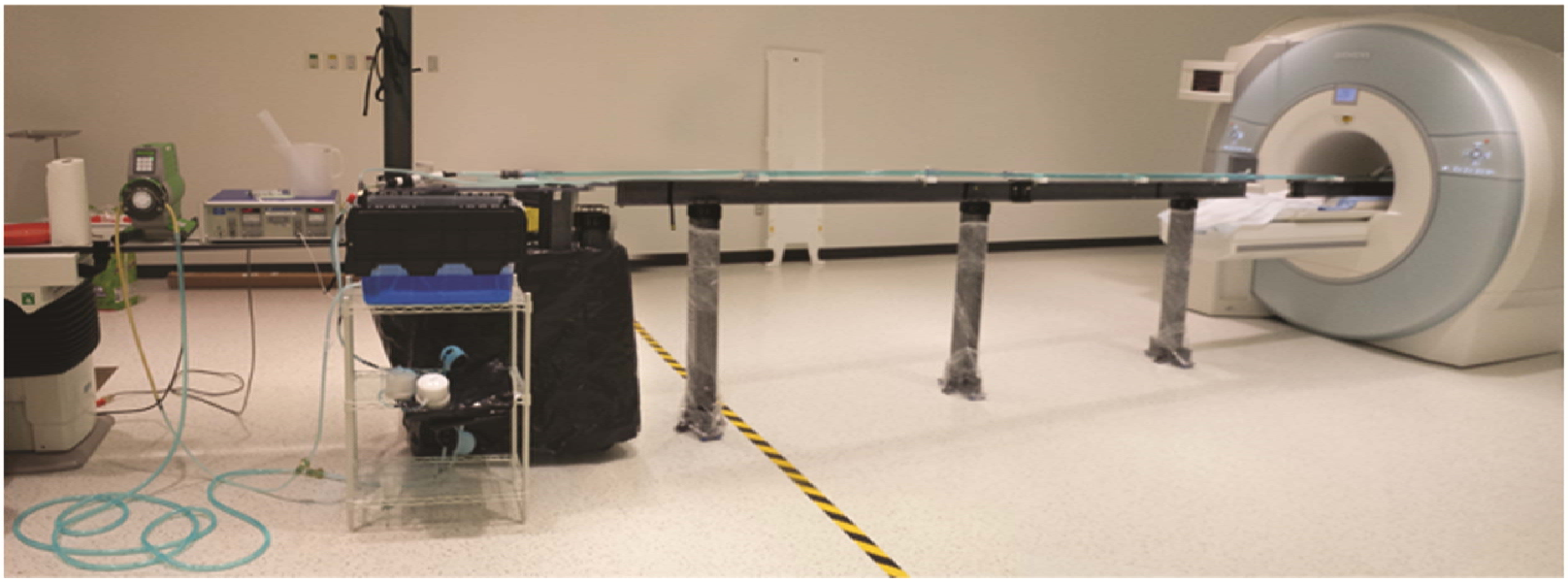

Figure 33: MRI setup.

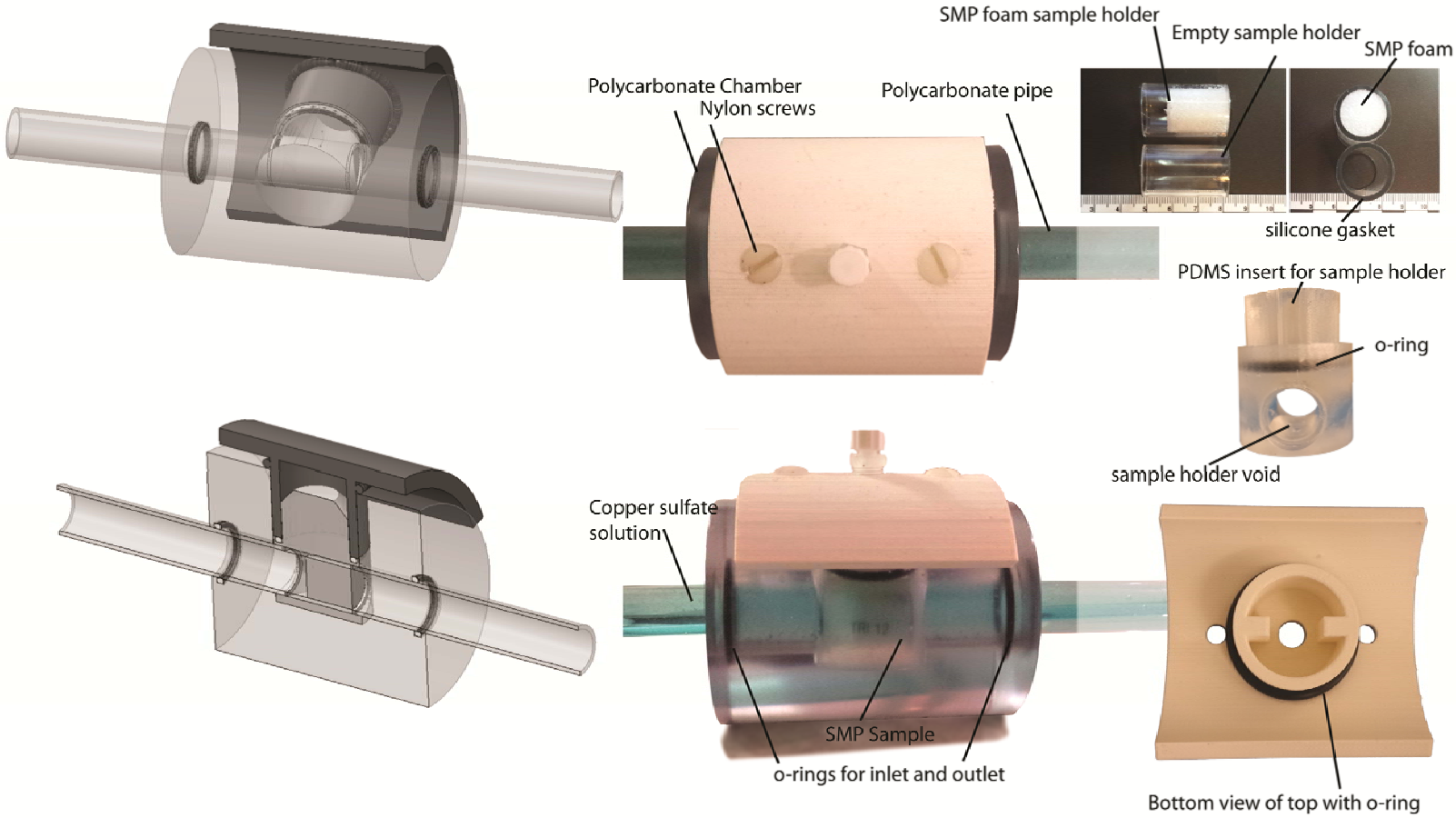

Figure 34: Close up of MRI measurement chamber.

Four samples of SMP foam and an empty chamber were imaged using the previously stated parameters at 400 and 800 ml/minute that resulted in Darcy velocities of 0.0334 and 0.0668 m/s respectively. The four samples chosen for imaging represented permeability and densities that were from the mid areas of the foam. All image sets were processed via Matlab (MathWorks®, Natick, MA) and viewed in Tecplot (Tecplot®, Bellevue, WA).

5.4 Results

5.4.1 Foam characterization

Figure 35 is a summary of SEM images of the amount of reticulation of the samples that were characterized in this study. The average density of the porous material was measured to be 0.013 ± 0.001 g/cm^3, with average porosity of the material was calculated via equation, $\Theta = (\rho_{neat} - \rho_{porous})/ \rho_{neat}$, to be 98.82% and the volume expansion of the foam was determined to be 85 X for 33 samples measured. As these are non-homogeneous blown foams, the densities, porosity, expansion ratio, aspect ratio and surface area were characterized for location within the batch were also measured and included measurements from the center, mid and outer portions of the foam (Figure 36 and 37). The densities were 0.012 ± 0.001, 0.013 ± 0.001, and 0.014 ± 0.001g/cm^3 for center, mid and outer regions of the foam respectively (Figure 36). The porosities were 98.93, 98.86 and 98.74% and the expansion ratios were 93.1, 87.4 and 79.1% from the center, mid and outer regions of the foam respectively (Figure 36). The aspect ratios for the center, mid and outer regions were 1.4, 1.7 and 2.5 respectively (Figure 36 and 38).

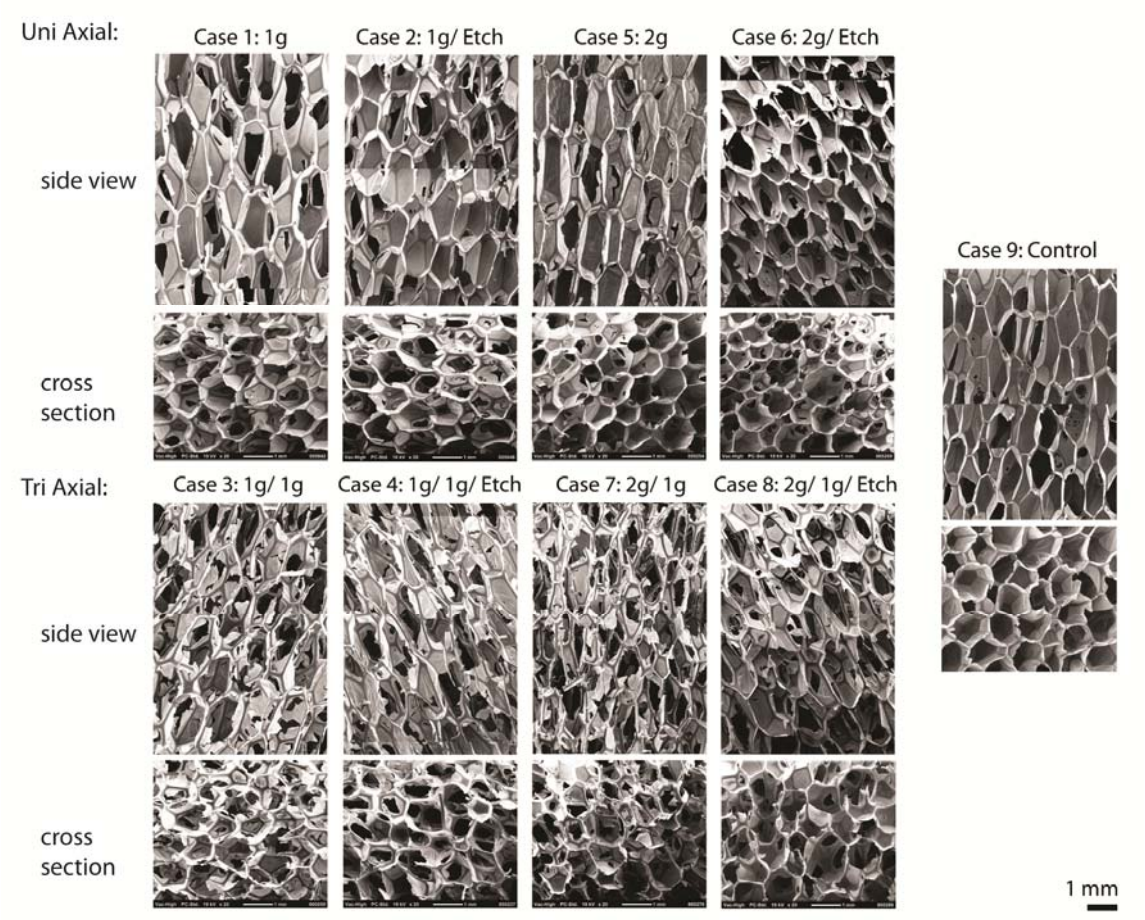

Figure 35: SEM imaging of mechanically reticulated SMP foam.

SMP Foam Region:	Center	Mid	Outer
Relative Foam Desity, g/cm^3	0.012 +/- 0.001	0.013 +/- 0.001	0.014+/-0.001
Surface Area, cm^2/cm^3	50.3 +/- 0.2	58.3 +/- 0.1	80.6 +/- 0.1
Pore Cell Volume, cm^3	0.989 +/- 0.177	0.989 +/- 0.100	0.987 +/- 0.117
Major DIA, mm	1.8 +/- 0.1	1.8 +/- 0.1	1.9 +/- 0.1
Minor DIA, mm	1.3 +/- 0.1	1.1 +/- 0.1	0.75 +/- 0.06
Aspect Ratio	1.4 +/- 0.4	1.7 +/- 0.3	2.5 +/- 0.5
Porosity, %	98.93 +/- 0.99	98.86 +/- 0.99	98.74 +/- 0.99
Expansion Ratio, (X)	93 +/- 3	87 +/- 3	79 +/- 2

Figure 36: Summary of foam characteristics for center, mid and outer regions of foam.

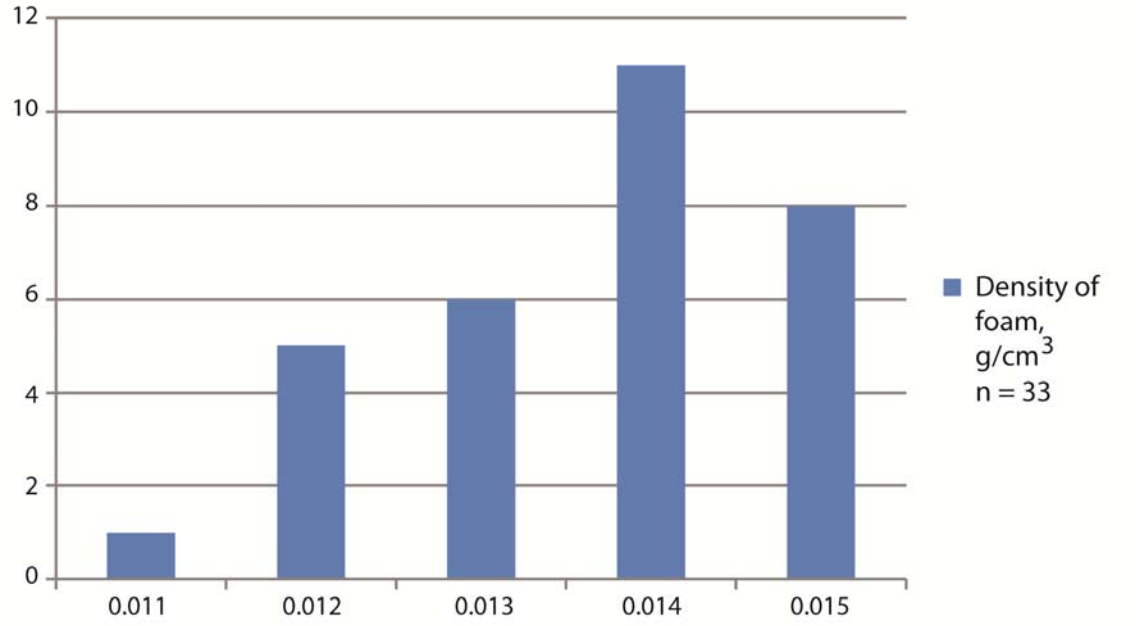

Figure 37: Histogram of density measurements of foam for total volume of foam.

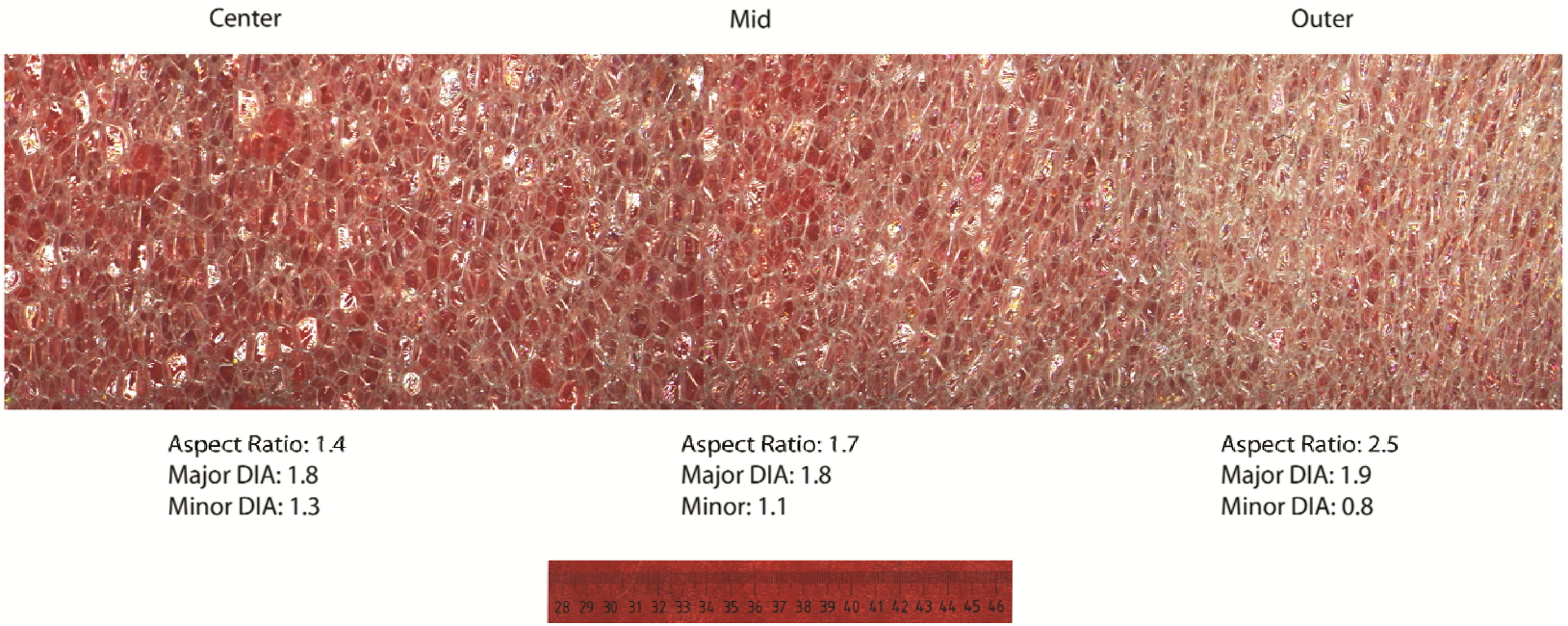

Figure 38: Example of the densification of foam from center to outer ring.

From micro CT (μ-CT) data the surface area of the struts of the foams were measured after the reconstructed data was made into a 3D model. The surface area of the struts of the foam was determined to be approximately 10 cm^2/cm^3. The struts were characterized via this method because the resolution of the μ-CT imaging was not high enough to capture membranes (5.96 μm/voxel resolution). The surface area was approximated via 3D hexagonal and pentagonal models that matched the major and minor diameters measured from microscopy images for the three regions (Figure 39). From these 3D models the surface area and volume of each pore was measured within Maya 2014 (Autodesk Inc., San Rafael, CA), a 3D software package. The number of pores per cm^3 was determined via subtraction of the sum of the pore volumes from total volume, such that the apparent density, mass and porosity of the modeled foam was equal to the measured apparent density of the foam from the three regions where the solid polymer has a density of 1.1 g/cm^3. Figure 36 is a summary of all of the foam characterizations that were made.

5.4.2 Permeability

All cases were graphed and fitted to the FHDD algorithm and are represented in figures 41, 43, and 45 and supplementary figures S1-9. The samples were also imaged via microscopy and are represented in figures 40, 42 and 44. The permeability of the control samples ranged from 1.1818 $x10^{-10}$ to 2.6815 $x10^{-10}$ m^2 and the form factor ranged from 1.096 $x10^6$ to 3.9582 $x10^5$ m^{-1} (Figure S1). The permeability of the 1 gram axially punched foam samples ranged from 1.6415 $x10^{-9}$ to 3.6668 x10-9 m^2 and the form factor ranged from 1.6744 $x10^4$ to 5.9197 $x10^4$ m^{-1} (Figure S2). The permeability of the 1 gram

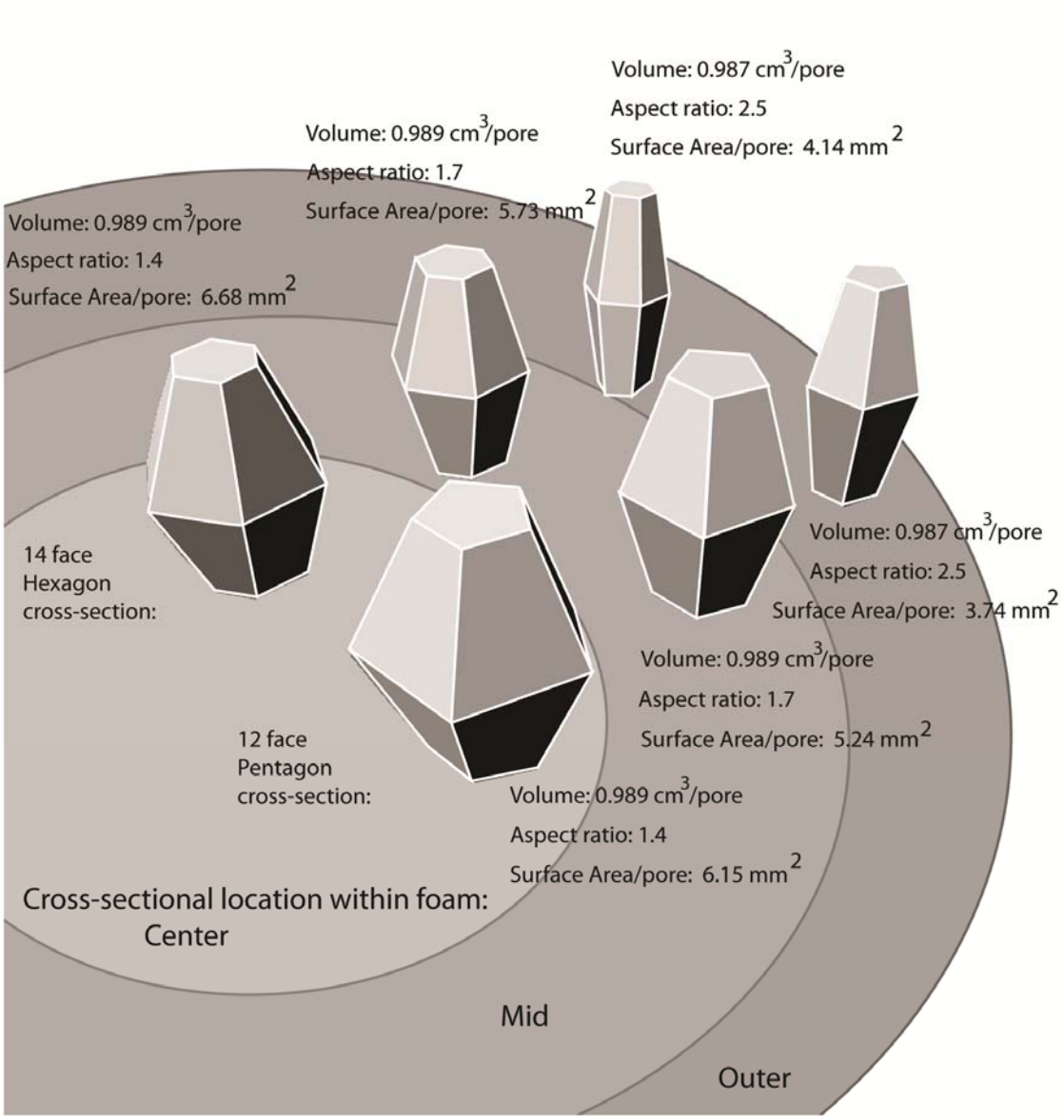

Figure 39: 3D models used to calculate surface area based off of aspect ratio measurements and morphology of the foams.

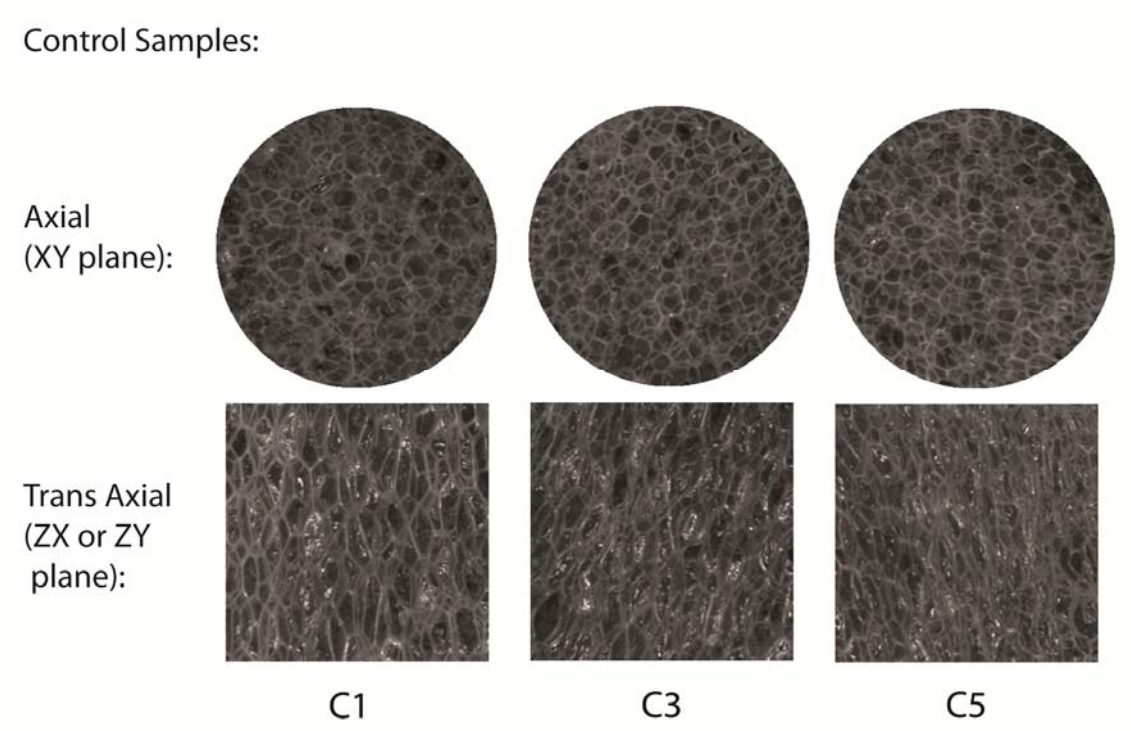

Figure 40: Microscopy images of the control samples.

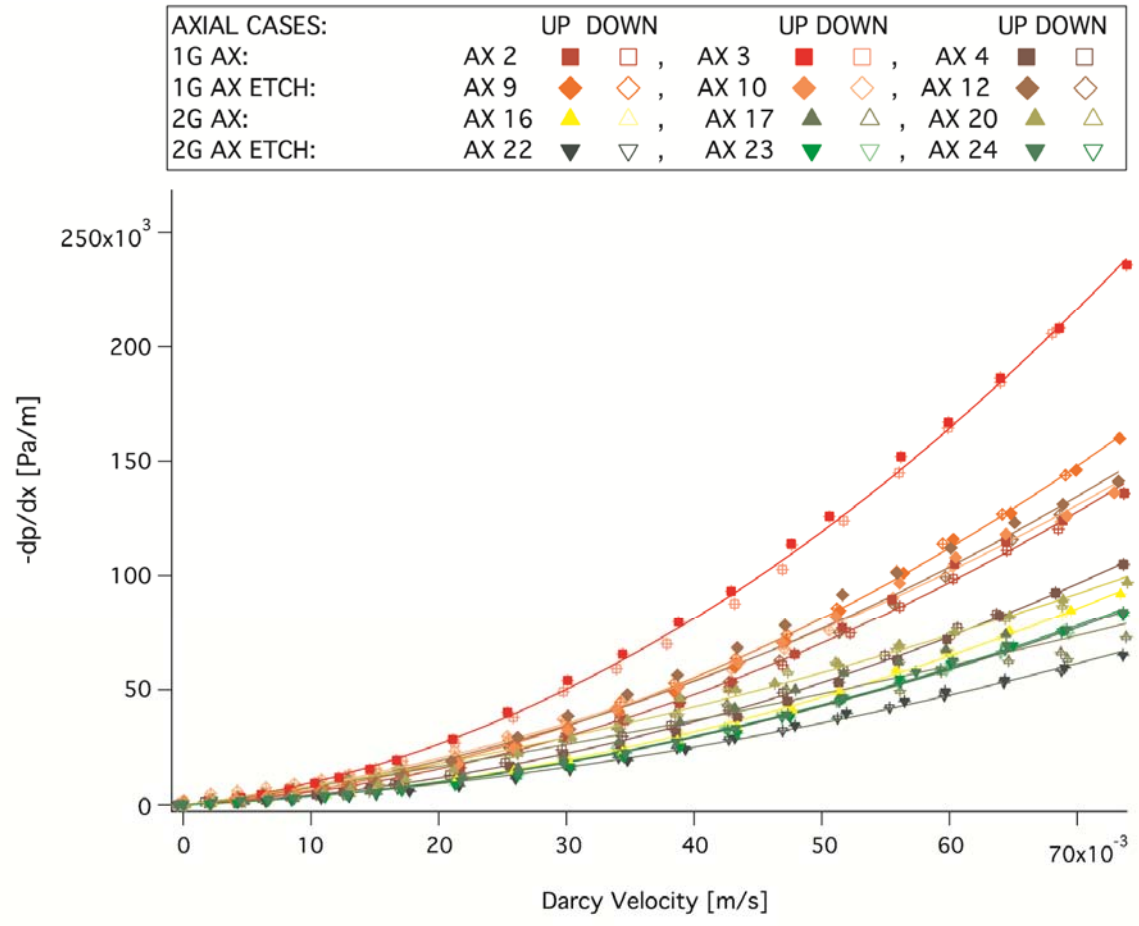

Figure 41: Permeability of all axial reticulated cases.

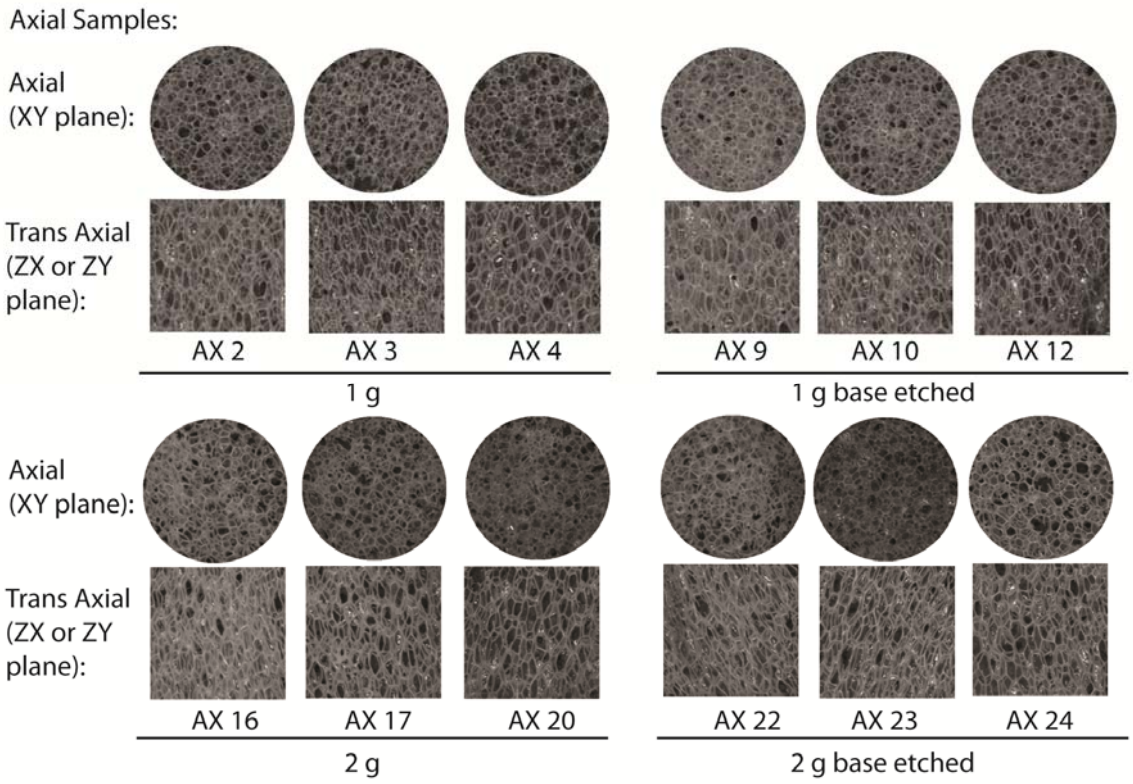

Figure 42: Microscopy imaging of all axial reticulated samples.

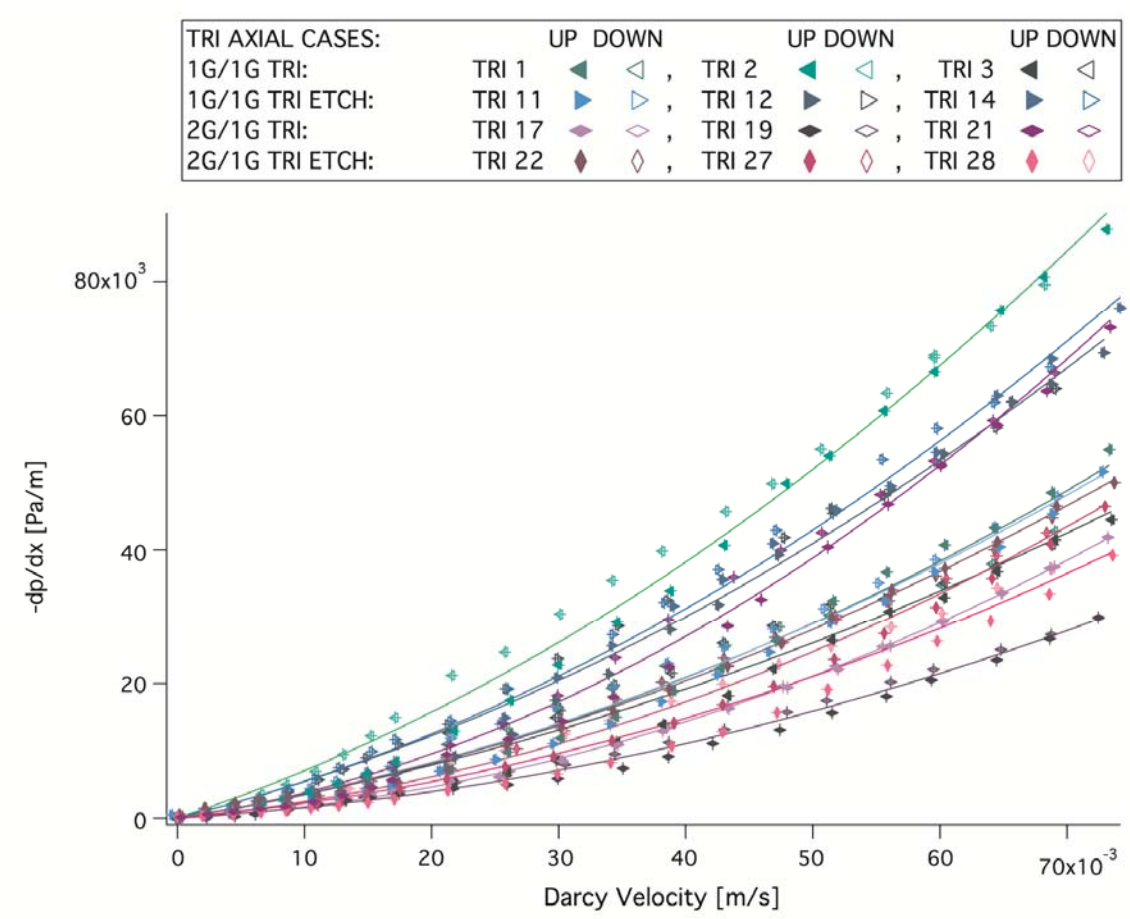

Figure 43: Permeability of tri axially reticulated cases.

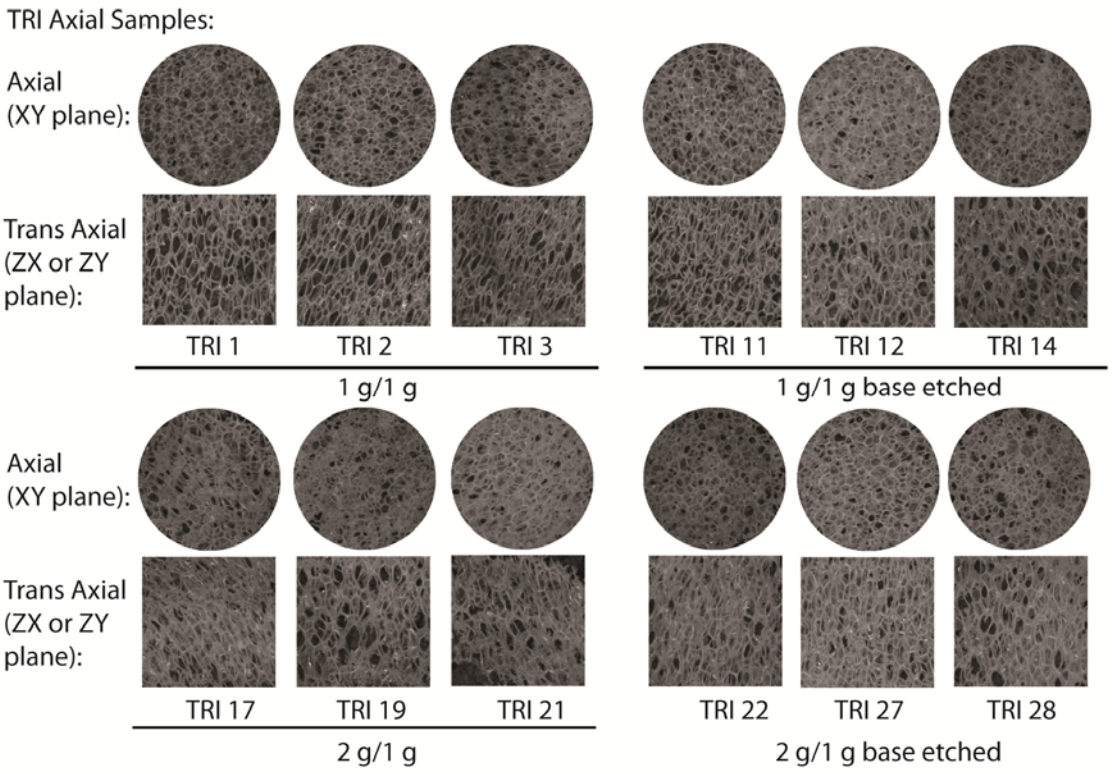

Figure 44: Microscopy imaging of all tri axially reticulated samples.

axially punched and base etched foam samples ranged from 1.50556 $x10^{-9}$ to 2.4589 $x10^{-9}$ m^2 and the form factor ranged from 1.8515 $x10^4$ to 2.5855 $x10^4$ m^{-1}(Figure S3). The permeability of the 2 gram axially punched foam samples ranged from 1.2924 $x10^{-9}$ to 4.5679 $x10^{-9}$ m^2 and the form factor ranged from 4.253 $x10^3$ to 1.5204 $x10^4$ m^{-1} (Figure S4). The permeability of the 2 gram axially punched and base etched foam samples ranged from 3.4054 $x10^{-9}$ to 4.1671 $x10^{-9}$ m^2 and the form factor ranged from 8.9562 $x10^3$ to 1.3153 $x10^4$ m^{-1}(Figure S5). Figures 41 and 42 are a comparison of all axial cases via microscopy and permeability. The permeability of the 1 gram/1 gram tri axially punched foam samples ranged from 1.6001 $x10^{-9}$ to 3.2762 $x10^{-9}$ m^2 and the form factor ranged from 4.6314 $x10^3$ to 5.9197 $x10^3$ m^{-1}(Figure S6). The permeability of the 1 gram/1 gram tri axially punched and base etched foam samples ranged from 2.1078 $x10^{-9}$ to 3.1708 $x10^{-9}$ m^2 and the form factor ranged from 5.7072 $x10^3$ to 8.3828 $x10^3$ m^{-1} (Figure S7). The permeability of the 2 gram/1 gram tri axially punched foam samples ranged from 3.5927 $x10^{-9}$ to 9.4619 x10-9 m2 and the form factor ranged from 4.2522 $x10^3$ to 1.0657 $x10^4$ m^{-1} (Figure S8). The permeability of the 2 gram/1 gram tri axially punched and base etched foam samples ranged from 3.2404 x10-9 to 5.8288 $x10^{-9}$ m^2 and the form factor ranged from 5.3521 $x10^3$ to 6.6565 $x10^3$ m^{-1} (Figure S9). Figure 43 and 44 summarizes the permeability and morphology of all of the tri axial cases. Figure 45 compares all cases on one graph. It was shown that all reticulated samples were an order of magnitude lower than the control samples in both permeability and form factor, which are summarized in figure 46 and 47 respectively. Figures 48 and 49 summarize the permeability and Form factor of the differently reticulated foams versus the idealized

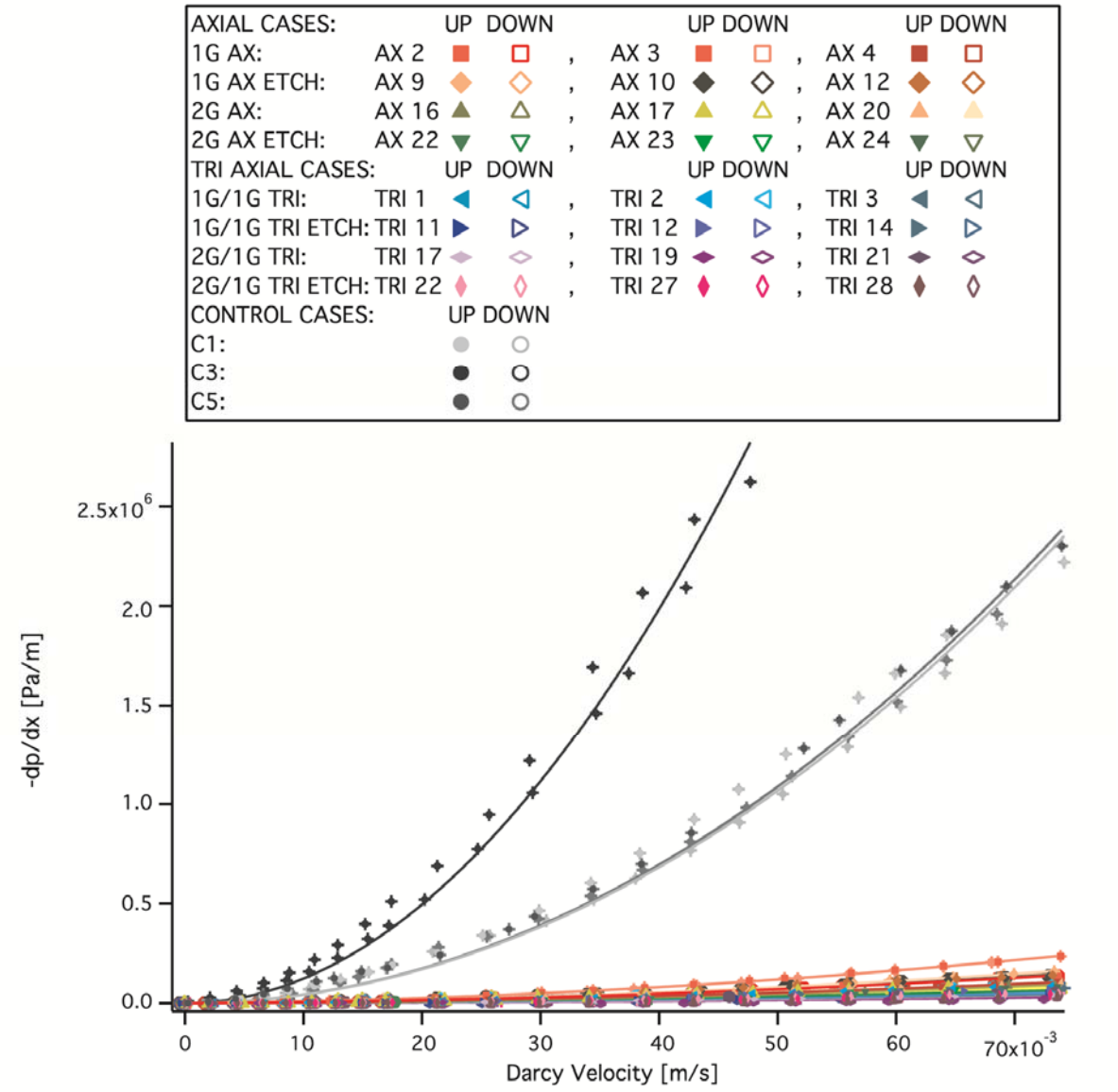

Figure 45: Permeability of all samples.

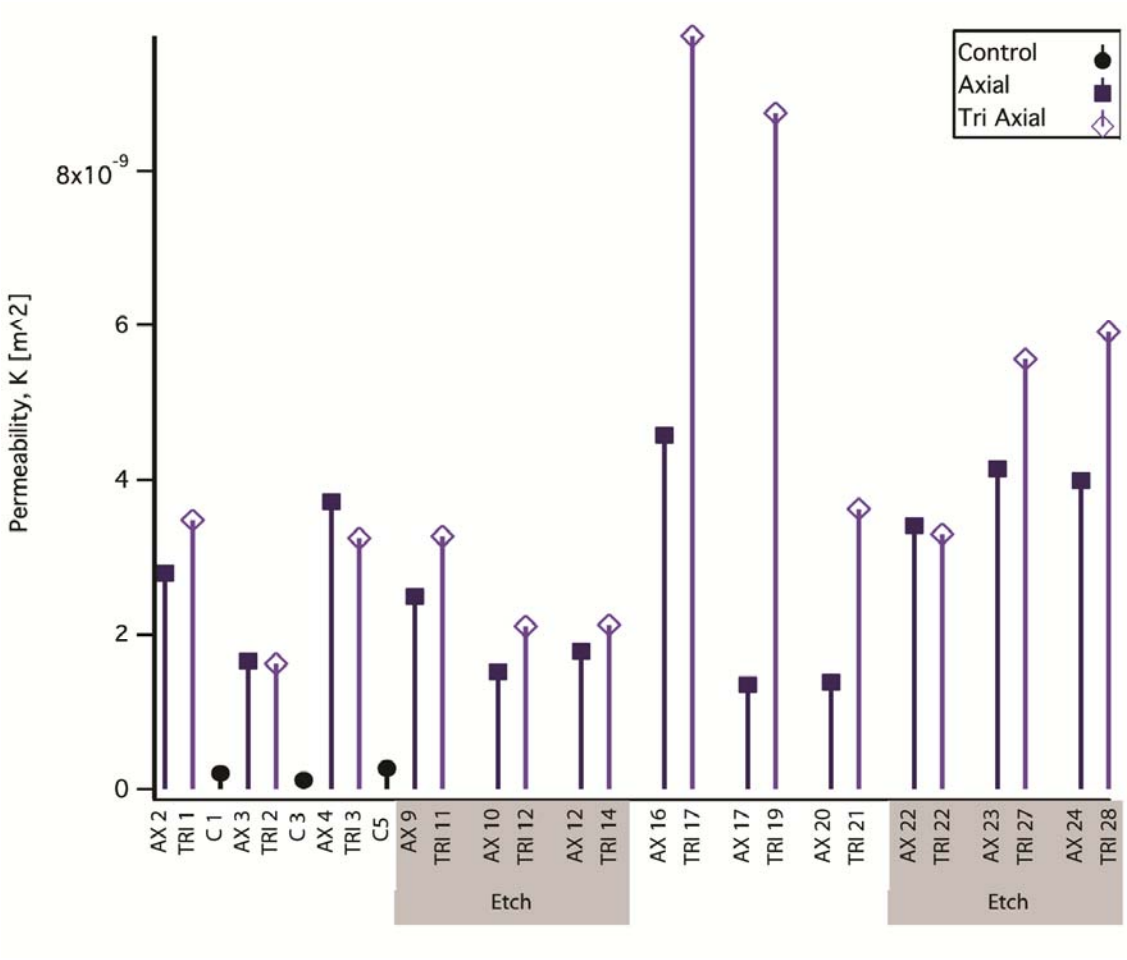

Figure 46: Permeability (K values) determined from FHDD fit of the measurements. Algorithm used to fit the K and C to the -dp/dx versus v curves gives a 95% confidence interval for the K and C values.

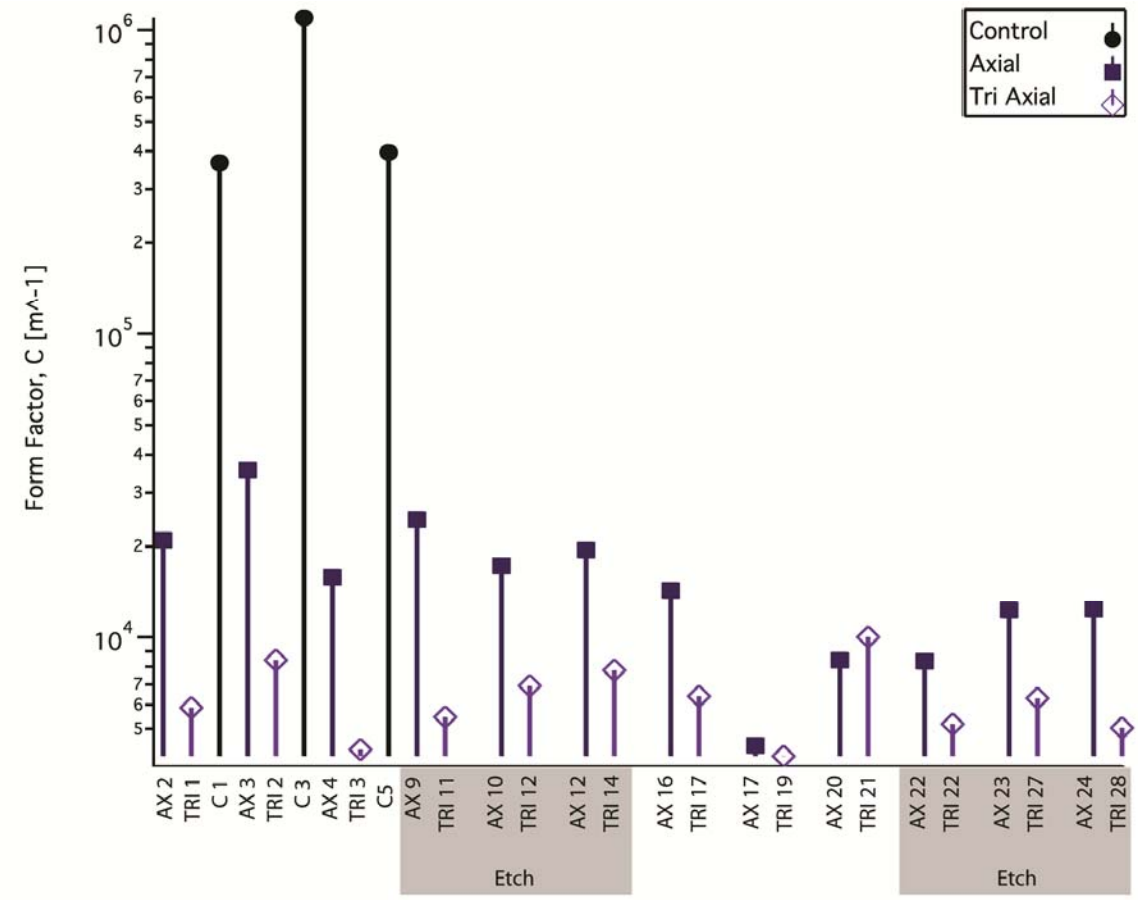

Figure 47: Form factor, C values, determined from FHDD fit of the measurements. Algorithm used to fit the K and C to the -dp/dx versus v curves gives a 95% confidence interval for the K and C values.

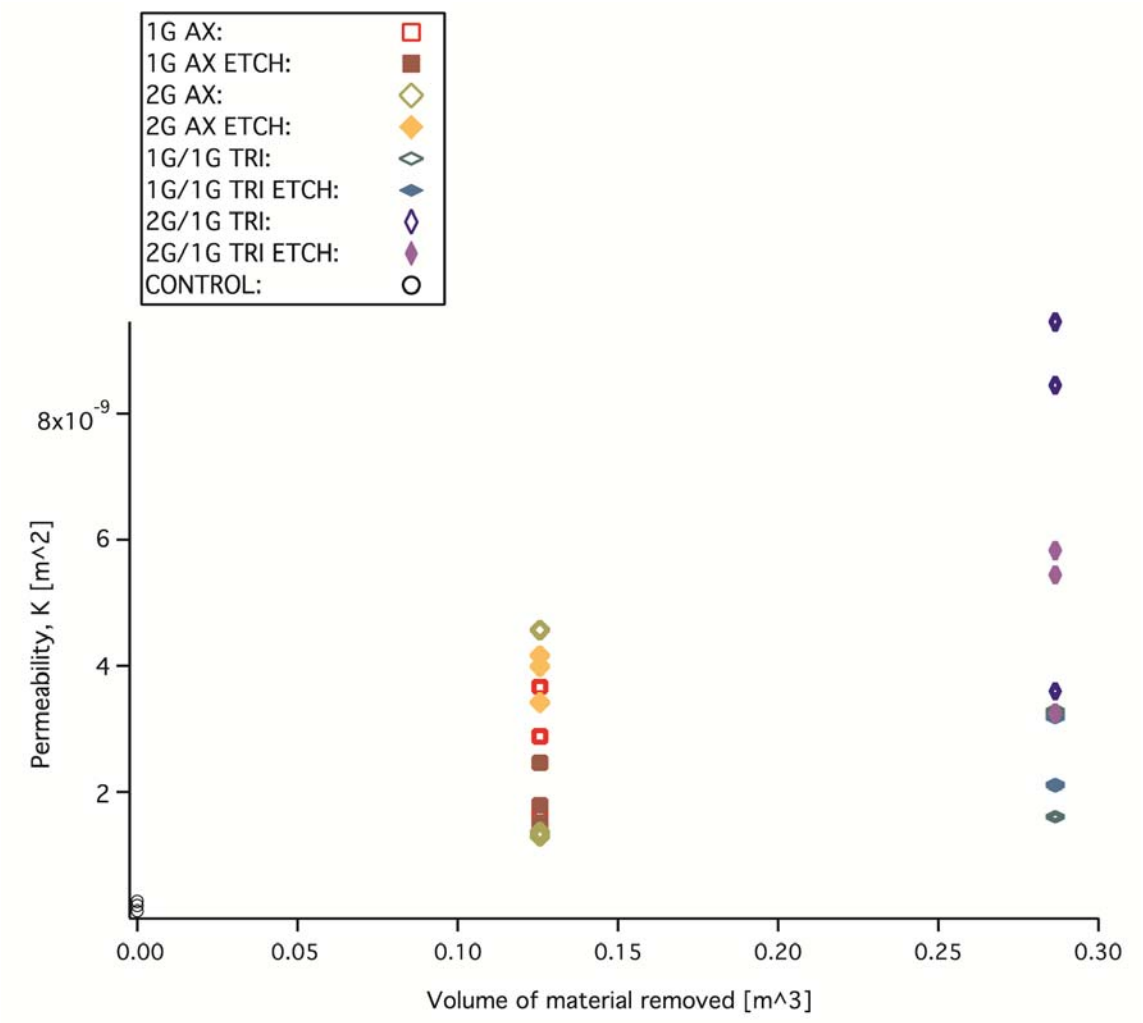

Figure 48: Permeability versus idealized volume of material removed per cubic meter of solid material via mechanical reticulation.

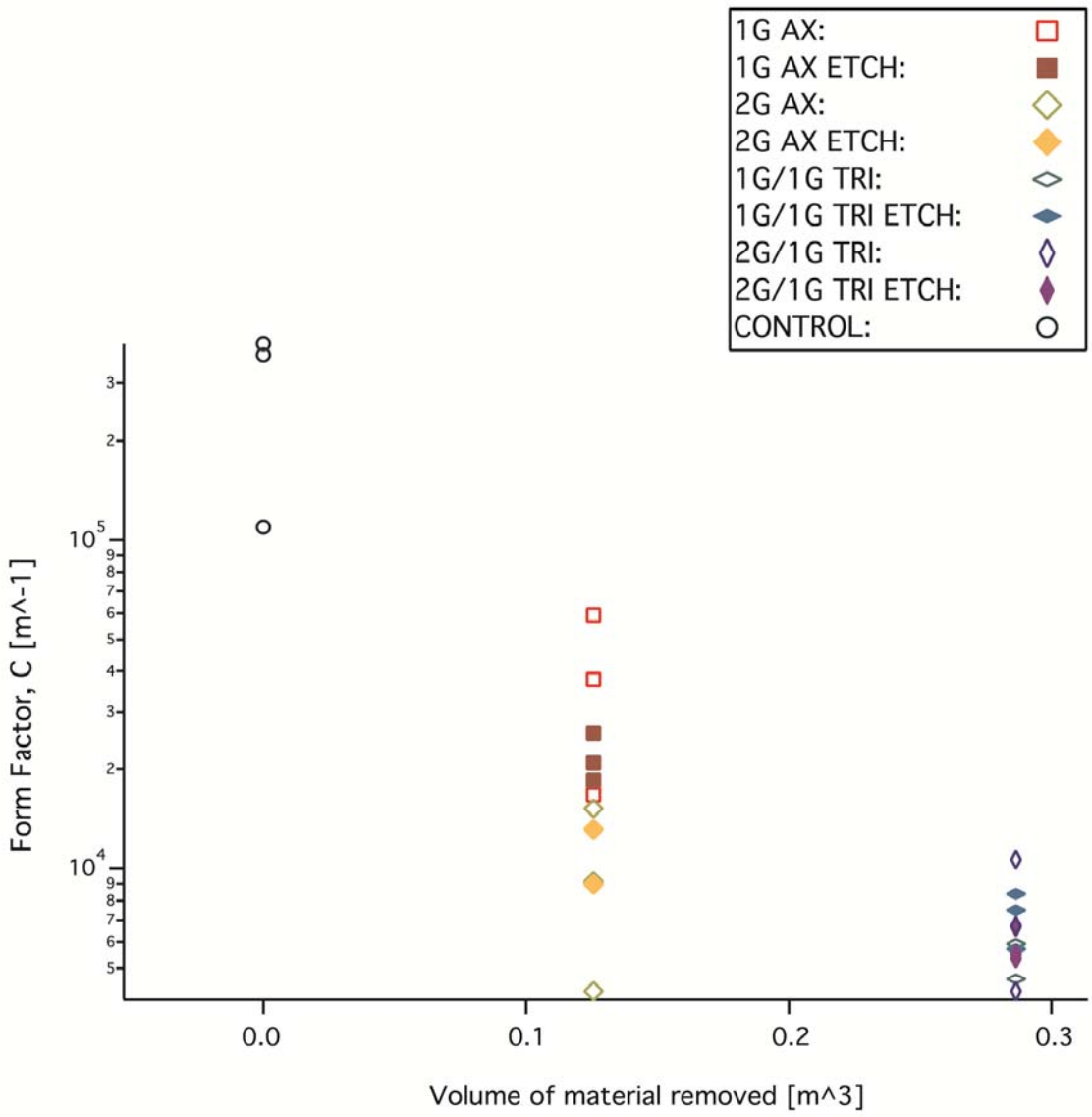

Figure 49: Form factor versus idealized volume of material removed per cubic meter of solid material via mechanical reticulation.

density of the material removed from the samples. Figure 50 is a graph of the friction factor versus Reynolds number for all samples and compared to samples from a previous study that measured SMP foams.

5.4.3 MRI imaging

From imaging of the control samples it is shown that the flow is fully developed within imaging frame (Figure 51 and 52), which was also observed on the inlet portion of the foam. The observed average velocity of the flow was between 0 and 0.1 m/s prior to the foam. Overall, at the lower flow rate, 400 ml/min, the MRI signal obtained by imaging was less than what was observed in the higher flow rate, 800 ml/min. It was also shown that on average, there was acceleration up to 0.25 m/s, and a deceleration of the flow down to -0.25 m/s within the foam that resulted in a mixture of both faster and slower velocities distal to the foam. However, it appears that more acceleration occurred within the axial cases than in the tri axial cases. From imaging with the larger slab slice, it was shown that that flow did become fully developed further distal to the foam (Figure 53 and 54).

5.5 Discussion

It has been shown that SMP foams have the potential to be aneurysm filler with superior healing responses in vivo.[77] It has also been shown that varying the level of reticulation of the foam affects the clotting time of the foams in vivo.[78] Characterization of the fluid interactions between the foam and water via permeability measurements and MRI imaging provided the preliminary steps towards observation of these materials in vivo. We were able to characterize the permeability of mechanically reticulated and

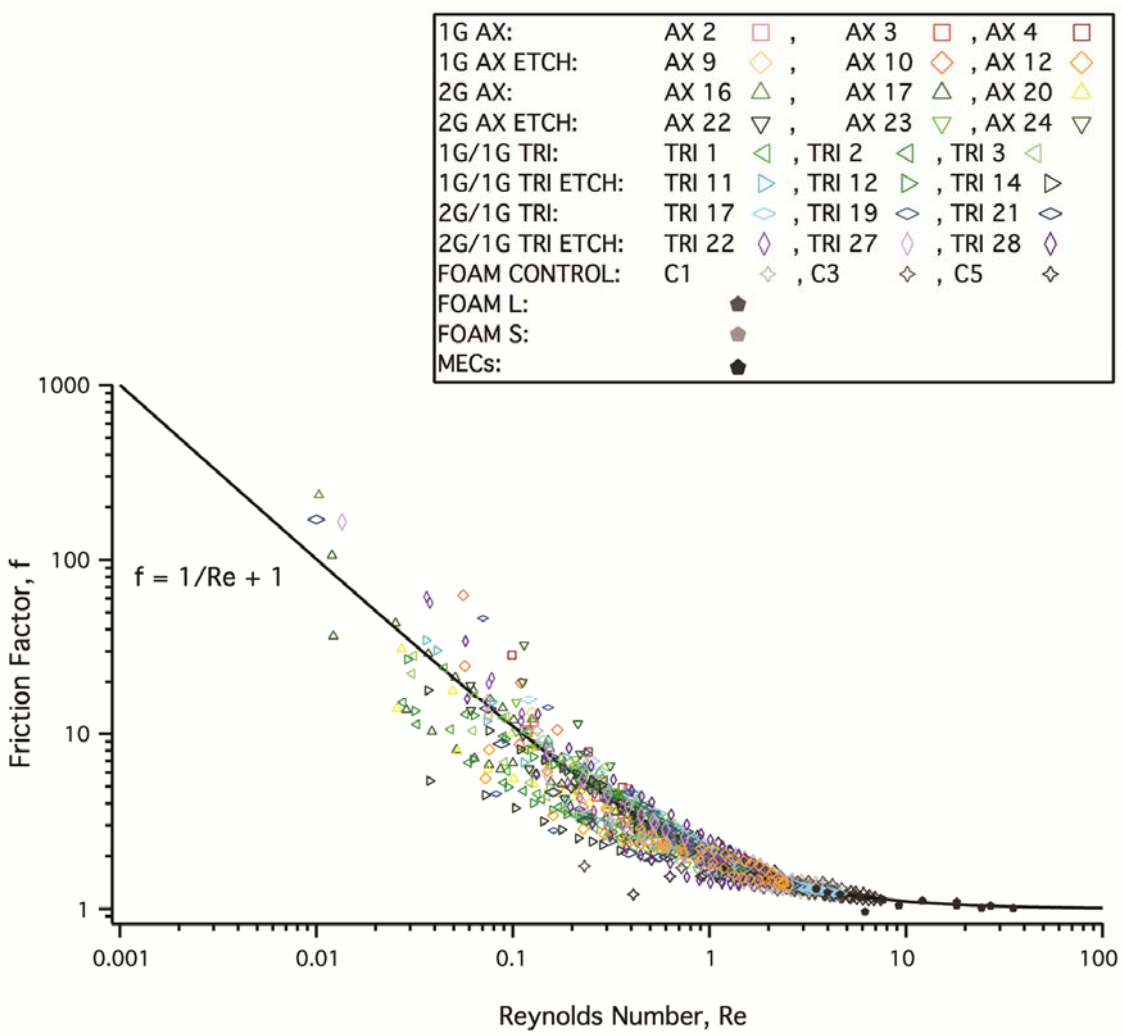

Figure 50: Friction factor versus Reynolds number for all cases and previous study reported by Muschenborn et. al, 2013, represented by foam l (large pore), foam s (small pore) and MECs (mock embolic coils).

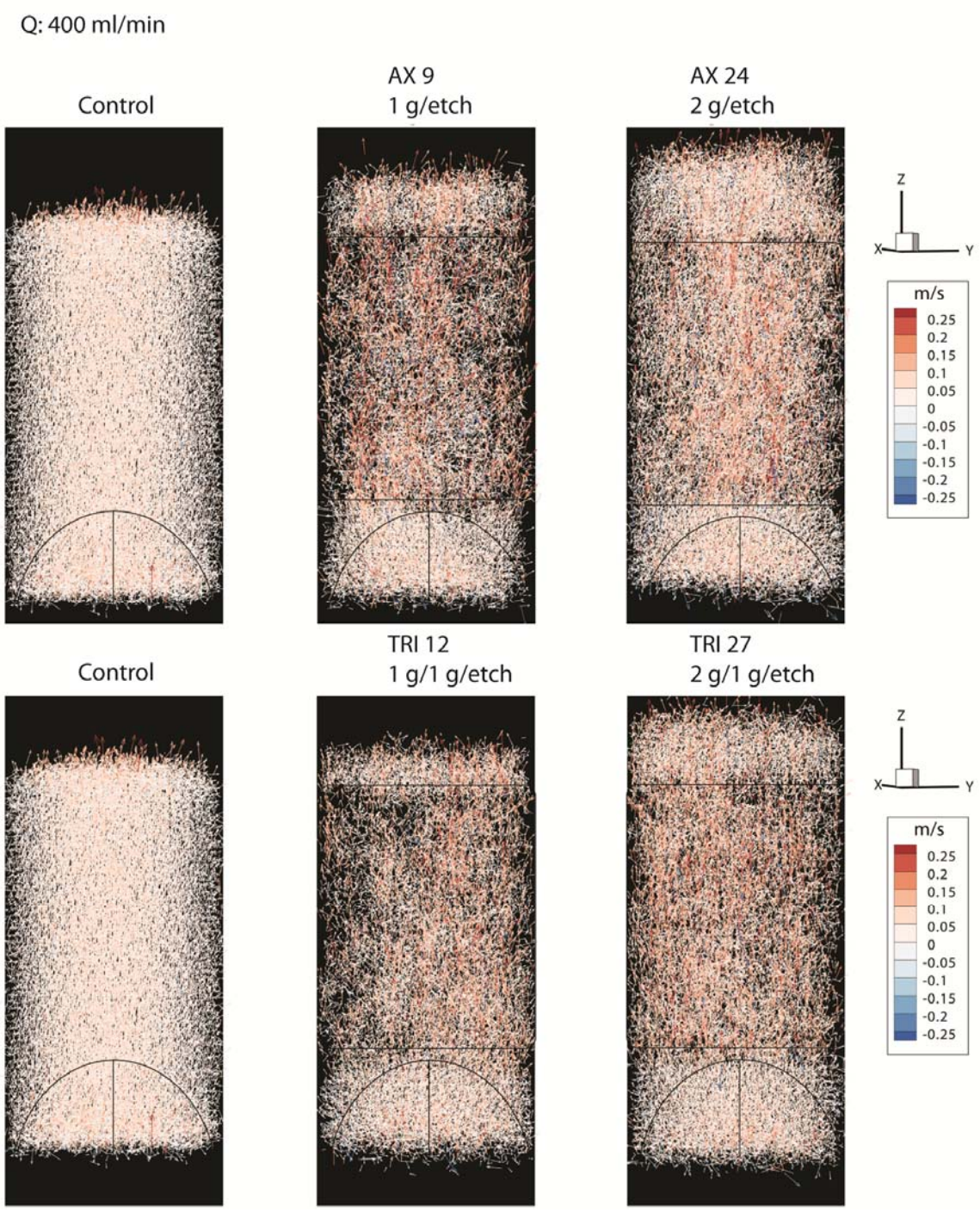

Figure 51: Velocity vectors from 400 ml/minute flow in control (empty chamber), axial and tri axial chambers. Black outline represents approximate location of SMP foam, which is approximately 2 cm.

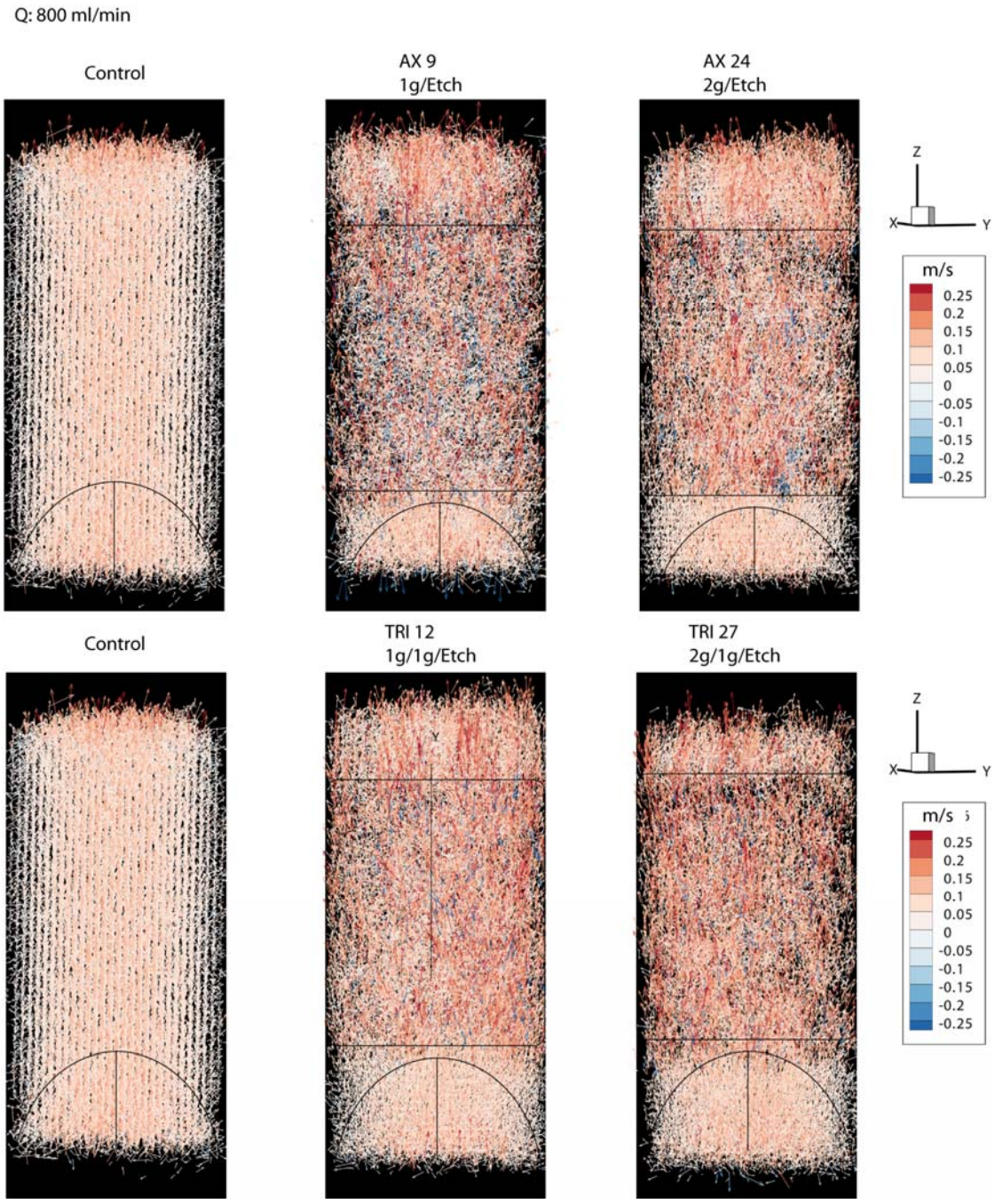

Figure 52: Velocity vectors from 800 ml/minute flow in control (empty chamber), axial and tri axial chambers. Black outline represents approximate location of SMP foam, which is approximately 2 cm.

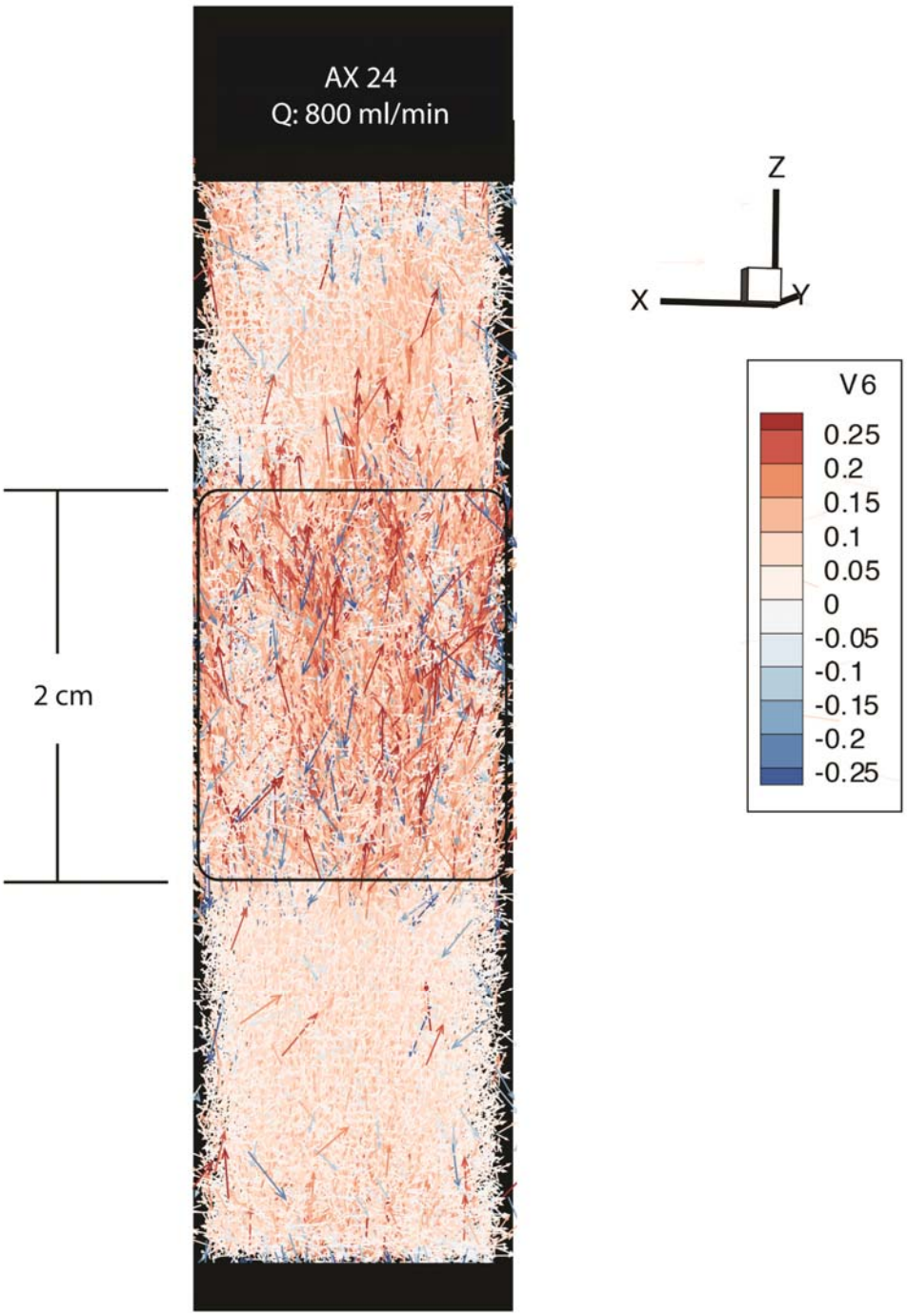

Figure 53: Velocity vectors from 800 ml/minute flow in axial and base etched foam. Permeability of 3.9908 e-9 m2 and form factor of 1.3153 e+4 m-1.

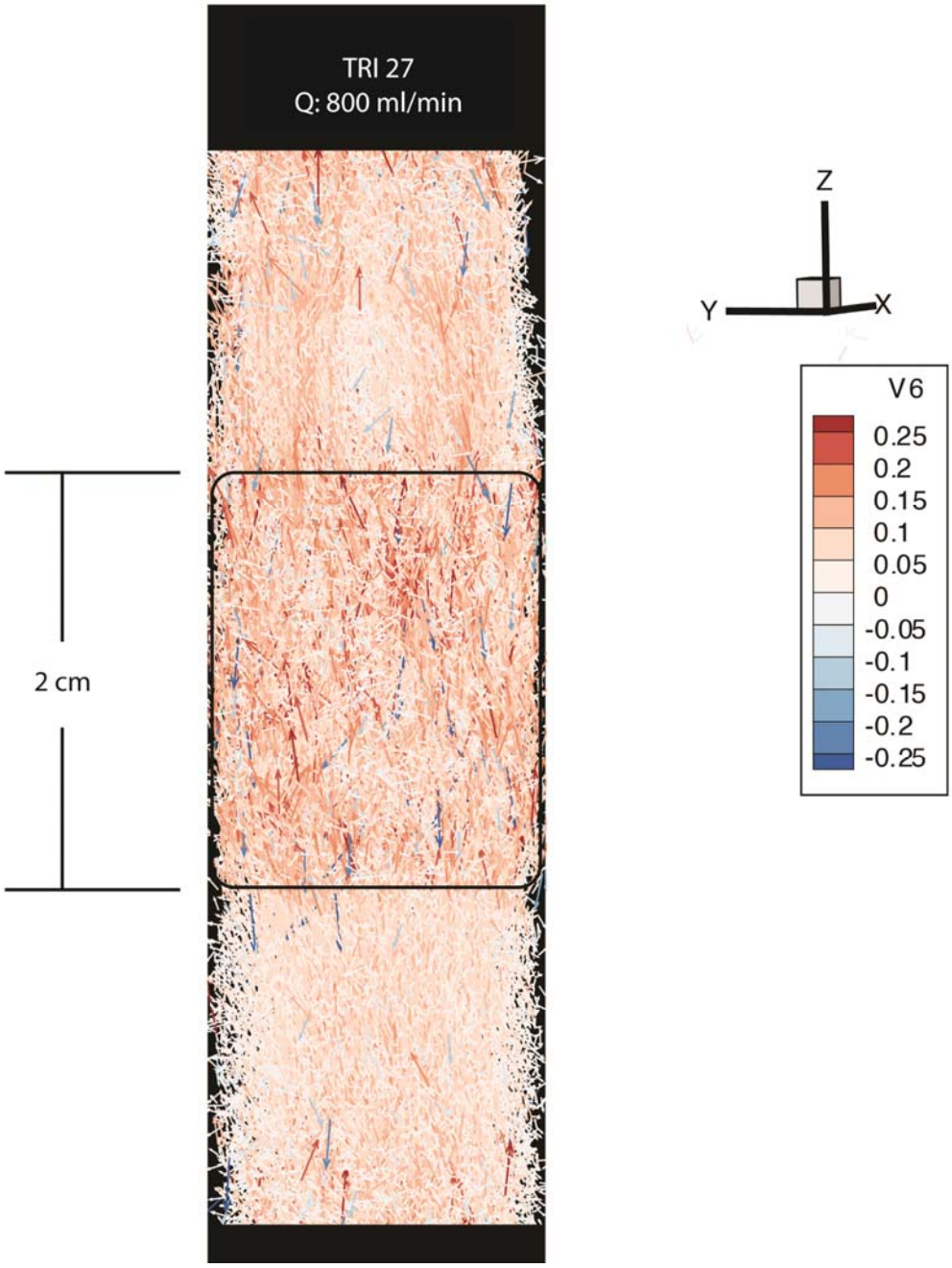

Figure 54: Velocity vectors from 800 ml/minute flow in tri axial and base etched foam. Permeability of 5.4433 e-9 m2 and form factor of 6.6565 e+3 m-1.

etched SMP foam at less than 5 Pa pressure drops across the foam and MRI image flow within the foam at a resolution that was sub pore cell sizes. The ability to characterize these materials at this level of detail will help the future development of these materials as aneurysm filling devices.

One drawback to characterization of these materials involved the creation of pathways for fluid to permeate into the pores for not only characterization, but also as a viable implantable material. This was due to the native closed cell morphology of this formulation of SMP foam. It became necessary to post cure process the foam via mechanical reticulation as a preliminary step as a means for the development of an SMP foam as an aneurysm filling device and also for characterization via permeability and MRV imaging. Currently, the optimal level of reticulation and morphology of SMP foam for thrombus formation within an SMP device is still unknown. In an effort to characterize different reticulation processes for these materials we looked at eight cases of reticulation and base etching and one control case. In order to characterize these materials under similar conditions in which the foam would experience in vivo, it was necessary to develop a permeability system that was sensitive enough to be able to measure small pressure drops across the sample at steady and low velocity flow rates. We were able to measure the permeability of mechanically reticulated foams with this system. This was a preliminary step toward optimization of design and fabrication of these foams as an SMP aneurysm-filling device. Beyond polymer design, permeability and morphology of these materials are also necessary parameters for computational fluid dynamics and understanding the basic fluid interactions with these materials in vivo.

The eight cases of post processing via reticulation and etching included axial and tri axial mechanically reticulated foams, which were shown to increase permeability by an at least an order of magnitude more than the control, or non-reticulated foams. An increase in the permeability of the foams permits more fluid to permeate throughout the volume of the foam. For the SMP foam to function as an aneurysm filler, or vasculature-occluding device, it was necessary to create paths for which blood may permeate and stagnate to facilitate the clotting process.

Mechanically reticulated foams in the axial direction increased permeability, K, by at least 10x more than the control foams. Tri axially reticulated foams increased permeability more than the axially reticulated foams by approximately 15x. These results imply that knowledge of the density, porosity anisotropy of the foams along with the level of reticulation one can potentially tailor the time and amount of clotting throughout the foam. However, optimization of these factors would vary between a vascular occluding device and an aneurysm-filling device. As a result, further studies would be necessary to determine the optimal characteristics of the foam devices.

The form factor was decreased by one to two orders of magnitude via mechanical reticulation and base etching. This was expected, due to the fact that mechanical reticulation is the act of removing membranes or windows of closed celled foams while the struts remain intact.[9] Through removal of the windows the cross-sectional area of porous material obstructing the flow perpendicular to the direction of the flow was decreased. In general, between the axial and tri axial cases, the form factor, f, decreased by an order of magnitude. The difference between the axial and tri axial samples was the

removal of membranes in one axis versus three respectively. Therefore, the decrease in form factor between the two is a reasonable result.

The difference between the two cases can be quantified via the hole density punched per face. The hole density of these samples was 4.0 x 10^6 holes/m2 per axis punched. For reticulated cases, if it was assumed that a straight cylindrical path was traveled for every pin (0.008" or 203 μm diameter, punched every 0.5 mm) through a cubic meter volume during reticulation, this punching pattern would result in the potential removal of 0.125664 m^3 and 0.286498 m^3 of material per cubic meter for axial and tri axial cases respectively, represented in figures 48 and 49. By these assumptions, the differences between the two reticulation methods results in up to a 2.3X increase in removal of membranes throughout the volume. From the samples measured, there was an average 1.5X increase in the permeability between the axial and tri axial cases (figure 48 and 49). In a previously reported permeability study performed on SMP foams[65], the permeability ranged between 5.7 x 10^{-9} to 1.27 x10^{-8} and 3.25 x 10^{-9} to 1.15 x 10^{-8} and form factors ranged between 2.72 x 10^3 to 7.26 x 10^3 and 2.80 x 10^3 to 6.19 x 10^3 for small (diameter = 0.73 mm) and large (diameter = 1.1 mm) celled foams respectively. The samples previously reported had hole punching densities of 0.9 x 10^5, 1.7 x 10^5, 3.5 x 10^5 and 6.9 x 10^5 holes/m^2. Although the hole pattern density was lower by an order of magnitude, the previously reported values for permeability were on the same order of magnitude up to an order of magnitude larger than the samples reported here. This may have resulted from the difference in mechanical reticulation applied to these samples or the foams themselves, as these materials were different SMP foam formulations

The difference between the previously reported cases and the cases reported here, was the difference in the mechanical mechanism of reticulation for puncturing the membranes between the pores. Previously, 300 μm diameter stainless steel needles were manually punched through the foam, aided with a rigid template used to create straight channels within the SMP foam material. For the samples reported here, the membranes were removed via free-floating, weighted, gravity driven, mechanically agitated nitinol pin assemblies. For this method of reticulation, the larger cylindrical weighted portion of the pins were free to move in the z-axis within a channel, while the nitinol pin portion was able to flex and stop when too much resistance was encountered as they penetrated the material. This design allowed for more tortuous paths to be made throughout the foam while preserving the integrity of the struts. Due to the less direct paths associated with this reticulation method, it is reasonable that the overall permeability would be lower for these samples even though the punching density was an order of magnitude greater than the previously reported samples. The lower permeability achieved by this reticulation method may result in a better device to occlude vessels due to the necessity of flow stagnation to aid in thrombus formation.[27] The previous study on SMP foams compared the permeability of two types of foams to mock embolic coils, and concluded that the SMP foams were more effective at reducing flow through the media and therefore, would be better suited to induce the desired hemodynamics within a treated aneurysm.[65]

The form factor versus Reynolds number plot of the samples follows the mathematical model of form factor in the region of Reynolds number, Re, greater than 1.

However, in the region of the plot of Re less than 1, the trends follow a similar pattern but diverge from the model as the Re values decrease. The previously reported permeability data for the different SMP foams and mock embolic coils were added to the plot and they spanned Reynolds numbers between 0.5 and 50. The data reported for these samples covered Reynolds numbers between 0.01 to 10, which covers the range of Reynolds numbers used by Ortega et al. for blood flow simulation within SMP foam.[70] The friction factors of all samples reported here are larger than the previously reported number from Muschenborn et al. in 2013.

Via MRV imaging we were able to visualize the interaction of the fluid within SMP foam while flow rates were varied. In general, it was shown that the lower flow rate, 400 ml/min, resulted in less tortuous flow patterns than the higher flow rate, 800 ml/min. However, the more reticulated tri axial foams showed a lower amount of variation in flow. This was expected due to the straighter channels within the axially reticulated foam than the more tortuous pathways exhibited tri axially reticulated foams; imaging of axial reticulated cases is most likely analogous to imaging flow in capillary tubes previously reported by Romenenko, et al. in 2011.[80]

We were able to visualize the average velocity vectors at a voxel resolution of 0.5 x 0.5 x 0.5 mm3. Although this resolution is sub pore cell size, smaller voxels would result in more visualization and quantification of flow within the foam. In other words, at the resolution imaged, we are not able to conclusively say that each velocity vector actually depicts the fluid and SMP foam interaction as they occur within the foam. We are only able to conclude that on average the velocity vectors depicted was what was

experienced within the foam. We were unable to image the non-reticulated, or control foams, due to the low permeability and high-pressure drop created across the sample. Another issue involved with imaging the control samples was the suspected resulting low signal from the small amount of native open membranes within the foam.

Signal was low in foams that were not evacuated overnight prior to imaging. This was expected due to the trapped air within the foam, which prevents the permeation of copper sulfate solution for increased contrast throughout the foam. It was also seen that signal was better in the higher flow rates than in the lower flow rates. For that reason, imaging was performed in the mid and higher flow rates of 400 and 800 ml/min. The flow rates reported in this study are higher than the blood flow within a basilar artery (~70-170 ml/min) reported by Jou et al. in 2003.[48] However, due to the large diameter of tubing that was used in these experiments, the Darcy velocities were very low and ranged between 0 and 0.071 m/s. Our Darcy velocities are much lower in comparison to the reported in Kato et al.[53] values for a normal artery (0.17-0.5 m/s). We obtained our Darcy velocity values via matching Reynolds number and were limited due to the cross sectional area of the foam, tubing and the capabilities of the pump. Additionally, these lower velocities compliment previous CFD simulations performed in SMP foam within basilar artery aneurysms.[70] The CFD results showed a significant deceleration in the fluid velocity within the foam[70], which was further validation of the use of these velocities. In addition to the previously mentioned reasons, these lower Darcy velocities compliment the previous study involving measurement of permeability in SMP foam at greater Darcy velocities.[65]

Previously, SMP foam with pore cells of approximately 200-300 μm in diameter, a density of 0.020 g/cc, a calculated volumetric void fraction of 98.4%, with a sample dimension of 4-mm-diameter by 10-mm-long cylinder of was imaged within silicone tubing having an inner diameter of 2.5 mm and a velocity of 0.013 m/s resulting in the foam being compressed to 62.5% of its original diameter was imaged via phase contrast MRV.[86] The resultant images had four slices with dimensions of 5 mm x 5 mm x 2 mm with a resolution of 39 μm x 39 x 2mm μm per voxel.[86] Although the in-plane resolution was more than an order of magnitude better than this study, the resolution of the velocity in the direction of the flow was 2 mm, or one quarter the resolution of the images that were achieved in this study. The imaging was performed with a "9.4 T with a Bruker Avance spectrometer and a Bruker Micro 2.5 microimaging probe equipped with a 5-mm coil".[86] For this study imaging was performed on a 3T clinical scanner. An increase in resolution by a smaller voxel size is feasible however; it greatly increases the imaging time. For this study we chose shorter imaging time to increase the number of averages in the velocity vectors, number of samples and flow rates imaged. The ability to image these materials with a clinical scanner with reasonable resolution implies that these methods may be used in the future to image these materials with blood either in vitro or in vivo. These studies laid the groundwork for more advanced characterizations of these materials, thereby facilitating further optimization them for clinical applications.

Basic characterizations of these foams were also performed in order to better understand the effects of the foam density, surface area, porosity and anisotropy. Although the foams were characterized in multiple locations via the previously

mentioned methods, not all densities were represented via permeability and MRI measurements. This would require much more samples, which was not feasible. Due to the heterogeneous nature of these blown foam materials, it has become evident that it was necessary to quantify the density and porosity of the material prior to sample preparation, evident by the variability in permeability of the materials after processing. Subsequently, this was also evident by the variation in form factor of samples that were prepared in the same manner, even though they were from the same batch of foam.

6. SUMMARY

This research sought to characterize shape memory polymer (SMP) foams by evaluating their micro-structure, biocompatibility, radio-opacity, and characterize their interaction in the presence of flow. The intention was to incorporate these results into the development of SMP foam technology that will result in a commercially available embolic treatment for aneurysms. The structure of SMP foam is a complex architecture of mostly closed cells, including struts, membranes and pores. Its structure contributes not only to the physical properties of the material, but the devices and their interaction with blood in vivo. These interactions include the hemodynamic disruptions caused by the presence of the foams and the resultant overall healing seen in vivo when used as an aneurysm occluding device. A component of this research explored the microstructure of SMP foam by micro computed tomography (μ-CT) imaging that provided data for structural characterization of the foam. Knowledge of the microstructure of the foams in three dimensions, not only allows for diameter histogram data to be acquired, but also allows for more complex computation fluid dynamic simulations to be performed on the resultant 3D models of the foam. Biocompatibility of SMP foams was evaluated for implants up to 90 days within a vein pouch porcine animal model, which ultimately determined the feasibility of these materials as a viable implantable medical device. For clinical relevance, the positioning and delivery of an aneurysm-filling device, such as the SMP embolic foam device, must be radio-opaque, or possess the ability to attenuate X-rays in order to be visible via fluoroscopy. One of the research goals of this research was to increase the radio-opacity of SMP foam. Beyond radio-opacity, this research also

demonstrated biocompatibility of the resultant composite materials that were made by making them radio-opaque. This research also set out to characterize fluid interactions between the foams when exposed to varied flow rates. The permeability of the porous media was characterized at varying flow rates, which compared to the clinically relevant flow rates that were demonstrated via computation fluid dynamics interactions. We were also able to visualize the hydrodynamic interaction between SMP foam and water with MRV at sub-pore cell size resolution, indicating that this technology could be adapted to visualization in vivo or with blood. This data may be an important first step toward understanding the initiation of clot formation within the volume of the aneurysm filling foam device; a valuable component of the biocompatibility of an aneurysm device.

6.1 Topics covered

6.1.1 Microstructure of SMP foams

First, I proposed to image SMP foam samples using micro-Computed tomography (μ-CT), using settings that will achieve high resolution (<5 μm/pixel) images, to be used for assessment of microstructure. This data was to be analyzed in three dimensions to characterize of the architecture of the foam. Assessment of the structure included such characteristics as a range of average pore cell diameters, strut length, and isotropy of the pores. Beyond characterization of foam, this data was used for 3D models to be used in computational fluid dynamics (CFD) simulations. This aim was met with the publication of the articles entitled "Ultra low density and highly crosslinked biocompatible shape memory polyurethane foams", published by Singhal et al. in 2012[85] and "Virtual treatment of basilar aneurysms using shape memory polymer

foam", published by Ortega et al. in 2013.[70] Expanding on this aim, data was also used in section five of this dissertation for the proposed publication of "4D Flow Visualization and Permeability of Mechanically Reticulated Shape Memory Polymer Foam for Aneurysm Treatment", by Rodriguez, et al. in 2014, in which the surface area of the foam was estimated via aspect ratio dimensions of the foam, the relative density of the foams and three dimensional models of individual pore cells. Possession of the complex 3D models and surface area of the foams helps to further increase the refinement of computational fluid dynamics simulations performed at Lawrence Livermore National Laboratory.

6.1.2 Biocompatibility of SMP foam

Second, I proposed to determine the biocompatibility of an SMP foam device when implanted in a porcine vein pouch aneurysm model. This aim was met with the publication of the articles entitled "In vivo response to an implanted shape memory polyurethane foam in a porcine aneurysm model" and "Opacification of shape memory polymer foam designed for treatment of intracranial aneurysms" by Rodriguez, et al. in 2014[77] and 2012[79] respectively. Both of these articles reported the biocompatibility of implanted SMP foams as aneurysm fillers within a porcine vein pouch aneurysm model. The latter of the two papers reported biocompatibility of tungsten doped SMP foams.

6.1.3 Radio-opacity and ppacification of SMP

Third, I proposed to determine the native opacity of our neat and foam versions of polyurethane SMP when imaged using X-ray based imaging methods, such as fluoroscopy. Once this data was acquired, I determined if there is a necessity for the

addition of High-Z element filler to the polymer that will aid in the attenuation of X-rays. X-rays are used in fluoroscopy, the imaging technology used by clinicians to place aneurysm filler devices. I proposed to determine the minimal concentration of High-Z element filler that is necessary for visualization of a crimped SMP foam device *in vivo***.** Experimentally it was determined that High-Z element filler was necessary for X-ray attenuation. It was determined that tungsten at 4% by volume was sufficient at creating enough radio-opacity in vivo when imaged with a porcine skull via fluoroscopy at small diameters. In addition to radio-opacity and biocompatibility, we demonstrated that by doping with a High-Z element particulate we can increase the mechanical properties of these materials. In essence the opacification research resulted in a composite material that was tougher than the original foams. This aim was met with the publication of the article entitled "Opacification of shape memory polymer foam designed for treatment of intracranial aneurysms" by Rodriguez, et al. in 2012.[79]

6.1.4 Imaging flow within an SMP foam using magnetic resonance imaging (MRI)

Fourth, I proposed to visualize the flow, specifically the mean velocity vectors of fluid within an SMP foam using magnetic resonance imaging (MRI), more specifically, magnetic resonance velocimetry (MRV). To achieve this goal I proposed to visualize a fluid within a SMP foam plug within a cylindrical model under constant flow at varying flow rates. Beyond imaging flow I also proposed to characterize the permeability of SMP foam. In order to achieve these goals, reticulation of SMP was necessary due to the native closed cell morphology of the foam. A sub aim of this fourth aim was to develop a non-destructive means for reticulation of the SMP foam. This was a large sub-aim,

which should have been an aim unto itself, as this aim was met with the intended publication of the article entitled "Reticulation of low density shape memory polymer foam for vascular occlusion" by Rodriguez, et al. in preparation for submission in 2014.[78]

This publication not only covers the process of mechanical reticulation used to open up the membranes of the foam, it also demonstrated the use of SMP foam as a vascular occlusion device in vivo within a porcine animal model. By varying the reticulation of SMP foam and implanting them as a vascular occlusion device we demonstrated that it might be possible to tailor future devices via mechanical reticulation for the optimal occlusion time based on further animal results. Finally, this aim was met with the intended publication of the article entitled "4D Flow Visualization and Permeability of Mechanically Reticulated Shape Memory Polymer Foam for Aneurysm Treatment" by Rodriguez, et al., also in preparation for submission in 2014. In this publication the permeability and MRV imaging of mechanically reticulated SMP foams were reported.

6.2 Impact of topics covered

Completion of these aims increased the understanding of the SMP foam devices and their overall interaction *in vivo*. The micro architecture of the foam impacts the mechanical behavior of the foams and how they interact with the body during the healing process. This knowledge of the micro architecture, aspect ratio, expansion ration and porosity, also determines the amount of material that can be compacted into one device during the temporary programming of the SMP. In effect, these characteristics

determine the amount of material that can be used for an occluding device that will be delivered via endovascular methods. Knowledge of their microstructure also determined that the individual pores need to be reticulated to allow for blood flow to permeate and begin the initial healing process.

After the foams have been mechanically reticulated by different means, by varying the axes punched, this changes their permeability. This change in the impedance of blood flow throughout the device has an impact on how long it takes for the device to occlude within the vessel and how completely the foam fills with blood. How completely the foam fills with blood in turn has an impact on how well the foams are incorporated into the healing tissue of the aneurysms. The clot acts as the architecture for which cellular components can come in and resolve the residual clot and lay down collagen, thereby stabilizing the aneurysm from future rupture.

The biocompatibility of an implanted device was determined at multiple time points and it was demonstrated that the foams were approximately 75% filled with cellular infiltrates, had low inflammation when compared to the suture materials used to make the aneurysms, and the device was isolated from the parent vessel with an endothelial cell layer. These results showed that SMP foam as aneurysm filling device is successful at achieving what both the GDC coils and surgical clipping aim to do, isolate the weakened portion of the vessel from the rest of the parent vasculature preventing future rupture.

Second to biocompatibility is visibility, or radio-opacity when the foam is implanted into an aneurysm, as far as the feasibility of these materials as becoming an

endovascularly deployed medical device. Radio-opacity was achieved by doping the foam with 4% by volume tungsten particulates. This process not only enabled contrast of the foam to be visible with the skull thickness of a pig, but was shown to be a tougher material and also biocompatible when implanted in vivo. We have shown that the particulates can be incorporated into these materials to increase mechanical properties and elicit radio-opacity, which can also be incorporated into future variations of these materials.

Healing is initiated by the clot formation within the foam that occurs within minutes of being exposed to blood with these materials. Varying the permeability by varying the reticulation of the foams allows for the future tailoring and design of occlusion devices by these materials. By characterizing the flow and fluid characteristics within the foam, it may be possible to predict the initial clotting process in vivo with computational fluid dynamics. CFD can also be validated by MRV imaging within the foam. With the proper settings, one could image the foam within an aneurysm as it was clotting using MRV methods. All of this research sought to advance these materials closer toward application as a viable medical device and to understand some basic science about the fluid and foam interactions. These characteristics are important factors that should be observed prior to commercialization of a medical device made of these materials. This research was a significant step toward the realization of these materials being used as aneurysm fillers within humans.

REFERENCES

1. Arthur, A. S., S. A. Wilson, S. Dixit, and J. D. Barr. Hydrogel-coated coils for the treatment of cerebral aneurysms: preliminary results. Neurosurg. Focus 18(2):1-9, 2005.

2. ASTM International, ASTM D638, Standard test method for tensile properties of plastics. West Conshohocken, P.A., 2010.

3. Baer, G., T. S. Wilson, D. L. Matthews, and D. J. Maitland. Shape-memory behavior of thermally stimulated polyurethane for medical applications. J. Appl. Polym. Sci. 103(6):3882-3892, 2007.

4. Bear, J. Dynamics of fluids in porous media. American Elsevier Publishing Company, Inc., New York, N.Y., 1988.

5. Bederson, J. B., I. A. Awad, D. O. Wiebers, D. Piepgras, E. C. Haley Jr, T. Brott, G. Hademenos, D. Chyatte, R. Rosenwasser, and C. Caroselli. Recommendations for the management of patients with unruptured intracranial aneurysms: a statement for healthcare professionals from the Stroke Council of the American Heart Association. Circulation 102(18):2300-2308, 2000.

6. Bederson, J. B., I. A. Awad, D. O. Wiebers, D. Piepgras, H. E. C. Jr, T. Brott, G. Hademenos, D. Chyatte, R. Rosenwasser, and C. Caroselli. Recommendations for the management of patients with unruptured intracranial aneurysms: a statement for healthcare professionals from the Stroke Council of the American Heart Association. Stroke 31(11):2742-2750, 2000.

7. Bederson, J. B., E. S. Connolly, H. H. Batjer, R. G. Dacey, J. E. Dion, M. N. Diringer, J. E. Duldner, R. E. Harbaugh, A. B. Patel, and R. H. Rosenwasser. Guidelines for the management of aneurysmal subarachnoid hemorrhage: A statement for healthcare professionals from a special writing group of the stroke council, American Heart Association. Stroke 40(3):994-1025, 2009.

8. Behl, M., M. Y. Razzaq, and A. Lendlein. Shape-memory polymers: multifunctional shape-memory polymers. Adv. Mater. 22(31):3388-3410, 2010.

9. Blair, E. A. Cell structure: Physical property relationships in elastomeric foams. Cellular Plastics, National Academy of Sciences, National Research Council, Proceedings, 143-152, 1966.

10. Brinjikji, W., A. A. Rabinstein, G. Lanzino, D. F. Kallmes, and H. J. Cloft. Effect of age on outcomes of treatment of unruptured cerebral aneurysms: a study of the national inpatient sample 2001–2008. Stroke 42(5):1320-1324, 2011.

11. Brinjikji, W., A. A. Rabinstein, G. Lanzino, D. F. Kallmes, and H. J. Cloft. Patient outcomes are better for unruptured cerebral aneurysms treated at centers that preferentially treat with endovascular coiling: a study of the national inpatient sample 2001–2007. Am. J. Neuroradiol. 32(6):1065-1070, 2011.

12. Britz, G. W., L. Salem, D. W. Newell, J. Eskridge, and D. R. Flum. Impact of surgical clipping on survival in unruptured and ruptured cerebral aneurysms: a population-based study. Stroke 35(6):1399-1403, 2004.

13. Broderick, J. P. Practical considerations in the early treatment of ischemic stroke. Am. Fam. Physician 57(1):73-80, 1998.

14. Brown, G. G. and W. H. Carnes. Primer of histopathologic technique. Appleton-Century-Crofts, New York, N.Y.,1969.

15. Cabanlit, M., D. Maitland, T. Wilson, S. Simon, T. Wun, M. E. Gershwin, and J. Van de Water. Polyurethane shape-memory polymers demonstrate functional biocompatibility. Macromol. Biosci. 7(1):48-55, 2007.

16. Cao, X., L. J. Lee, T. Widya, and C. Macosko. Polyurethane/clay nanocomposites foams: processing, structure and properties. Polymer 46(3):775-783, 2005.

17. Cebral, J. R., F. Mut, J. Weir, and C. Putman. Quantitative characterization of the hemodynamic environment in ruptured and unruptured brain aneurysms. Am. J. Neuroradiol. 32(1):145-151, 2011.

18. Cekirge, H. S., I. Saatci, M. H. Ozturk, B. Cil, A. Arat, M. Mawad, F. Ergungor, D. Belen, U. Er, S. Turk, M. Bavbek, Z. Sekerci, E. Beskonakli, O. E. Ozcan, and T. Ozgen. Late angiographic and clinical follow-up results of 100 consecutive aneurysms treated with Onyx reconstruction: largest single-center experience. Neuroradiol. 48(2):113-126, 2006.

19. Chu, C. C., J. A. von Fraunhofer, and H. P. Greisler. Wound closure biomaterials and devices. CRC Press, Boca Raton, F.L., 1997.

20. Cognard, C., A. Weill, L. Spelle, M. Piotin, L. Castaings, A. Rey, and J. Moret. Long-term angiographic follow-up of 169 intracranial berry aneurysms occluded with detachable coils. Radiology 212(2):348-356, 1999.

21. Coley, S., M. Sneade, A. Clarke, Z. Mehta, D. Kallmes, S. Cekirge, I. Saatci, D. Roy, and A. Molyneux. Cerecyte coil trial: procedural safety and clinical outcomes in patients with ruptured and unruptured intracranial aneurysms. Am. J. Neuroradiol. 33(3):474-480, 2012.

22. Cui, J., K. Kratz, M. Heuchel, B. Hiebl, and A. Lendlein. Mechanically active scaffolds from radio-opaque shape-memory polymer-based composites. Polym. Adv. Technol. 22(1):180-189, 2011.

23. Currie, S., K. Mankad, and A. Goddard. Endovascular treatment of intracranial aneurysms: review of current practice. Postgrad. Med. J. 87(1023):41-50, 2011.

24. Dalyai, R. T., C. Randazzo, G. Ghobrial, L. F. Gonzalez, S. I. Tjoumakaris, A. S. Dumont, R. H. Rosenwasser, and P. Jabbour. Redefining Onyx HD 500 in the flow diversion era. Int. J. Vasc. Med. 2012:1-9, 2012.

25. De Nardo, L., R. Alberti, A. Cigada, L. Yahia, M. C. Tanzi, and S. Farè. Shape memory polymer foams for cerebral aneurysm reparation: effects of plasma sterilization on physical properties and cytocompatibility. Acta Biomater 5(5):1508-1518, 2009.

26. Doerfler, A., I. Wanke, T. Egelhof, U. Dietrich, S. Asgari, D. Stolke, and M. Forsting. Aneurysmal rupture during embolization with Guglielmi detachable coils: causes, management, and outcome. Am. J. Neuroradiol. 22(10):1825-1832, 2001.

27. Einav, S. and D. Bluestein. Dynamics of blood flow and platelet transport in pathological vessels. Ann. NY Acad. Sci. 1015:351-366, 2004.

28. Elkins, C. and M. Alley. Magnetic resonance velocimetry: applications of magnetic resonance imaging in the measurement of fluid motion. Exp. Fluids 43(6):823-858, 2007.

29. Elkins, C. J., M. Markl, N. Pelc, and J. K. Eaton. 4D Magnetic resonance velocimetry for mean velocity measurements in complex turbulent flows. Exp. Fluids 34(4):494-503, 2003.

30. Findlay, J. M. and T. E. Tim E. Darsaut. Endovascular management of cerebral aneurysms: work in progress. Can. J. Neurol. Sci. 34(1):1-2, 2007.

31. Gall, K., M. L. Dunn, Y. Liu, D. Finch, M. Lake, and N. A. Munshi. Shape memory polymer nanocomposites. Acta. Mater. 50(20):5115, 2002.

32. Gall, K., M. L. Dunn, Y. Liu, G. Stefanic, and D. Balzar. Internal stress storage in shape memory polymer nanocomposites. Appl. Phys. Lett. 85(2):290-292, 2004.

33. Gent, A.N., Rusch,K.C. Viscoelastic behavior of open-cell foams. Rubber Chemistry and Technology, 39(2):389-396, 1966.

34. Gibson, L. J. and M. F. Ashby. Cellular Solids Structure and Properties. Cambridge University Press, London, U.K., 1997.

35. Goods, S. H., C. L. Neuschwanger, L. L. Whinnery, and W. D. Nix. Mechanical properties of a particle-strengthened polyurethane foam. J Appl Polym Sci 74(11):2724-2736, 1999.

36. Guglielmi, G., C. Ji, T. F. Massoud, A. Kurata, S. P. Lownie, F. F. Viñuela, and J. Robert. Experimental saccular aneurysms. Neuroradiology 36(7):547-550, 1994.

37. Guglielmi, G., F. Viñuela, I. Sepetka, and V. Macellari. Electrothrombosis of saccular aneurysms via endovascular approach. Part 1: Electrochemical basis, technique, and experimental results. J. Neurosurg. 75(1):1-7, 1991.

38. Gunnarsson, T., P. Klurfan, K. G. terBrugge, and R. A. Willinsky. Treatment of intracranial aneurysms with hydrogel coated expandable coils. Can. J. Neurol. Sci. 34(1):38-46, 2007.

39. Hampikian, J. M., B. C. Heaton, F. C. Tong, Z. Zhang, and C. P. Wong. Mechanical and radiographic properties of a shape memory polymer composite for intracranial aneurysm coils. Mat. Sci. Eng. C-Bio. S. 26(8):1373-1379, 2006.

40. Hayakawa, M., Y. Murayama, G. R. Duckwiler, Y. P. Gobin, G. Guglielmi, and F. Viñuela. Natural history of the neck remnant of a cerebral aneurysm treated with the Guglielmi detachable coil system. J. Neurosurg. 93(4):561-568, 2000.

41. Higashida, R. T., B. J. Lahue, M. T. Torbey, L. N. Hopkins, E. Leip, and D. F. Hanley. Treatment of unruptured intracranial aneurysms: a nationwide assessment of effectiveness. Am. J. Neuroradiol. 28(1):146-51, 2007.

42. Hong, B., N. V. Patel, M. J. Gounis, M. J. DeLeo, I. Linfante, J. C. Wojak, and A. K. Wakhloo. Semi-jailing technique for coil embolization of complex, wide-necked intracranial aneurysms. Neurosurgery 65(6):1131-1138, 2009.

43. Horowitz, M., P. Purdy, T. Kopitnik, K. Dutton, and D. Samson. Aneurysm retreatment after Guglielmi detachable coil and nondetachable coil embolization: report of nine cases and review of the literature. Neurosurgery 44(4):712-720, 1999.

44. Horowitz, M., D. Samson, and P. Purdy. Does electrothrombosis occur immediately after embolization of an aneurysm with Guglielmi detachable coils? Am. J. Neuroradiol. 18(3):510-513, 1997.

45. Horowitz, M. B., C. A. Jungreis, and J. Genevro. Delayed rupture of a previously coiled unruptured anterior communicating artery aneurysm: case report. Neurosurgery 51(3):804-806, 2002.

46. Hwang, W., B. L. Volk, F. Akberali, P. Singhal, J. C. Criscione, and D. J. Maitland. Estimation of aneurysm wall stresses created by treatment with a shape memory polymer foam device. Biomech. Model Mechan. 11(5):715-729. 2012.

47. Johnston, S. C., S. Zhao, R. A. Dudley, M. F. Berman, and D. R. Gress. Treatment of unruptured cerebral aneurysms in California. Stroke 32(3):597-605, 2001.

48. Jou, L. D., C. M. Quick, W. L. Young, M. T. Lawton, R. Higashida, A. Martin, and D. Saloner. Computational approach to quantifying hemodynamic forces in giant cerebral aneurysms. AJNR Am. J. Neuroradiol. 24(9):1804-1810, 2003.

49. Kallmes, D. F., A. D. Williams, H. J. Cloft, M. B. Lopes, G. R. Hankins, and G. A. Helm. Platinum coil-mediated implantation of growth factor-secreting endovascular tissue grafts: an in vivo study. Radiology 207(2):519-523, 1998.

50. Kallmes, D. F., N. H. Fujiwara, D. Yuen, D. Dai, and S. T. Li. A collagen-based coil for embolization of saccular aneurysms in a New Zealand white rabbit model. Am. J. Neuroradiol. 24(4):591-596, 2003.

51. Kampmann, C., R. Brzezinska, M. Abidini, A. Wenzel, C. -F. Wippermann, P. Habermehl, M. Knuf, and R. Schumacher. Biodegradation of tungsten embolisation coils used in children. Pediatr. Radiol. 32(12):839-843, 2002.

52. Karaca, E., A. S. Hockenberger, and H. Yildiz. Investigating changes in mechanical properties and tissue reaction of silk, polyester, polyamide, and polypropylene sutures in vivo. Tex. Res. J. 75(4):297-303, 2005.

53. Kato, T., T. Indo, E. Yoshida, Y. Iwasaki, M. Sone, and G. Sobue. Contrast-Enhanced 2D Cine Phase MR angiography for measurement of basilar artery blood flow in posterior circulation ischemia. Am. J. Neuroradiol. 23(8):1346-1351, 2002.

54. Kipshidze, N., K. Sadzaglishvili, M. Panarella, E. A. Rivera, R. Virmani, and M. B. and Leon. Evaluation of a novel endoluminal vascular occlusion device in a porcine model: early and late follow-up. J. Endovasc. Ther. 12(4):486-494, 2005.

55. Kumar, V., A. Abbas, N. Fausto, and R. Mitchell. Robbins basic pathology. Saunders Elsevier, Philadelphia, P.A., 2007.

56. Linn, F. H. H., G. J. E. Rinkel, A. Algra, and J. Van Gijn. Incidence of subarachnoid hemorrhage : role of region, year, and rate of computed tomography: a meta-analysis. Stroke 27(4):625-629, 1996.

57. Macdonald, R. L. Evidence-based treatment of subarachnoid hemorrhage: current status and future possibilities. Clin. Neur. 53:257-266, 2006.

58. Markl, M. Velocity encoding and flow Imaging. http://ee-classes.usc.edu/ee591/library/Markl-FlowImaging.pdf, 2005.

59. Markl, M., A. Harloff, T. A. Bley, M. Zaitsev, B. Jung, E. Weigang, M. Langer, J. Hennig, and A. Frydrychowicz. Time-resolved 3D MR velocity mapping at 3T: Improved navigator-gated assessment of vascular anatomy and blood flow. J. Magn. Reson. Imaging 25(4):824-831, 2007.

60. Metcalfe, A., A. C. Desfaits, I. Salazkin, L. Yahia, W. M. Sokolowski, and J. Raymond. Cold hibernated elastic memory foams for endovascular interventions. Biomaterials 24(3):491-497, 2003.

61. Molyneux, A. J., S. Cekirge, I. Saatci, and G. Gal. Cerebral aneurysm multicenter european Onyx (CAMEO) trial: Results of a prospective observational study in 20 european centers. Am. J. Neuroradiol. 25(1):39-51, 2004.

62. Molyneux, A. J., R. S. C. Kerr, L. M. Yu, M. Clarke, M. Sneade, J. A. Yarnold, and P. Sandercock. International subarachnoid aneurysm trial (ISAT) of neurosurgical clipping versus endovascular coiling in 2143 patients with ruptured intracranial aneurysms: a randomised comparison of effects on survival, dependency, seizures, rebleeding, subgroups, and aneurysm occlusion. Lancet 366(9488):809-817, 2005.

63. Murayama, Y., Y. L. Nien, G. Duckwiler, Y. P. Gobin, R. Jahan, J. Frazee, N. Martin, and F. ViÃuela. Guglielmi detachable coil embolization of cerebral aneurysms: 11 years' experience. J. Neurosurg. 98(5):959-966, 2003.

64. Murayama, Y., F. Vinuela, S. Tateshima, J. K. Song, N. R. Gonzalez, and M. P. Wallace. Bioabsorbable polymeric material coils for embolization of intracranial aneurysms: a preliminary experimental study. J. Neurosurg. 94(3):454-463, 2001.

65. Muschenborn, A., J. Ortega, J. Szafron, D. Szafron, and D. Maitland. Porous media properties of reticulated shape memory polymer foams and mock embolic coils for aneurysm treatment. Biomed. Eng. Online 12(1):103, 2013.

66. Nam, P. H., P. Maiti, M. Okamoto, T. Kotaka, T. Nakayama, M. Takada, M. Ohshima, A. Usuki, N. Hasegawa, and H. Okamoto. Foam processing and cellular structure of polypropylene/clay nanocomposites. Polym, Eng. Sci. 42(9):1907-1918, 2002.

67. Ortega, J., J. Hartman, J. Rodriguez, and D. Maitland. Post-treatment hemodynamics of a basilar aneurysm and bifurcation. Ann. Biomed. Eng. 36(9):1531-1546, 2008.

68. Ortega, J., D. Maitland, T. Wilson, W. Tsai, O. Savas, and D. Saloner. Vascular dynamics of a shape memory polymer foam aneurysm treatment technique. Ann. Biomed. Eng. 35(11):1870–1884, 2007.

69. Ortega, J. M. A porous media model for blood flow within reticulated foam. Chem. Eng Sci. 99:59-66, 2013.

70. Ortega, J. M., J. Hartman, J. N. Rodriguez, and D. J. Maitland. Virtual treatment of basilar aneurysms using shape memory polymer foam. Ann. Biomed. Eng. 41(4):725-743, 2013.

71. Osterman, Floyd A. Jr. MD, W. R. M. Bell, R. J. D. Montali, G. R. L. Novak, and White, Robert I. Jr. Natural history of autologous blood clot embolization in swine. Invest. Radiol. 11(4):267-276, 1976.

72. Peuster, M., C. Fink, and C. von Schnakenburg. Biocompatibility of corroding tungsten coils: in vitro assessment of degradation kinetics and cytotoxicity on human cells. Biomaterials 24(22):4057-4061, 2003.

73. Pierot, L., C. Cognard, F. Ricolfi, and R. Anxionnat. Mid-Term anatomic results after endovascular treatment of ruptured intracranial aneurysms with guglielmi detachable coils and matrix coils: Analysis of the CLARITY series. Am. J. Neuroradiol. 33(3):469-473, 2012.

74. Putt, F. A. Manual of histopathological staining methods. John Wiley and Sons, New York, NY, 1972.

75. Raymond, J., F. Guilbert, A. Weill, S. A. Georganos, L. Juravsky, A. Lambert, J. Lamoureux, M. Chagnon, and D. Roy. Long-term angiographic recurrences after selective endovascular treatment of aneurysms with detachable coils. Stroke 34(6):1398-1403, 2003.

76. Rhee, J. Y., S. M. Trocciola, R. Dayal, S. Lin, R. Chaer, N. Kumar, A. Mousa, J. Bernheim, P. Christos, M. Prince, M. L. Marin, R. Gordon, J. Badimon, V. Fuster, K. C. Kent, and P. L. Faries. Treatment of type II endoleaks with a novel polyurethane thrombogenic foam: Induction of endoleak thrombosis and elimination of intra-aneurysmal pressure in the canine model. J. Vasc. Surg. 42(2):321-328, 2005.

77. Rodriguez, J. N., F. J. Clubb, T. S. Wilson, M. W. Miller, T. W. Fossum, J. Hartman, E. Tuzun, P. Singhal, and D. J. Maitland. In vivo response to an implanted shape memory polyurethane foam in a porcine aneurysm model. J. Biomed. Mater. Res. Part A 102(5): 1231-1242, 2013.

78. Rodriguez, J. N., M. W. Miller, A. Boyle, C. -. Yang, T. S. Wilson, W. Small, L. Nash, H. Skoog, and D. J. Maitland. Reticulation of low density shape memory polymer foam with an in vivo demonstration of vascular occlusion. J. Mech. Behav. Biomed. Submitted, 2014.

79. Rodriguez, J. N., Y. J. Yu, M. W. Miller, T. S. Wilson, J. Hartman, F. J. Clubb, B. Gentry, and D. J. Maitland. Opacification of shape memory polymer foam designed for treatment of intracranial aneurysms. Ann. Biomed. Eng. 40(4):883-897, 2012.

80. Romanenko, K. and B. Balcom. Permeability mapping in porous media by magnetization prepared centric-scan SPRITE. Exp. Fluids 50(2):301-312, 2011.

81. Saatci, I., H. S. Çekirge, M. M. Firat, F. Balkanci, T. Özgen, V. Bertan, and S. Saglam. Placement of mechanically detachable spiral coils in the endovascular treatment of intracranial aneurysms. Work in progress. J. Vasc. Interv. Rad. 7(1):75-79, 1996.

82. Saha, M. C., M. E. Kabir, and S. Jeelani. Enhancement in thermal and mechanical properties of polyurethane foam infused with nanoparticles. Mat. Sci. Eng. C-Bio. S. 479(1-2):213-222, 2008.

83. Seldinger, S. I. Catheter replacement of the needle in percutaneous arteriography; a new technique. Acta. Radiol. 39(5):368-76, 1953.

84. Singhal, P., A. Boyle, M. L. Brooks, S. Infanger, S. Letts, W. Small, D. J. Maitland, and T. S. Wilson. Controlling the actuation rate of low-density shape-memory polymer foams in water. Macromol. Chem. Physic. 214(11):1204-1214, 2013.

85. Singhal, P., J. N. Rodriguez, W. Small, S. Eagleston, J. Van de Water, D. J. Maitland, and T. S. Wilson. Ultra low density and highly crosslinked biocompatible shape memory polyurethane foams. J. Appl. Polym. Sci. Part B: Polymer Physics 50(10):724-737, 2012.

86. Small, W., E. Gjersing, J. L. Herberg, T. S. Wilson, and D. J. Maitland. Magnetic resonance flow velocity and temperature mapping of a shape memory polymer foam device. Biomed. Eng. Online 8(1):42, 2009.

87. Sokolowski, W., A. Metcalfe, S. Hayashi, L. Yahia, and J. Raymond. Medical applications of shape memory polymers. Biomed. Mater. 2(1):S23-S27, 2007.

88. Szikora, I., P. Seifert, Z. Hanzely, Z. Kulcsar, Z. Berentei, M. Marosfoi, S. Czirjak, J. Vajda, and I. Nyary. Histopathologic evaluation of aneurysms treated with Guglielmi detachable coils or Matrix detachable microcoils. Am. J. Neuroradiol. 27(2):283-288, 2006.

89. van der Schaaf, I., A. Algra, M. J. Wermer, A. Molyneux, M. Clarke, J. van Gijn, and G. Rinkel. Endovascular coiling versus neurosurgical clipping for patients with aneurysmal subarachnoid hemorrhage. Stroke 37(2):572-573, 2006.

90. van Gijn, J. and G. J. E. Rinkel. Subarachnoid hemorrhage: diagnosis, causes and management. Brain 124(2):249-278, 2001.

91. Wang, C. and X. Xie. Treatment of an unraveled intracerebral coil. Catheter. Cardio. Inte. 76(5):746-750, 2010.

92. Wardlaw, J. M. and P. M. White. The detection and management of unruptured intracranial aneurysms. Brain 123(Pt. 2):205-221, 2000.

93. Warlow, C. P. Epidemiology of stroke. Lancet 352(Suppl 3):SIII1-SIII4, 1998.

94. Weber, W., R. Siekmann, B. Kis, and D. Kuehne. Treatment and follow-up of 22 unruptured wide-necked intracranial aneurysms of the internal carotid artery with Onyx HD 500. Am. J. Neuroradiol. 26(8):1909-1915, 2005.

95. Whittle, P. and A. L. Gilchrist. "The psychophysics of contrast brightness." In: Lightness, Brightness, and Transparency. Lawrence Erlbaum Associates, Hillsdale, N.J.,1994.

96. Willinsky, R. A. Detachable coils to treat intracranial aneurysms. CMAJ 161(9):1136, 1999.

97. Wilson, T. S., J. P. Bearinger,1 J. L. Herberg, J. E. Marion, W. J. Wright, C. L. Evans, and D.J.Maitland. Shape memory polymers based on uniform aliphatic urethane networks. J. Appl. Poly. Sci. 106(1):540-551, 2007.

98. Wilson, T. S. and D. J. Maitland. Shape memory polymer foams for endovascular therapies. United States Patent Application Publication, US 2005/0075405 A1, 2005.

99. Wilson, T. S., W. Small, W. J. Benett, J. P. Bearinger, and D. J. Maitland. Shape memory polymer therapeutic devices for stroke. Proc. SPIE The International Society for Optical Engineering 6007:157-164, 2005.

100. Yu, S. C. H., W. K. So, A. C. S. Chung, K. T. Lee, and G. K. C. Wong. A compartmentalized volumetric system for outcome analysis of coiled cerebral aneurysms: aneurysm-coil mass-neck outcome assessment. Neurosurgery 64(1):149-155, 2009.

APPENDIX

Table S1: Summary of residual fibrin remaining in the aneurysm dome determined by histology.

Implantation time, days	Number of Aneurysms	>50% fibrin score = 5	26-50% fibrin score = 4	11-25% fibrin score = 3	6-10% fibrin score = 2	<5% fibrin score = 1	0% fibrin score = 0
0	2	-	-	-	2 of 2	-	-
30	7	1 of 7	-	3 of 7	3 of 7	-	-
90	8	-	-	1 of 8	-	7 of 8	-

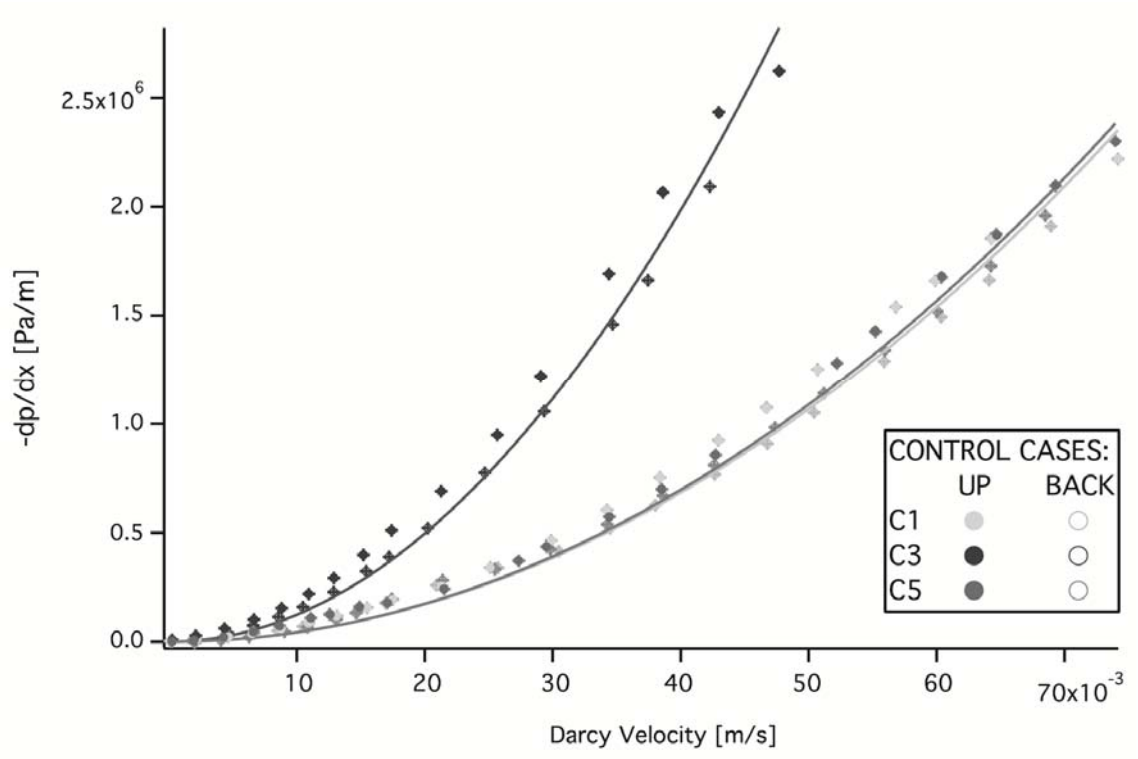

Figure S1: Permeability of the control samples.

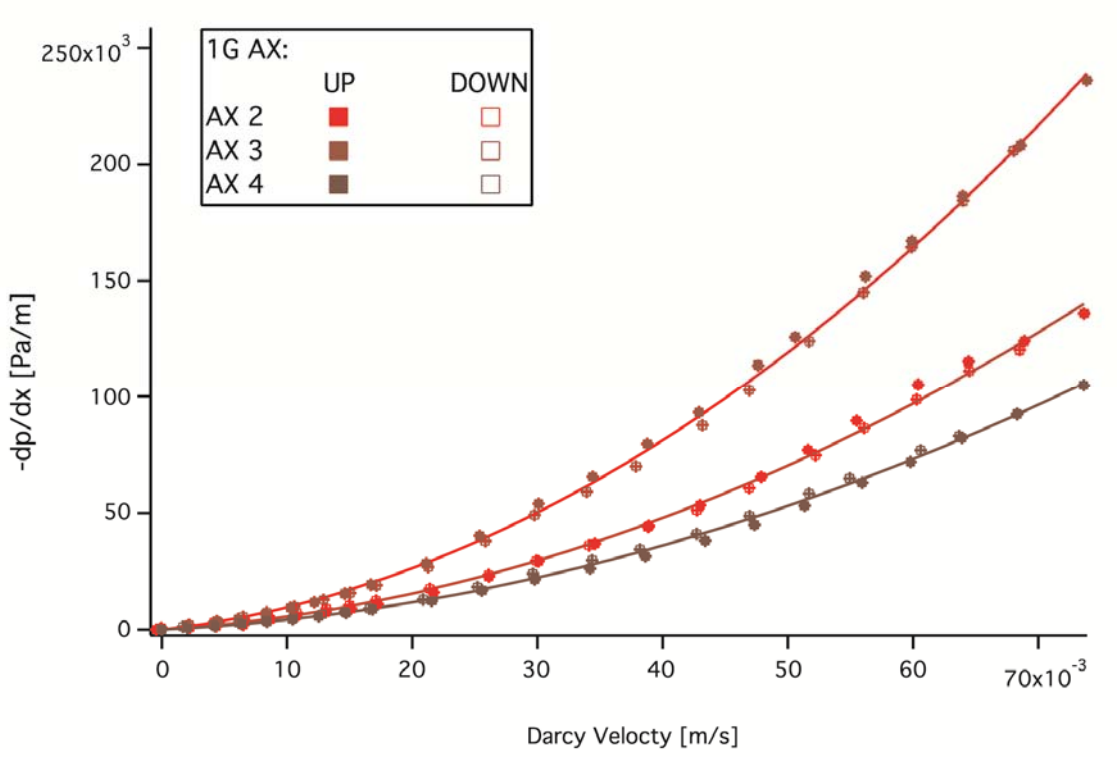

Figure S2: Permeability of 1gram axial reticulated cases.

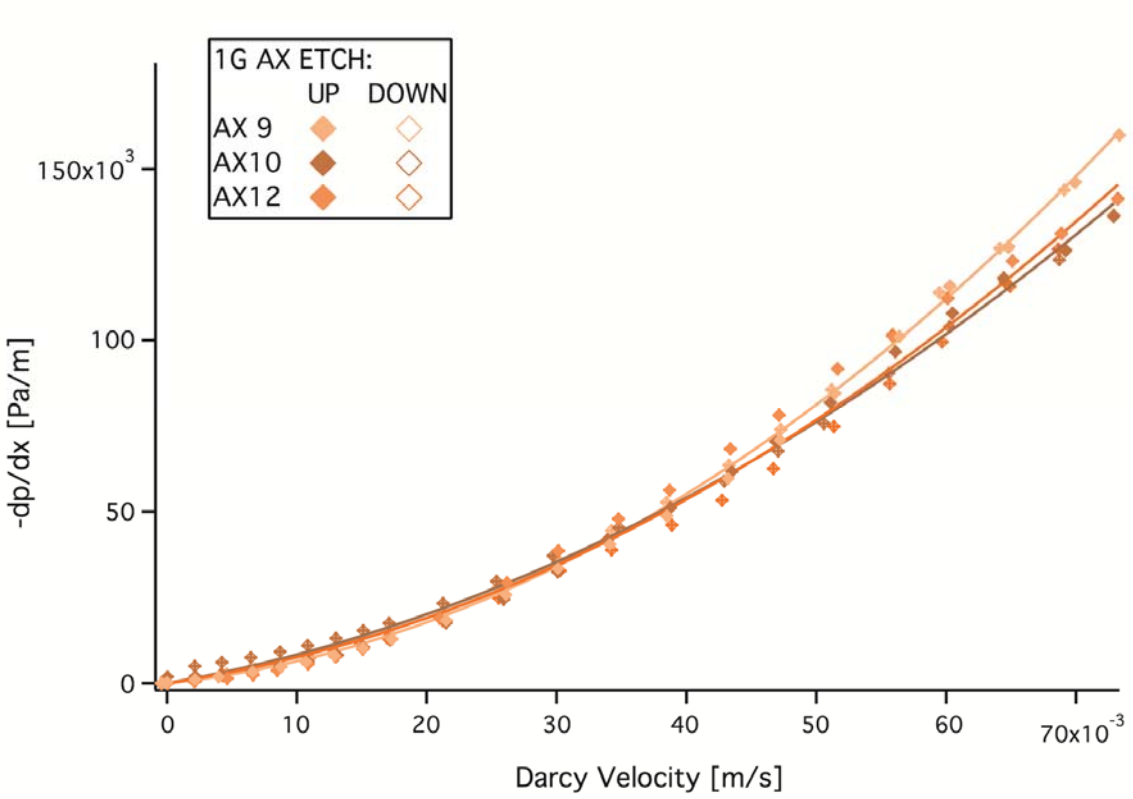

Figure S3: Permeability of 1 gram axial and base etched reticulated cases.

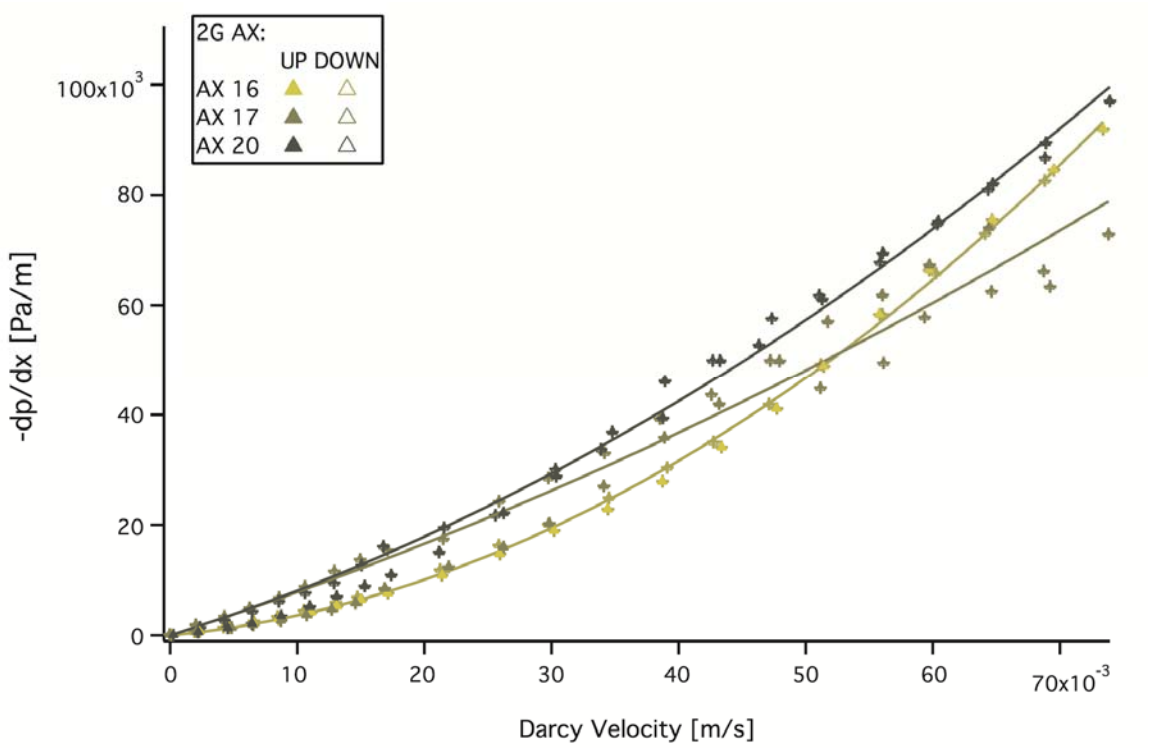

Figure S4: Permeability of 2 gram axial reticulated cases.

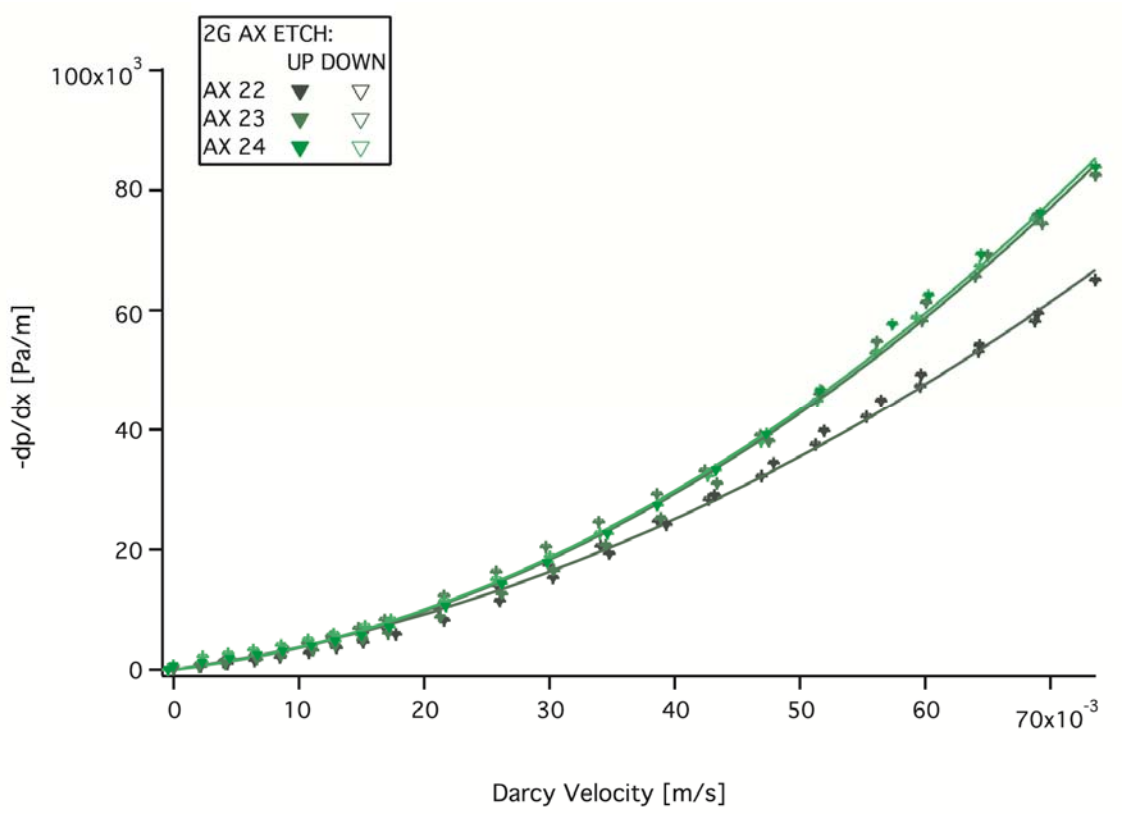

Figure S5: Permeability of 2 gram axial and base etched reticulated cases.

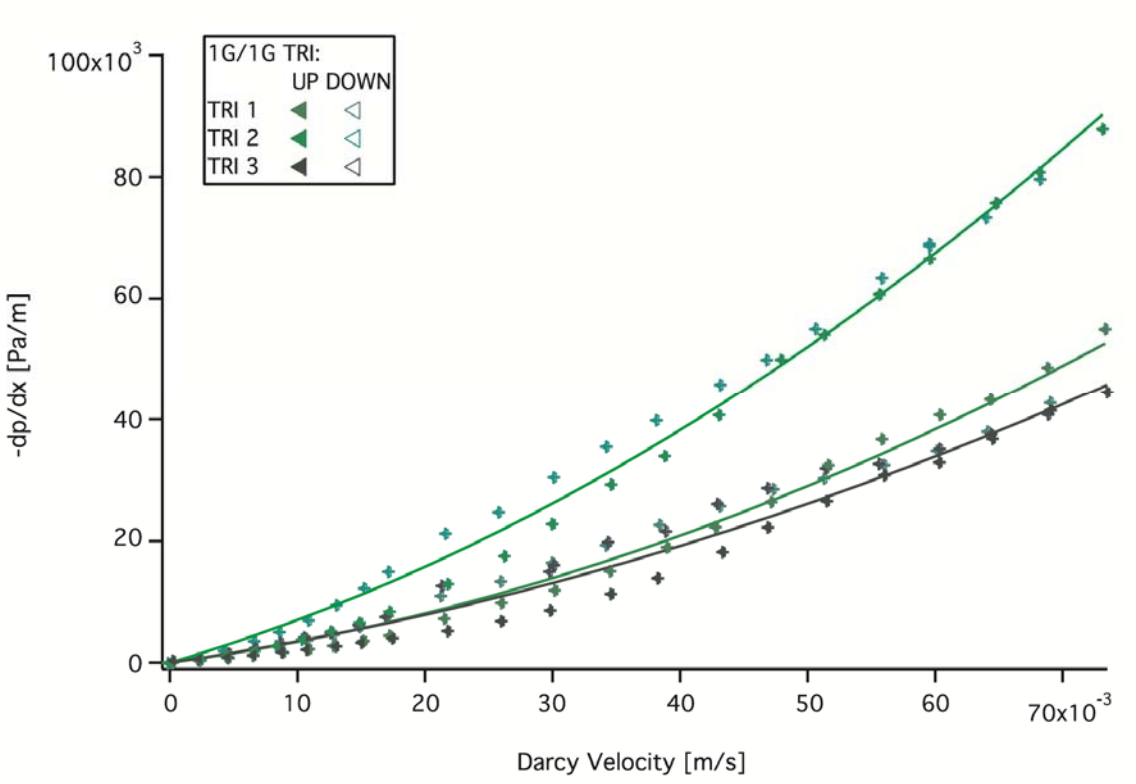

Figure S6: Permeability of 1g/1g tri axially reticulated cases.

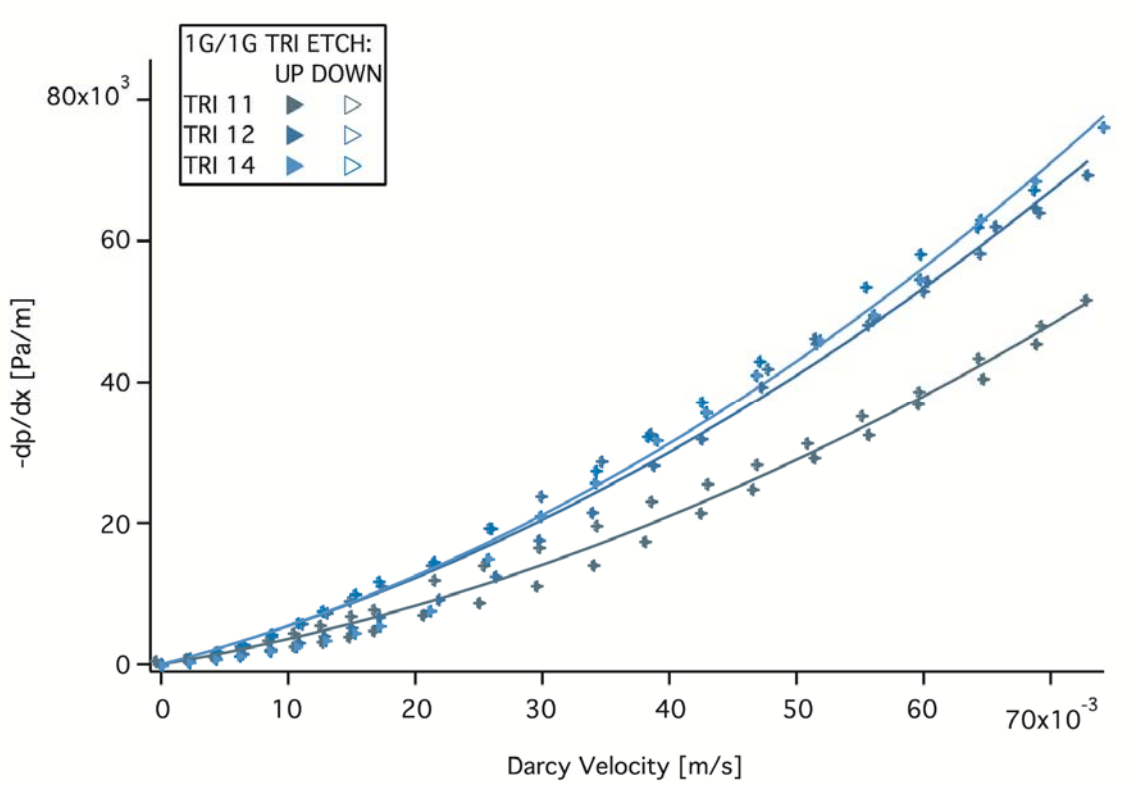

Figure S7: Permeability of 1g/1g tri axially and base etched reticulated cases.

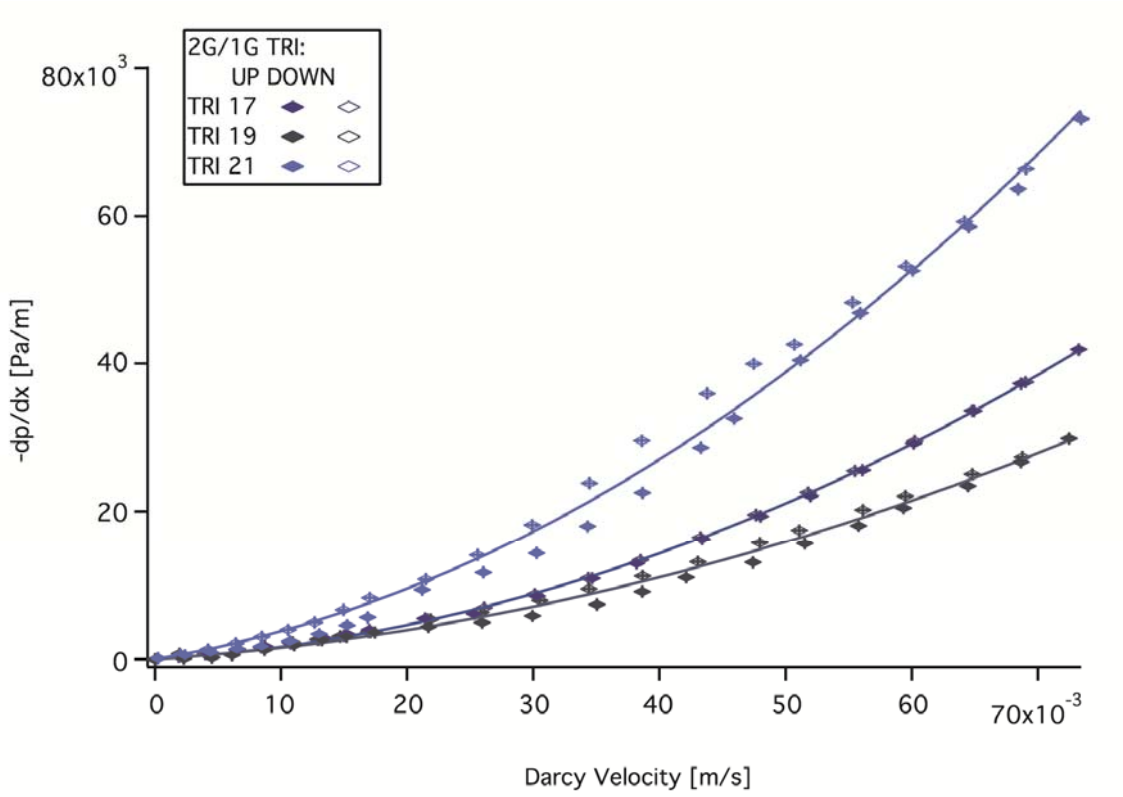

Figure S8: Permeability of 2g/1g tri axially reticulated cases.

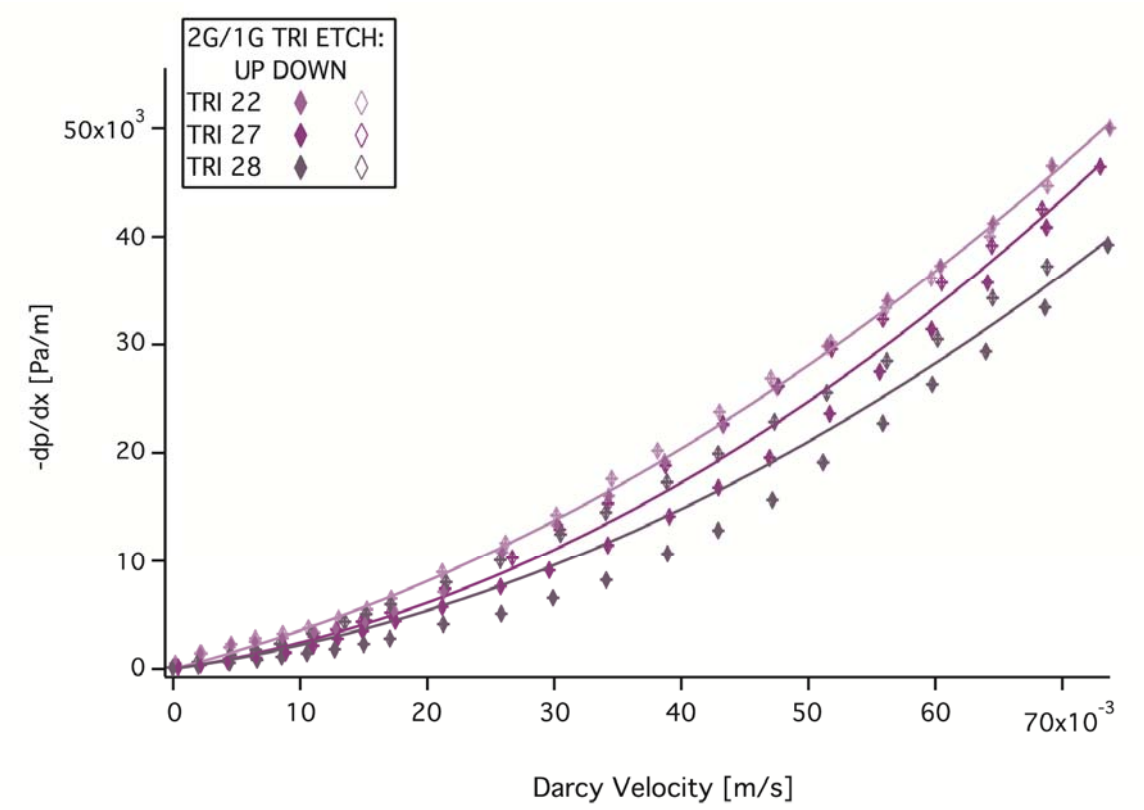

Figure S9: Permeability of 2g/1g tri axially and base etched reticulated cases.